https://ntrs.nasa.gov/search.jsp?R=19660011723 2020-03-16T22:35:10+00:00Z

NASA CR-65211

Pesco Products DIVISION OF BORG-WARNER CORPORATION

ENGINEERING REPORT NO. 3530

A STUDY OF ELECTRIC MOTORS FOR USE IN LIQUID AND GASEOUS HELIUM

FOR

NATIONAL AERONAUTICS AND SPACE ADMINISTRATION
MANNED SPACECRAFT CENTER
UNDER CONTRACT NO. NAS 9-4923

March 9, 1966

Prepared by F. W. Bott Title Project Engineer-Electrical

Prepared by G. H. Caine Title Project Engineer Specialist Cryogenics

Prepared by A. V. Pradhan Title Project Engineer Specialist Heat Transfer

Approved by J. H. Redmond Title Project Manager

Approved by John F. DiStefano Title Chief Engineer-Development

© Copyright 1966, Borg-Warner Corporation
Printed by Pesco Publications Department

USAF ZERO DEFECTS

aerospace equipment BORG WARNER®

Engineering Report 3530

TABLE OF CONTENTS

ABSTRACT			i
SECTION			PAGE
1.0	INTRODUCTION		1.1
2.0	STUDY BASIS		2.1
	2.1	Statement of Work	2.1
	2.2	Problem Areas	2.2
		2.2.1 Structure	2.2
		2.2.2 Bearings	2.3
		2.2.3 Heat Rejection	2.3
3.0	GENERAL APPROACH		3.1
	3.1	In-House Information Correlation	3.1
	3.2	Literature Search	3.1
	3.3	Industry Search	3.1
	3.4	Computations	3.2
4.0	CONCLUSIONS		4.1
	4.1	Recommended Structural Design	4.1
	4.2	Bearings	4.1
	4.3	Heat Rejection	4.2
	4.4	Electrical and Magnetic Design	4.3
	4.5	Effects of Fluid	4.4
5.0	RECOMMENDATIONS		5.1

USAF ZERO DEFECTS

aerospace equipment BORG WARNER®

SECTION			PAGE
6.0	DISCUSSION		6.1
	6.1	Mechanical Design Considerations	6.1
		6.1.1 Material Property Data Compilation	6.1
		6.1.2 Design Evaluation	6.2
		6.1.3 Bearings	6.6
		6.1.3.1 Bearing Manufacturers Reports and Recommendations	6.6
		6.1.3.2 Bearing Considerations	6.9
		6.1.3.3 Bearing Types	6.11
	6.2	Electro-Magnetic Design	6.14
		6.2.1 Motor Computer Program	6.16
		6.2.2 Active Volumes to be Studied	6.18
		6.2.3 Basic Geometry of Laminations	6.18
		6.2.4 Windings	6.20
		6.2.5 Effect of Temperature on Performance	6.20
		6.2.6 Insulation	6.23
		6.2.7 Conductor Materials	6.26
		6.2.8 Magnetic Material	6.27
		6.2.9 Results of Electro-Magnetic Design Study	6.28
		6.2.10 Other Factors Affecting Motor Design	6.31
	6.3	Heat Rejection Study	6.34
		6.3.1 Effect of Fluid Density on Fan Performance	6.35
		6.3.2 Compensating for Fluid Density Variations	6.38
		6.3.3 Heat Transfer Calculation	6.57
	6.4	Effect of Fluids	6.70
	6.5	Test Description and Results	6.73

Engineering Report 3530

Table of Contents

SECTION

APPENDICES -

APPENDIX I - Sample Calculations

APPENDIX II - Bibliography

ADDENDUM - Motor Selection Guide

USAF ZERO DEFECTS

aerospace equipment BORG WARNER®

Engineering Report 3530

FIGURE INDEX

FIGURE NO.		Following Page
6.1-1	Structural Materials Properties Chart	6.1
6.1-2	Structural Design I	6.3
6.1-3	Structural Design II	6.3
6.1-4	Structural Design III	6.4
6.1-5	Structural Design IV	6.4
6.1-6	Example Design	6.5
6.2-1	Computer Input Sheet for Lamination & Winding Calculations (Data for sample motor included)	6.17
6.2-2	Explanation of Symbols used on Computer Input Sheet for Lamination & Windings	6.17
6.2-3	Computer Print-Out for Lamination & Winding Calculations (Data for Sample Motor Included)	6.17
6.2-4	Computer Print-Out, Sample Motor Performance, Windings at +350°F	6.17
6.2-5	Computer Print-Out, Sample Motor Performance, Windings at -452°F	6.17
6.2-6	Active Volumes Studied and Some Pertinent Dimensions	6.18
6.2-7	Speed-Torque Curves, Sample Motor, Windings at +350°F and -452°F	6.22
6.2-8	Power Input and Current versus Torque, Sample Motor, Windings at +350°F and -452°F . .	6.22
6.2-9	Efficiency versus Torque, Sample Motor, Windings at +350°F and -452°F	6.22
6.2-10	Power Factor versus Torque, Sample Motor, Windings at +350°F and -452°F	6.22
6.2-11	Magnet Wire Flexibility in Liquid Helium	6.25
6.2-12	Average Electrical Breakdown Voltage for Insulated Wire	6.25
6.2-13	Resistivity of Copper and Some Copper Alloys versus Temperature	6.26
6.2-14	Resistivity of Copper and Some Constant Resistivity Materials versus Temperature	6.26
6.2-15	Mechanical Properties of Copper and Some Copper Alloys	6.26
6.2-16	Saturation Density @ Ambient Temperature - Saturated Density @ Absolute Zero versus Ambient Temp. - Curie Temp. . . .	6.27

USAF ZERO DEFECTS

aerospace equipment BORG WARNER®

FIGURE NO.		Following Page
6.2-17	Continuous Output versus Active Volume	6.30
6.2-18	Motor Efficiency versus Active Volume	6.30
6.2-19	Power Consumed by Fan versus Active Volume . . .	6.30
6.2-20	Losses Dissipated versus Active Volume	6.30
6.3-1	Helium Density versus Temperature, Motor Envelope	6.37
6.3-2	Helium Density versus Temperature, Fan Envelope.	6.37
6.3-3	Variable Pitch Fan.	6.43
6.3-4	Blade Angle Determination	6.43
6.3-5	Estimated Fan Performance	6.52
6.3-6	Estimated Fan Power	6.53
6.3-7	Estimated Fan Performance @ 610°R	6.54
6.3-8	Thermal Model	6.57
6.3-9	Typ. Computer Print-Out for Heat Transfer Rates	6.59
6.4-1	Fluid Loss Coefficients	6.72
6.5-1	Test Motor	6.73
6.5-2	Test Motor - Disassembled	6.73
6.5-3	Instrumentation Schematic	6.73
6.5-4	Test Dewar - Flange Mounted	6.73
6.5-5	Test Horizontal Mounting	6.73
6.5-6	Test Data	6.74
6.5-7	Test Bearing (Front)	6.75
6.5-8	Test Bearing (Rear)	6.75

USAF ZERO DEFECTS

aerospace equipment BORG WARNER®

ABSTRACT

This report covers the information and data generated by a study of the application of electric motors in a helium environment.

It was sponsored by NASA Manned Spacecraft Center, Houston, Texas under Contract No. NAS 9-4023.

In general, the application of high frequency electric motors over broad temperature environments requires a compromise of design, performance, and/or weight to accommodate the worst, and therefore, controlling environment. In the specific case of required continuous operation over the range of +70°F gaseous helium to -452°F liquid, a severe cooling penalty exists for the +70°F operation when compared to -452°F operation. Low heat rejection rates not only restrict the output ability of the motor, but also compromise the bearing life. Since the bearing may not use a conventional lubricant because of low temperature operation, the "cryogenic" bearing construction used must be modified to assist operation at the more nominal conditions. The use of molybdenum di-sulfide lubricant carried in a glass reinforced Teflon cage has exhibited promising results for both the high and low temperature conditions. Although the scope of this study did not allow long term testing, the results of the short test period coupled with satisfactory long term results reported by the bearing manufacturer for similar environments encourages the use of the bearing-lubricant configuration for further test evaluation.

Structural design must not only provide suitable rotor and bearing mounting means but must also counteract or absorb clamping action and distortion inherent in multi-metal assemblies due to temperature differential contraction. Such action, if uncompensated, can result in severe axial or radial loading of the bearing and overstressing of structural members.

A single metal assembly is impractical since no one metal has all the necessary physical properties to be suitable for structural, bearing and shaft applications for light weight assemblies.

A tri-metal assembly is proposed and analyzed as a practical method of providing a free action mounting for the bearing, reasonable stress in structural members and light weight construction.

Cooling of the motor and bearings requires heat rejection into the ambient gas or liquid environment. For effective heat removal, a flow of the fluid must be created through the motor to provide maximum contact between cooling the media and the motor heat generating areas.

The fan or impeller normally used for forced circulation exhibits an extreme loading variation as a direct result of the fluid density variation. A fluid density range of .0068 lbs/ft^3 to 15 lbs/ft^3 could constitute a fan power input range of the same order of magnitude or 2200:1. Therefore, a compensating method of coolant circulation must be used to assure both an adequate flow for sufficient heat removal and acceptable power absorption. Alternate schemes are presented to accomplish this aim. The most promising appears to be a bi-metal fan blade which due to its change in angle with temperature prevents undue loading in high density fluid.

Two sample bearing test motors were built and tested in LH_2 and 70°F He verifying the feasibility of the bearing mounting method and operation of the motor over the wide temperature range.

Motor performance varies substantually with temperature due to conductor resistance change, especially for the rotor conductors. Some compensation can be made by using alloys having a lower coefficient of temperature resistivity and a higher (than copper) initial resistance. However, alloys which exhibit an almost constant resistance over +350°F to -450°F temperature range, unfortunately also possesses extremely high initial resistance (based on 70°F) making then unusable as conductors without suffering a severe penalty in size and weight of the motor.

SECTION 1.0

INTRODUCTION

This developmental study of electrical motors for use in helium was sponsored by NASA Manned Spacecraft Center, Houston, Texas under Contract No. NAS 9-4023.

The intent of the study is to develop data by state-of-the-art and theoretical investigation to demonstrate the feasibility of operation of A.C. motors in liquid helium and helium vapor. This study is to produce information on and relationships between envelope, weight, efficiency, and power output for motors operating in the required environment and to present a design recommendation for a two-pound unit. Only one type of motor is considered, that is, the squirrel cage induction motor operating from a 3-phase, 400 cycles per second, 208 line-to-line voltage power system.

All of the pertinent design parameters such as electrical power generation, speed of operation, bearing type and configuration, and cooling methods, are to some degree inter-related. It has therefore been necessary to evaluate not only the effects of variables in each specific area of study, but also to evaluate the effect of these variables on the performance of the dependent parameters.

For example, the ability of a motor to produce continuous power is dependent on insulation temperature as well as power generated. Therefore, the heat rejection effectiveness is equal in important to electro-magnetic sizing for determining the final machine size.

Optimization, an ambitious goal in itself, can be approached only if specific guidance is available to set the criteria for evaluating the importance of the various trade-off areas. To this end the work statement has been used as a guide and in addition, it has been assumed that light weight is a primary goal. Much of the time has been spent on researching basic materials, physical and electrical characteristics and state-of-the-art designs and experience,

especially on bearings. Much of the design input has been obtained from Pesco experience on previous hardware programs involving cryogenic fluid pumping units some of which were cryogenic electric motor driven.

It should be noted that Pesco has found the various information sources extremely cooperative and helpful in supplying available material.

Also, bearing manufacturers have been willing to disclose their recommendations and experience data to aid in the selection of the best choice based on existing data and knowledgeable estimates.

SECTION 2.0

STUDY BASIS

The "Statement of Work" contained in NASA Contract NAS 9-4023 forms the basis of this study. The Work Statement is reproduced here as a reference.

2.1 Statement of Work

SPECIFICATION FOR THE DEVELOPMENT OF ELECTRICAL MOTORS FOR USE IN LIQUID HELIUM

1.0 SCOPE

1.1 This specification defines the requirements for liquid helium motor developmental study, hereinafter referred to as the motor study. This study shall demonstrate the feasibility of the operation of electric motors in liquid helium and helium vapor.

2.0 REQUIREMENTS

2.1 This motor study shall be based upon the following design parameters:

2.1.1 Frequency of the power unit - 400 cps
2.1.2 Number of phases of the power unit - 3
2.1.3 Phase to phase voltage of the power unit - 208 v
2.1.4 Phase to neutral voltage of the power unit - 120 v
2.1.5 Current - alternating, sinusoidal
2.1.6 Dielectric strength - 1000 v DC ± 10%
2.1.7 Weight - less than 2 pounds

2.2 Dependent upon the results and/or progress of the motor study, initiation of motor fabrication shall be determined.

2.2.1 These motors shall be capable of operating submerged in liquid or gaseous helium over a pressure range of 10 to 3000 psia for 1000 hours of continuous running and 10,000 on-off cycles. Maximum fluid temperature for design shall be 70°F.

2.3 These motors shall be optimized for use in the specified fluid as follows:

2.3.1 Final motor design shall be optimized using parametric data which will be presented as a part of the results of the study.

2.3.2 Parametric data which will be presented will include, but not be limited to the following:

2.3.2.1 Power requirements versus fluid density and viscosity.
2.3.2.2 Efficiency versus temperature
2.3.2.3 Weight versus power
2.3.2.4 Effects of using a different fluid
2.3.2.5 Envelope dimensions versus power
2.3.2.6 Electrical design trade-offs

2.2 Problem Areas

Certain areas of design required special consideration primarily due to the broad temperature and pressure range of the environment. Most of these could be anticipated with some prior knowledge of cryogenic behavior of materials and therefore the study directed accordingly.

2.2.1 Structure

There are two basic design considerations for the main housing and bearing supports. First, the inherent physical characteristics of available materials at both normal and cryogenic temperatures must be suitable for the expected loads and intended usage. Second, the fits and differential expansions between dissimilar materials must result in a workable assembly; not over-stressed nor with over-large clearances where not desirable. Controlled fits and clearances are especially important in the successful application of bearings.

2.2.2 Bearings

The operating life of the motor is expected to be its bearing life. The bearing thus becomes the controlling item and deserves primary consideration. Very limited experience data is available for bearing operation at both liquid and gaseous fluid conditions with the associated temperature levels. Lubrication and cooling methods must be predictable and adequate for the full operating range. Various types of bearings are available for consideration, each having its own particular advantages and disadvantages.

2.2.3 Heat Rejection

Heat rejection rates constitute one limiting factor on the continuous power available from a motor. Since no external heat sink is offered by the Work Statement, it must be assumed that the environmental fluid must constitute the heat sink and that it is sufficient to absorb the quantities of heat required. The rate of transfer is dependent on the method of heat removal, the rate of fluid flow involved, and the fluid thermal characteristics. While the liquid state of the fluid has high heat capacity, its gaseous 70°F state has heat removal characteristics poorer that the normally used room ambient air.

In addition, circulating the fluid poses a problem in power absorption due to its wide density variation from gaseous to liquid state and the resulting variation in the power required.

SECTION 3.0

GENERAL APPROACH

Predicting the performance and establishing weight and size relationships requires a correlation of electrical and mechanical designs. Existing information must be utilized and supplemented with calculated data for operating characteristics and material characteristics. The plan of attack to accomplish these objectives was -

3.1 In-House Information Correlation

Much usable data on motor performance, bearing operation, structural configuration, and materials has been generated by prior and current programs for pumping cryogenic fluids. These data have been used where applicable and the referenced documents appear in the bibliography.

3.2 Literature Search

Many sources were consulted to obtain listings of pertinent publications. Those contacted are reported in the bibliography as sources and the pertinent documents are listed as references.

3.3 Industry Search

In order to obtain the latest information regarding material characteristics (electrical and mechanical) a survey of industrial concerns and government testing agencies was made. It was felt that this was especially important for bearing application and testing experience information.

3.4 Computations

Computations were made for the mechanical design (stresses and fits), electrical performance and heat rejection. Design calculations were necessary over a wide range of sizes and speeds to establish meaningful relationships of wieght versus power output and cooling ability.

SECTION 4.0

CONCLUSIONS

This study has demonstrated the feasibility of motor operation in liquid and gaseous helium within the limits of present art. Certain performance and size restrictions are imposed by bearing knowledge, heat rejection rates, and feasible magnetic densities. An example design is included to demonstrate a suggested configuration for both mechanical and electrical considerations. A bearing test motor was built and tested to demonstrate the ability of the mechanical structure to maintain accurate bearing alignment and secure mounting over the temperature range of +70°F to -425°F. A description and results of the test is presented in Section 6.5.

4.1 Recommended Structural Design

Figure 6.1-6 shows a drawing of the basic design. This structure is basically the recommended design for motors to meet the requirements of the Work Statement.

The structure is a tri-metal assembly in order to accommodate the inherent differences in coefficient of expansion without undue stresses. Also, for good bearing operation it was deemed necessary to prevent any uncontrolled pre-loading axially or radially due to contractions. Section 6.1.2 gives the detail information concerning stresses for the example design.

4.2 Bearings

Radial type ball bearings have been selected as the best suited for the required application. This type modified to an angular contact style have good load carrying characteristics for both radial and thrust loads. The angular contact arrangement requires that the thrust loads must be oriented and maintained in one direction. The advantage of the angular contact type is that the ball cage need not be formed of two pieces to allow assembly. A snap

assembly method is used where the balls and cage are forced over the shallow inner race shoulder. Thus, the cage can be precision machined of one-piece reducing inaccuracies in ball to cage contact and cage to race fit.

Lubrication to suit the high and low temperature environment is a solid material wiped from the cage by the ball contact. For the sample test motor, a glass filled Teflon cage impregnated with MoS_2 was used representing the type of bearing having the most available data on wide temperature range operation.

In general, the reliability and life of a bearing is a function of its DN value (bore diameter mm x rpm) temperature, load and lubrication. While these parameters are fairly well established for normal temperature oil lubricated applications by many tests and service experience, this is not true for cryogenic applications. Predictability of life for cryogenic applications is questionable. For combination cryogenic and hot temperature operation, there is even less experience. For this reason, it is best to use existing data with caution and rely on general guide lines for applying the bearing. Light loads, low speeds, and adequate cooling all enhance bearing life. Special attention should be paid to assure square and concentric mounting. With these precautions, it is reasonable to expect the required 1000 hours life.

4.3 Heat Rejection

Heat rejection rates determine the allowable power out of a motor to maintain reasonable insulation temperatures; normal methods of cooling is to reject the motor losses into the surrounding environment, gas or liquid as the case may be.

In this study, the environment can vary through both a gaseous and liquid state and over a wide range of densities and temperatures. As a consequence, the heat absorption ability also varies over a wide range and at the high temperature condition the least cooling effect can be expected. Accordingly, any cooling method must be designed around this worst case condition.

A forced flow of coolant through the motor offers the most efficient heat removal since it allows direct contact with the heat generating areas. Special methods of propelling the coolant must be used because a normal type fan designed for low density gas operation exhibits an impossibly high load when subjected to a high density liquid. A suggested method for partially compensating the load change is a bi-metallic fan blade that changes angle as a function of temperature.

Where a motor is not wholly dependent on environment heat sinking, as in the case where intermittent operation is required, structural conduction may eliminate the need for forced cooling.

4.4 Electrical and Magnetic Design

The basic electrical and magnetic design of the standard squirrel cage induction motor has been used. This type of motor is less susceptible to extreme environmental conditions and offers good possibilities for low weight to power.

Selection of insulations is done primarily on the basis of their physical properties at cryogenic temperatures and their temperature ratings for the higher ambient. Fortunately, those materials reported having the better cryogenic physical properties also have good high temperature ratings. These include Teflon and DuPont ML film which are both good for operation above 200°C.

Conductor materials, generally copper or copper alloys, can be used without hesitation at cryogenic temperatures, since most all of these metals exhibit good physical characteristics. The variation in electrical resistance does tend to restrict the application of motors. Stator winding resistance reduction as the temperature lowers results in a slight increase in maximum torque. Rotor cage conductor reduction in resistance directly affects the slip and inversely the starting torque. Therefore, to obtain a reasonable starting torque at low temperatures necessitates a rotor resistance value which produces high slip (reduced speed) at normal temperature. The use of alloys having "flat" coefficient of resistivity curves versus temperature could compensate this relationship. However, those metals known to date also have large initial resistivities in the order of 20 to 25 times as great as copper. The increase in size and weight to accommodate these alloys is not warranted.

Those magnetic materials normally used for high performance motors are usable throughout the temperature range specified for this study. Approximately 25% increase in iron losses can be expected as reported in the literature, but magnetization remains almost constant.

4.5 Effects of Fluid

The effect of the environment fluid, which we assume will pass through the motor as a coolant, can be either chemical or physical or both. One of the first considerations is the compatibility of the fluid with the materials and whether deleterious or hazardous combinations might exist. The electrical properties of the fluid are also important as they may establish unusual spacing of conductors and affect size. Fortunately, the common cryogenic fluids, LN_2, LOX, LH_2, and LH_e have adequate electrical characteristics to be used in 200 volt machinery without difficulty. Insulations are available that are usable at low temperatures and compatible with the fluids. One cautioned area is the use of oxygen due to the possibility of material ignition in the case of an electrical fault. Applications in O_2 deserve extra consideration to minimize the probability of failure or to protect against prolonged fault conditions that may result in local ignition temperatures.

Chemically, the LH_2 atmosphere is probably the most unfavorable for bearing operation due to its strong reducing influence tending to breakdown ball track oxide films.

Some loss in power is realized due to the rotational losses especially in the higher density fluids. These losses are a function of the surface condition, surface speed fluid viscosity, and fluid density. In general, the value of losses is not expected to constitute a problem but will have to be estimated and applied as an anticipated load on the motor. Reduction in losses can be realized by paying particular attention to minimizing rotor and stator irregularities and by careful selection of rotor diameter to length ratios. The generalized expression for loss is -

$$HP = K N^3 D^5 \omega$$

where: K is an operational function based on Reynolds number

ω = fluid density
N = rpm
D = diameter of rotor

SECTION 5.0

RECOMMENDATIONS

Calculations of performance and cooling have been presented as part of this study. The degree of compliance of calculated to actual is expected to be good especially for motor performance based on generally accepted procedures and past experience. Heat transfer predictions and calculations are, due to their nature, always best augmented with empirical coefficients of heat transfer.

Predicting bearing life accurately for the specified environments and operation is questionable. Little data is available and the theoretical analysis of normally lubricated bearings is not applicable.

In order to obtain additional data for the application of bearings over the wide environmental range, a hardware and test program should be undertaken. It is felt that such a program would add to both the knowledge of bearing performance and the structure integrity.

SECTION 6.0

DISCUSSION

6.1 Mechanical Design Considerations

6.1.1 Material Property Data Compilation

The requirements for motor operation over the wide range of temperature has placed emphasis on the determination of material properties and the selection of materials that will be both structurally and thermally compatible with the design goals. To aid in the evaluation of possible materials, Figure 6.1-1, Structural Materials Properties Chart was constructed from sources made available during the literature survey.(1) This table compiles material properties such as thermal expansion, modulus of elasticity, yield strength, and Poissons ratio for a variety of materials including aluminum, carbon steel, stainless steel, Invar, and Inconel. As can be seen from the table, a great difference appears in the thermal expansion rate of the selected bearing material (440 C stainless steel), and popular light weight housing alloys such as aluminum. It is this difference that causes extreme design complexities. Although 440 C is a satisfactory material for the construction of bearings, sleeves, and other small items, it is considered too brittle a material particularly at cryogenic temperatures for the fabrication of a light weight motor housing.

(1) Air Force Materials Laboratory, Cryogenic Materials Data Handbook, No. AD 609562, Clearinghouse for Federal Scientific and Technical Information, August, 1964.

Material	Thermal Expansion $(L_T - L_{68})/L_{68}$ In/In X 10^{-5}		Average Coeff. of Linear Thermal Exp. In/In/°F X10^{-5}		Modulus of Elasticity, psi X 10^6			Yield Stress, psi X 10^3			Poisson's Ratio		
	T = 350°F	-450°F	68° to 350°	68° to 450°	350°	68°	-450°	350°	68°	-450°	350°	68°	-450°
Al 356T6	+345.0	-390.0	+1.223	-.753	+ 9.5	+11.0	+13.0	+11.0	+24.0	+37.0			
Al 7075T6	+370.0	-430.0	+1.311	-.830	+ 9.0	+11.0	+12.0	+45.0	+74.0	+100.0			
Steel 1075	+190.0	-200.0	+ .674	-.386	+29.0	+30.0	+31.5	+90.0	+103.0	+280.0			
Steel 440C	+170.0	-185.0	+ .603	-.357	*+30.5	*+31.5	*+33.0	*+110.0	*+135.0	*+230.0			
Stainless 304	+260.0	-300.0	+ .922	-.579	+28.0	+28.5	+29.0	+60.0	+60.0	+80.0	.283	.25	
Invar 36	+ 30.0	- 40.0	+ .106	-.077	+23.0	+21.5	+19.0	+75.0	+90.0	+170.0			
Inconel	+205.0	-230.0	+ .727	-.444	+30.0	+31.0	+32.0	+45.0	+35.0	+30.0			
Inconel 750X	+220.0	-220.0	+ .780	-.425	+30.0	+30.0	+30.0	+108.0	+110.0	+122.0		.295	.298

* Approximated from (1) 400 series.

STRUCTURAL MATERIALS PROPERTIES CHART

FIGURE 6.1-1

6.1.2 Design Evaluation

For long life and good wearing properties, the bearing races are best fabricated from 440C stainless steel. For lightness, the motor housing is best constructed from aluminum alloy. Since the differential expansion rate between the aluminum housing and bearing materials is great, a bearing liner is required. Alternately, the housing could be made from a material with a more compatible thermal coefficient of expansion.

Although the current NASA operating range is between +70°F and -453°F, additional power can be obtained from the motor active ingredients by allowing a motor temperature rise to +350°F. To allow such a temperature rise, the bearings will have to operate over a temperature range of 800°F.

To further point out the design problem to be overcome, we must consider the coefficient of thermal expansion for the materials used in the construction of the motor. The following coefficients are given for the range +350 to -453°F.

AMS 7074 AlAlloy	-	80×10^{-4} in/in
304 S/S	-	56×10^{-4} in/in
440 C	-	35.5×10^{-4} in/in
Inconel 750X	-	44.0×10^{-4} in/in

A line to line fit on a .75 in. O.D. 440C bearing race in an aluminum housing at -453°F will result in a .0033 loose fit at +350°F. This looseness is unacceptable for maintaining shaft and rotor alignment and will result in short bearing life. This approach to the solution of the problems is to use a sleeve to take up the difference in thermal contraction.

Axial expansion rate differential must also be considered. Assuming a 2-inch separation between bearing raceways, a .0072 inch differential length results at cryogenic temperature. This problem can be overcome by using a bearing preload spring of proper rate to accommodate the dimensional change and to provide a desirable thrust load on the bearings.

Several possible designs were investigated to overcome the thermal differential problem within the 2-pound design weight goal. These designs are presented below:

Aluminum Housing (Baseline for Study - Figure 6.1-2)

This design was considered to obtain a baseline for the study. The motor housing is fabricated from AMS 7075 aluminum alloy bar stock. The housing walls are .125 in. thick and the bearing supports .156 in. thick for rigidity.

To prevent stator/rotor misalignment, the stator is positioned into the housing with a maximum working stress respectively in the housing and stator at cryogenic temperatures. The housing wall thickness supplies a factor of safety of 2. As indicated in the general discussion above, a line to line fit of the bearing to housing at -453°F results in .0034 looseness at +350°F. From these calculations, it is seen that either a bearing sleeve or a housing of more compatible material is required. The aluminum housing weight is estimated at approximately .3 pounds. Stresses for this configuration are shown in Appendix I as well as the method of calculation.

Aluminum Housing with Invar Sleeve (Figure 6.1-3)

To reduce the .0033 inch clearance between the aluminum housing and bearing, a sleeve of low thermal expansion Invar was considered. The difference in expansion is taken up as stress in the Invar sleeve. Stress calculations show that to maintain the same bearing to sleeve clearance at both +350 and -453°F, a ratio of sleeve to housing wall thickness of 1:1 is required. The resulting maximum stress would be 50,600 psi and 52,100 psi in the sleeve and housing respectively. Although, this method of bearing mounting is possible, further analysis of Invar revealed that the thermal coefficient of expansion is not linear throughout the operating temperature range causing possible binding at the midpoint temperature. For this reason this design was discarded.

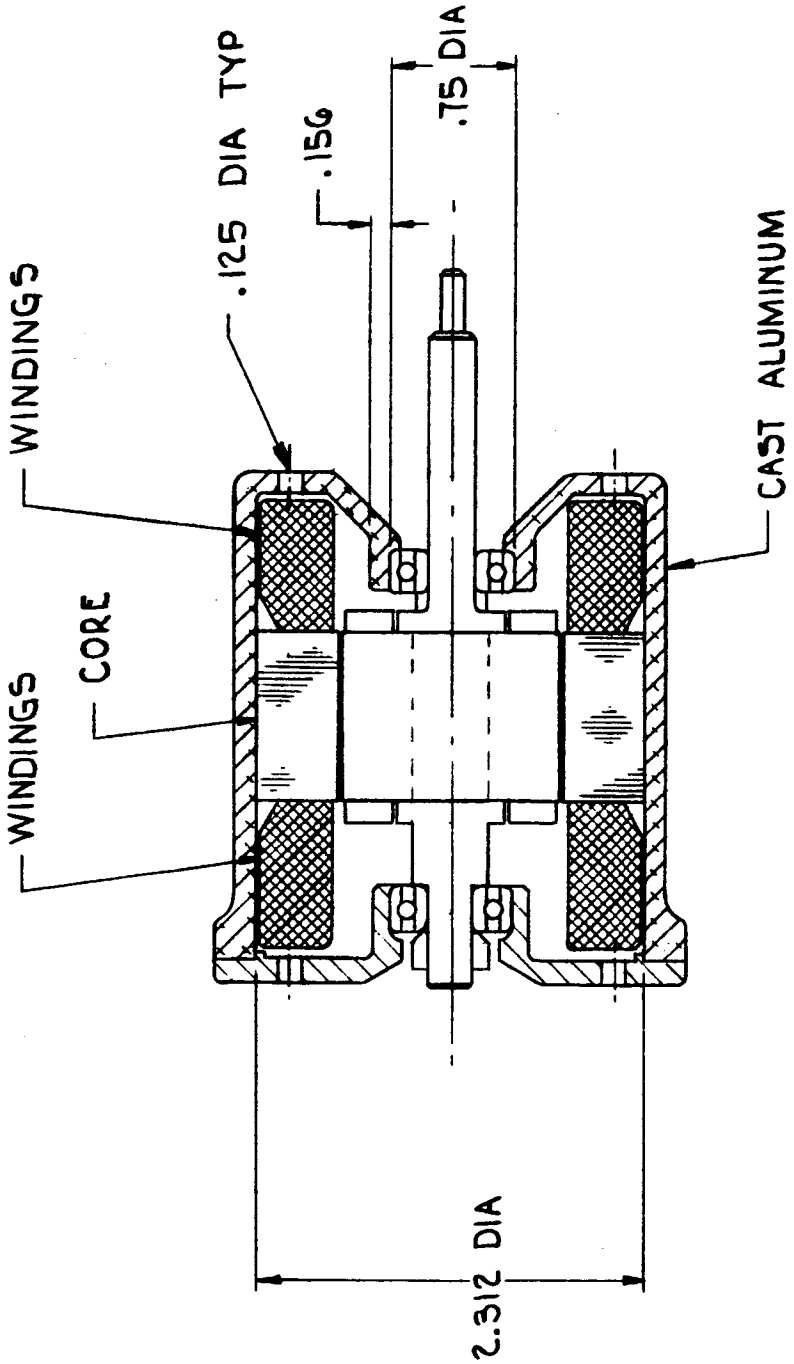

Structural Design I
(Aluminum & 440C)

FIGURE 6.1-2

USAF ZERO DEFECTS

aerospace equipment BORG WARNER®

USAF ZERO DEFECTS

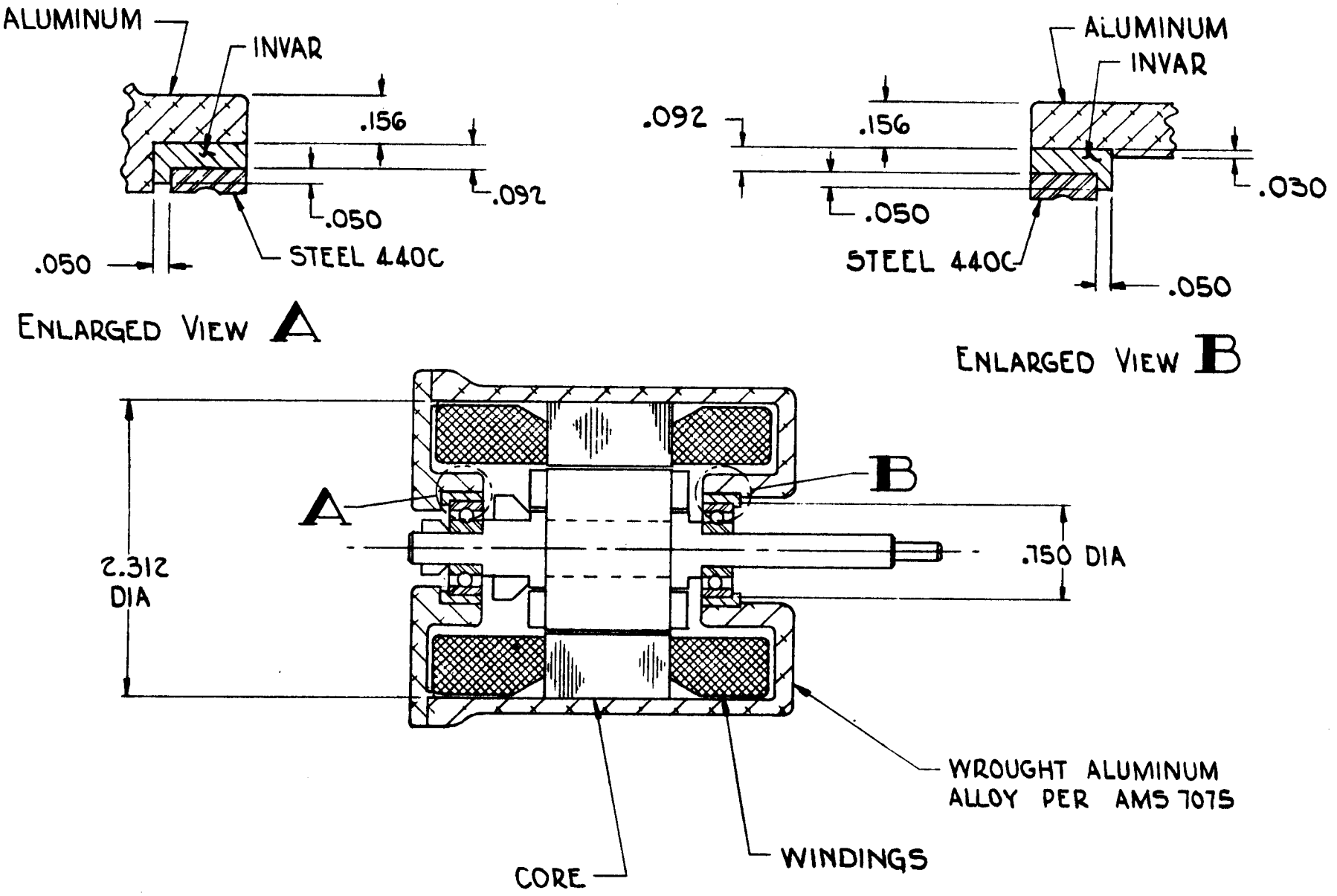

Structural Design II
(Aluminum, Invar, 440C)

FIGURE 6.1-3

Pesco Products DIVISION OF BORG-WARNER CORPORATION
aerospace equipment BORG WARNER ®

Inconel Housing (Figure 6.1-4)

The use of a housing made of Inconel was considered. Inconel with a thermal coefficient of expansion of 5.4×10^{-6} in/in°F over the considered 800°F operating temperature range is more compatible with the 440C bearing race material (thermal coefficient of expansion = 4.4×10^{-6} in/in/°F) than aluminum. A line to line fit at -453°F between an Inconel housing and a 440°C outer bearing race will result in only .0006 looseness at +350°F. Likewise, a line to line fit of an Inconel shaft to 440C bearing inner race at -453°F will result in a .0002 tight fit at +350°F. The use of an Inconel shaft seems feasible in all designs. Preliminary weight estimates of a fabricated Inconel housing indicate a total housing weight of .65 pounds. Since the weight of an Inconel housing does not appear to be within the weight requirements of flight type units, and since difficult fabrication problems are expected in manufacturing a sheet metal Inconel housing, this design was discarded.

Aluminum Housing with 440C Sleeve and Star Tolerance Ring (1) (Figure 6.1-5)

A tolerance ring (tentative selection P/N AN 112037S) is inserted between a 440C sleeve and the aluminum housing to absorb the differential in thermal expansion. The tolerance ring is a corrugated, open ring of 301 S.S. with straight rims at the ends of the corrugations. It serves as a wedging shim between the two cylindrical members. If the clearance between the sleeve and housing is set at -453°F, then as the housing warms the thermal expansion is absorbed by the tolerance ring. Close design analysis revealed that the manufacturing tolerances of the rings are too large for the precision clearances required in the helium motor design. This design was subsequently discarded. In addition, it is obvious that radial clamping of the bearing outer ring will occur preventing free axial movement which is necessary to prevent uncontrolled preloading.

(1) Trade name of corrugated sleeve manufactured by Roller Bearing Company of America.

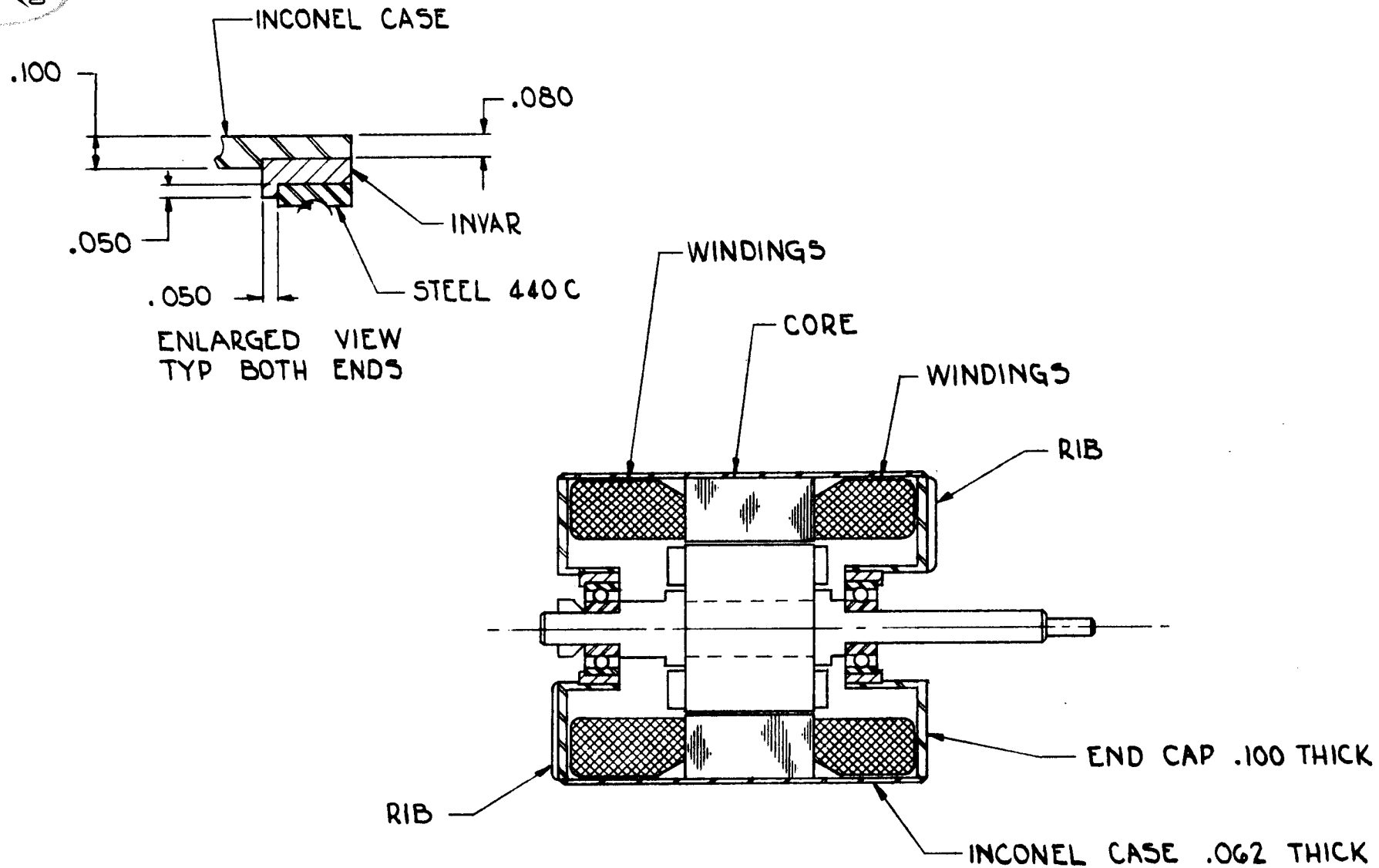

Structural Design III
(Inconel, Invar, 440C)

FIGURE 6.1-4

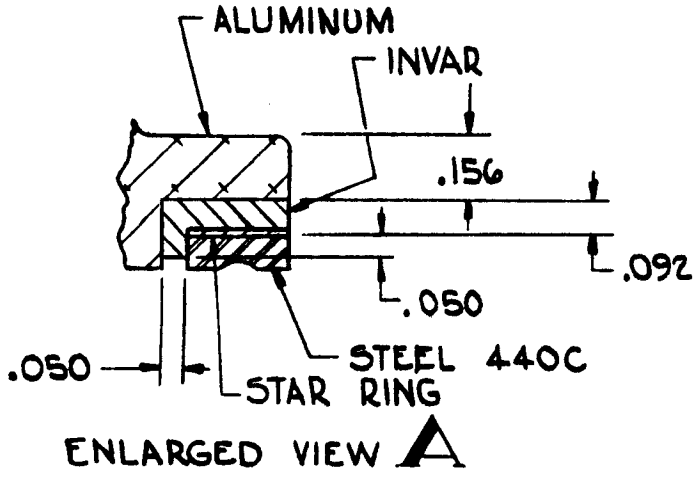

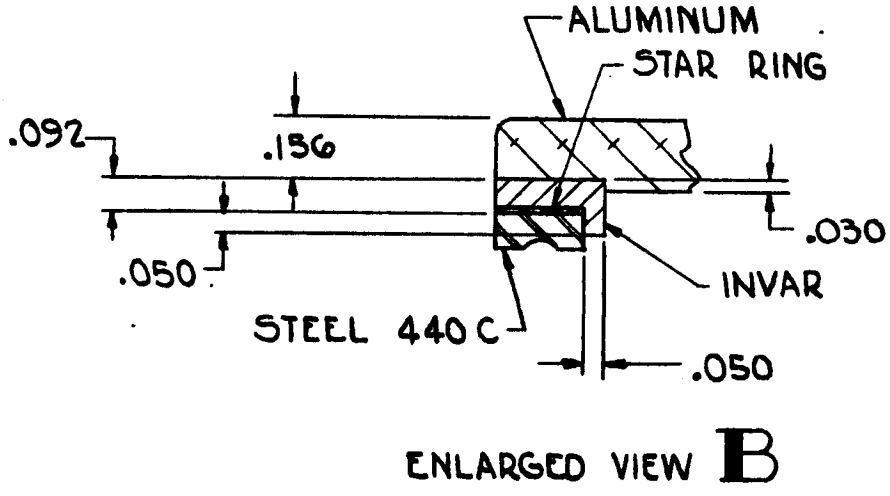

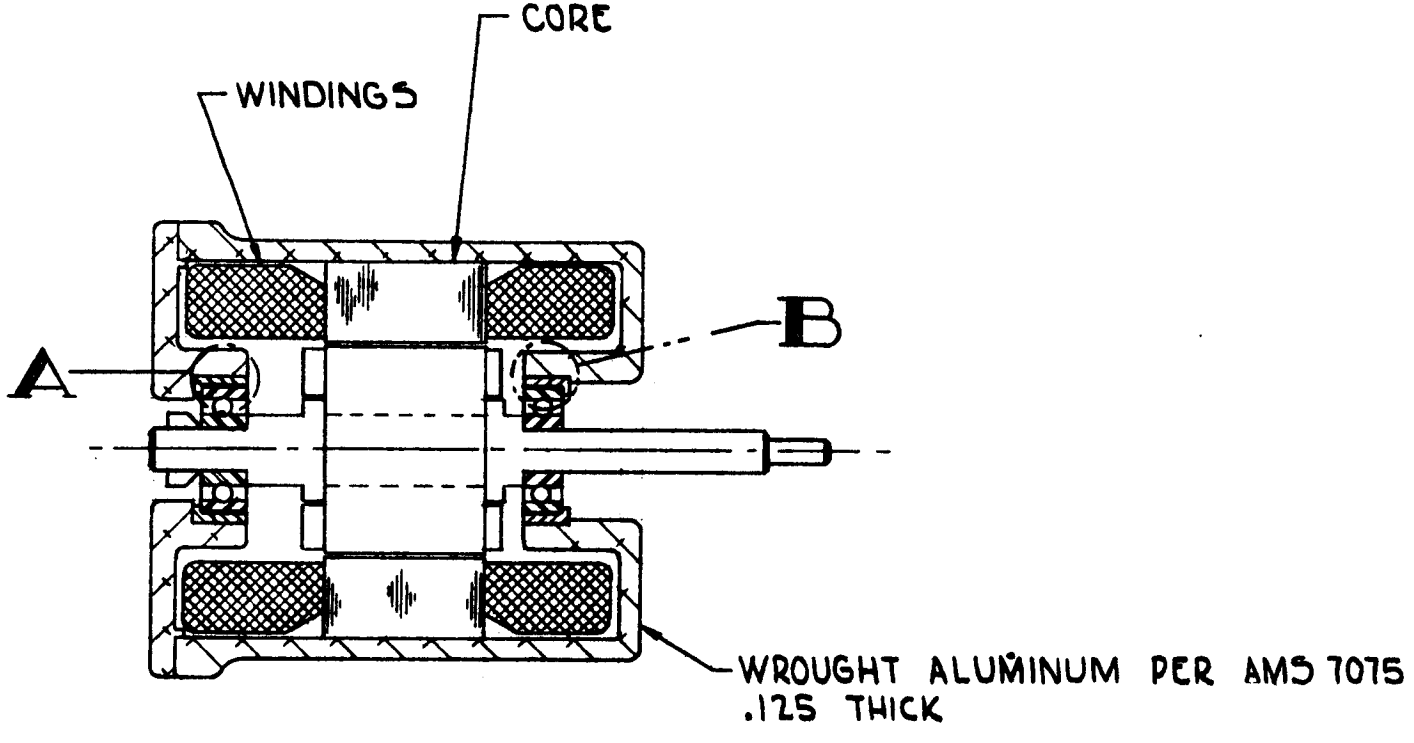

Structural Design IV
(Aluminum, Invar, Star Ring)

FIGURE 6.1-5

Aluminum Housing with 440C Sleeve (Not shown)

A 440 C sleeve is used in place of Invar of Figure 6.1-3. The difference in thermal expansion is taken up as stress in the sleeve. The sleeve is matched in line with the aluminum housing at +350°F. Detailed stress analysis of this configuration disclosed that over-stressing of the aluminum housing and sleeve would occur at -453°F. The analysis also indicated that a workable design could be obtained if an intermediate sleeve with a thermal expansion coefficient somewhere between the 440C sleeve and aluminum was used as a buffer. Inconel was examined as a possible choice and the final design presented below was evolved.

Final Design of Test Unit - Model 214976-100

Model 214976-100-01 shown on Figure 6.1-6 is the example design used for this study. The calculated stresses are noted on the drawing. It incorporates an AMS 7075-T6 aluminum alloy housing. This material has the advantage of light weight, superior strength, and good machinability. The rotor is supported by a central shaft fabricated from Inconel 750X. The central shaft is supported by two angular contact Barden SR4ABSSX112K6 bearings with Bartemp cages. The SR4A size was chosen as a compromise between the lower static contact stress levels of a larger bearing versus the lower centrifugal ball and cage loads of a smaller bearing. The balls and races of this bearing are made from hardened 440 C stainless steel.

An adapter sleeve made from Inconel 750X is used as a buffer between the aluminum housing and a 440 C sleeve surrounding the bearing outer race. The difference in thermal expansion between the aluminum housing and 440 C sleeve is taken up as stress in the Inconel 750X adapter. Clearances have been arranged in such a manner to allow free bearing axial movement under all temperature and pressure conditions to permit compensation for axial differential expansion.

The rotor stack is pressed over raised serrations of the central shaft. The stator stack is shrunk into the housing. During assembly, the housing is heated to +350 and the stator at room temperature inserted. A set screw insures secure stator positioning under all operating conditions.

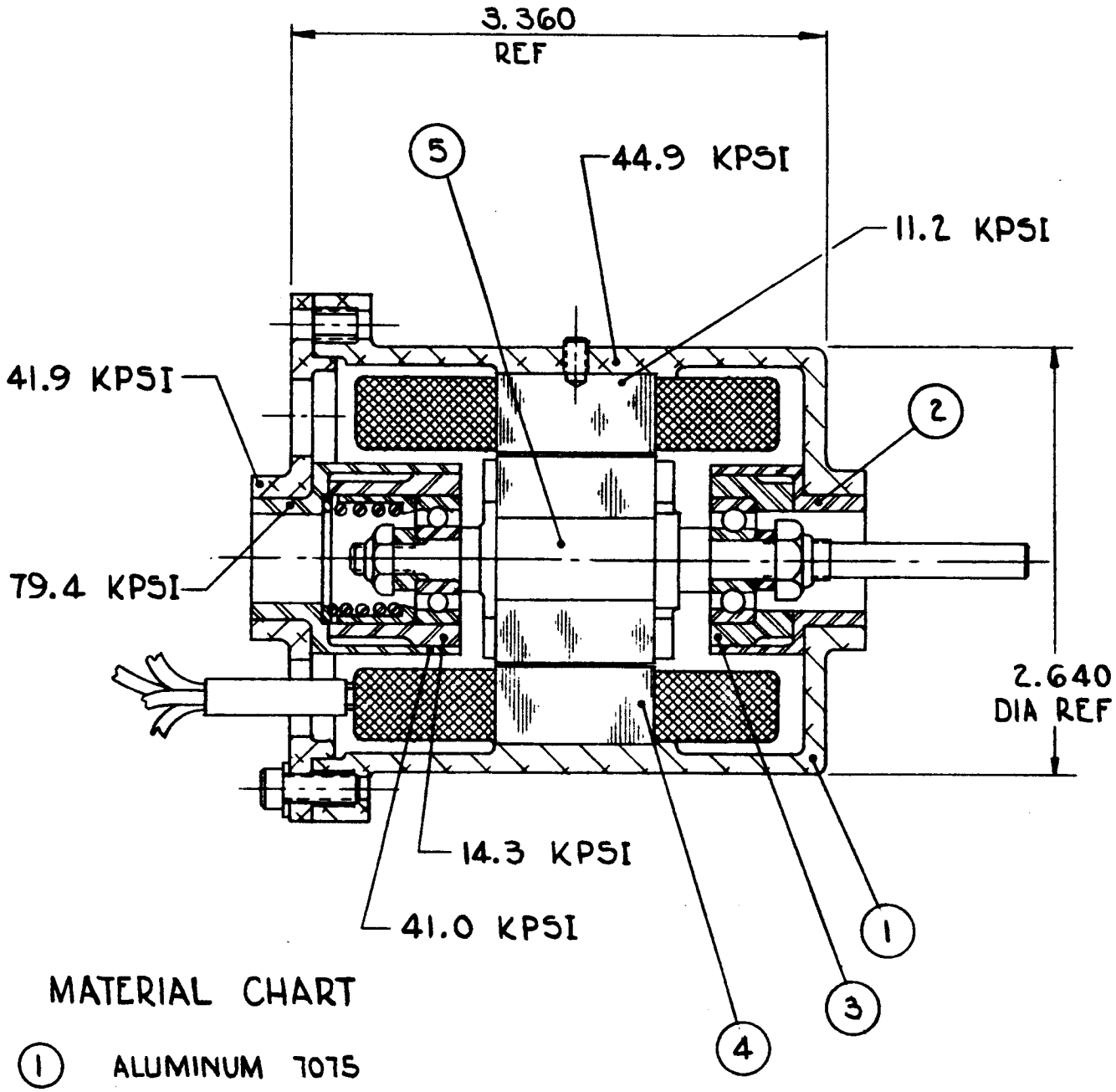

MATERIAL CHART

(1)	ALUMINUM 7075
(2)	INCONEL 750 X
(3)	440C STEEL
(4)	3% SILICON STEEL
(5)	INCONEL 750 X

NOTE :
STRESS SHOWN AT -450°F

Example Design Model 214976-100

FIGURE 6.1-6

The bearing inner races are held to the shaft with stainless steel lock nuts. The bearing outer races are free to slide in their respective sleeves (made from 440C stainless steel of some thermal expansion coefficient). To prevent ball skidding during motor acceleration, a helicoil preload spring is provided. This spring places the bearings under a minimum load of .5 pounds at all times.

An electromagnetic speed pickup is mounted on the housing. This pickup senses the passing of the hex corners of the lock nut mounted on the shaft and converts this motion into electric pulses to be recorded on a Berkley counter.

Because of the wide operating range of this unit, cooling is expected to be somewhat of a problem. Since Model 214976-100 is a test device to determine feasibility of bearing mounting methods, no provisions have been made for internal coolant flow. Instead, the internal temperature was regulated by controlling the motor input voltage. In a final design, cooling could be supplied by a variable pitch fan.

Provisions are made on the cover assembly for motor mounting. Power is transmitted through a .200/.201 inch diameter shaft extension.

6.1.3 Bearings

6.1.3.1 Bearing Manufacturers Reports and Recommendations

Of 18 bearing manufacturers contacted, 11 replies were received. Six mechanical bearing manufacturers were interested in working with Pesco in the helium motor study. Due to the unusual operating parameters and size requirements, the other five (mainly sleeve bearing manufacturers) did not wish to participate. Summary of the replies of these manufacturers is included.

In general, the six mechanical bearing manufacturers selected 440 C stainless steel for the balls and races. The materials suggested for the ball retainer were plastics in all cases, ranging from Rulon A, Duroid 5813, Salox M, Armalon, Vespel, and Bartemp. These materials are varieties of impregnated Teflons.

The replies indicate that the contact area, cage design, and heat transfer is of great importance. A race curvature somewhere between 53 and 60 per cent is desirable to give small ball surface twist. The question of greatest importance appears to be which race curvature is the best and what combinations of curvature should be used for the inner and outer races to provide an optimum design.

The size recommended ranged between a bearing with a .2500 bore and .6250 O.D. and a .3150 bore and .8661 O.D.

Mechanical Bearings

Barden

The current production bearing recommended by Barden is the SR4ABSSX112K6 (Bartemp type). This bearing has 440C balls and races and the Bartemp one-piece cage and is an angular contact type.

Marlin-Rockwell-Company

MRC recommends a type 1900-R bearing. MRC indicates a bearing with an inner race curvature between 56 and 58%, an outer race curvature of 52%, a cage made of Armalon or Salox M, balls and races of 440 C, and wave spring preload is the best. The speed should be kept as low as possible for long life. MRC data sheet T-1408 supplies additional design information.

New Departure

Recommends an angular contact type bearing with straight through ball pocket separator. The bearing size could range from one with a .2500 bore and .6250 O.D. to .3150 bore and .8661 O.D. Materials recommended include rings and balls of 440 C and cages of Duroid 5813 or Rulon "A". The spring load should be 2 to 8 pounds. Internal fit up depends upon shaft and housing fits and the bearing size; normally this would be .0005 to .0008 radial play.

Fafnir Bearing Company

Bearings required to operate with marginal lubricants have short life. A wider race curvature for both inner and outer rings with an internal clearance that will provide a 20 degree contact angle is considered optimum for this application. Fafnir recommends size 38K which weighs .02 pounds with a one-piece Rulon retainer. To insure adequate internal radial clearance, an extra loose radial fit of .0008 to .0011 is recommended. A 303 stainless steel housing with a 440 C sleeve or a 440 C annealed housing is suggested.

Miniature Precision Bearings, Incorporated

MPB recommends a R4 size bearing as a compromise between the lower static contact stress levels of larger bearings versus the lower centrifugal ball loads of a smaller bearing. The ball separator is machined and slotted of Duroid 5813 or Vespel. The bearing is deep groove construction and is capable of thrust loads in either direction. The quality should be ABED 7 or better.

The bearing mounting should provide approximately .0018 total end play at -452°F. The shaft O. D. and housing liner mounting diameters should be machined to .0001 TIR maximum out of roundness, eccentricities, and squareness.

The material recommended as first choice for the rings and balls is 440 C. Haynes Stellite No. 3 or No. 25 alloy may be a possible second material choice.

Industrial Tectonics, Incorporated

ITI reported that they have had specific experience with electric motor bearings operated at cryogenic temperatures. ITI No. 7149 has operated successfully for 500 hours in a 20,000 rpm electric motor in gaseous hydrogen below -100°F. ITI does not have specific experience in helium, nitrogen, or oxygen in this type of application, but believes that hydrogen is the more difficult operating fluid due to its reducing tendency. The ITI No. 7149 is recommended for this application. This bearing has a .3150 inch bore and .8661 inch O. D.

6.1.3.2 Bearing Considerations

To obtain reliable long bearing life over the bearing operating range of -450°F to +350°F, many parameters must be considered. In consulation with Mr. T. Barish (private bearing consultant), Pesco engineers discussed helium motor design requirements in detail. Mr. Barish agreed with the recommendations of the manufacturers queried. The type bearing mutually agreed upon is:

a. Counterbore type (angular contact type)

b. Shallow shoulder inner race

c. One-piece ball separator

d. Ball separator fabricated from glass stabilized Teflon composition.

e. Contact angle should be low indicating a race curvature between 53 and 60 per cent.

In order to minimize surface twist of the balls on the races, the race curvature should be somewhere between 53 and 60%. In this respect, a 57% curvature is felt to be superior to the 52% curvature. One question that must be resolved by testing is: What is the optimum race curvature combination that will result in long life and high reliability?

The cage best suited to this application appears to be a non-metallic type made from an impregnated Teflon. Some of the promising cage materials to select from include:

Trade Name		Teflon Filler
Bartemp	-	glass and MoS_2
Armalon	-	glass
Salox M	-	bronze
Rulon A	-	glass
Duroid 5813	-	glass and MoS_2

Since these materials are relatively weak (tensile strength 1000 to 2000 psi) aluminum reinforcing side rails may be required depending on size and speed. A one-piece ball separator is preferred to the conventional two-piece riveted construction commonly found in lower speed applications. This type of cage offers a more uniform ball pocket for film transfer lubrication.

The diametrical cage clearance is an important factor in obtaining reliable bearing operation. At present, an outer land riding cage with .010 to .015 radial clearance is felt to be the optimum. An inner race to cage clearance of .050 inch or larger with ball pocket clearances of .010 inch also appears to be desirable.

The control of mount squareness should be as close as possible. Good squareness will help in reducing ball speed problems. Misalignments in excess of .0005 TIR squareness or concentricity will result in an elliptical ball paths with subsequent acceleration and deceleration of the balls and excessive ball pocket wear. The tolerances in the final design are held to less than 0.0005 TIR.

To prevent skidding of the balls during rapid motor acceleration, a moderate bearing spring preload is required. For this particular application, the spring preload is slightly larger than the maximum expected dynamic radial load.

The Barden type SR4ABSSX112K6 bearings tested by Pesco generally fit the criteria discussed above and were also recommended by the Barden Corporation as the best choice of off-the-shelf items to fulfill the helium motor requirements. These bearings have 440 C balls and races and a Bartemp one-piece cage.

There are many possible internal design configurations which could be experimentally evaluated before the optimum bearing could be selected for long life and reliability. Various ball contact angles, race curvatures, cage clearances and materials, and cooling methods should be considered and evaluated.

6.1.3.3 Bearing Types

Four types of bearings were considered for application in the helium motor. Roller, plain journal, hydrodynamic (self-pressurizing) gas, and radial ball bearings were analyzed per the NASA operating requirements.

Roller Bearings

Roller bearings offer the highest radial load carrying capacity of the four types of bearings considered. Because of the large surface contact areas, they are used for relatively slow moving applications where radial loads are heavy, where shock loads are present, and long life is desired. The general construction of roller bearings makes them more suitable for heavy duty power generating, transmitting, and absorbing machinery as opposed to the extremely light loads and high speeds developed in the helium motor application.

Journal Bearings

Characteristically, high speed, lightly loaded plain journal bearings are difficult to design and build. These bearings are difficult to lubricate and cool and are subject to self-induced vibrations.

Bearing instability offen results from low stiffness of the journal bearing at low eccentricity and because the shaft center motion is at right angles to the load. These bearings require lubrication and adequate cooling. In the helium motor, a source of liquid lubrication is not available thus dictating bearing journal materials made from such materials as Teflon or impregnated Teflon compounds for lubrication. These plastic materials are limited to low PV values. Although the construction of plain journal bearing for the application may be feasible, bearing cooling becomes quite critical and is difficult to control. Also, plastic bearing materials act as insulators making cooling extremely difficult. Pesco has experimented unsuccessfully in the past with cryogenic journal bearings of various materials, and therefore, believes that development efforts would not be as productive in the area of plain sleeve bearings as efforts directed in the area of anti-friction bearings.

Gas Lubricated Bearings

Gas lubricated bearings have for some time been successfully used in precision instruments. The advantages of a hydrodynamic (self-pressurizing) gas bearing are: 1) Low friction, 2) Indefinite life for continuous operation, 3) Insensitivity to temperature changes, 4) Does not contaminate environment with lubricants, 5) High speed capability, and 6) Insensitivity to radiation. However, these bearings are not without disadvantages. The load carrying capacity is low per unit area, and the bearings are prone to whip and whirling instabilities. Because of the bearing self-pressurizing aspect, scuffing occurs during equipment start-up and shutdown.

The requirements of the helium motor does not appear to fit into the general design aspects of the hydrodynamic gas bearing. The 10,000 on-off cycles would cause severe wear problems degrading the precision finish and fits required, resulting in bearing failure or performance reduction. An other complication arises in the helium ambient pressure ranges between 10 and 3000 psia causing large variances in bearing load supporting capability over the operating envelope. Since the bearing load carrying capacity is quite low per unit area, the helium motor application would require journals of considerable length extending the present envelope and requiring ultra-fine machining to obtain the high precision required along the entire length of the bearing bore. For these reasons, the use of gas bearing, in the helium motor is not considered optimum.

Radial Ball Bearings

Radial contact bearings are well suited to high speed and thrust load applications. Because of the small surface contact area, only a limited amount of energy is lost in the form of heat, thus making cooling requirements less critical than in other bearing systems. Although, ball bearings are basically intended for radial loads, they also accept thrust loads of equal magnitude and accurately position the shaft in respect to the housing components. Although the temperature and pressure envelope has not previously been explored with radial ball bearings in helium, the .07 million DN operating point should be well within the current state-of-the-art. Pesco, as well as many other aero-space component and engine manufacturers, have had excellent success with radial ball bearings in liquid and gaseous hydrogen at DN values many times the DN operating design value of the helium motor.

Since the experience of ball bearings operated in cryogenic applications has been excellent at Pesco, and the helium design requirements closely match the capabilities of radial ball bearings, this type of bearing was selected for closer evaluation as described in the detailed section on bearings.

6.2 Electro-Magnetic Design

The purpose of this section is to describe the electrical and magnetic circuit designs for motors to operate in the specified ambients. The electrical circuit consists of the stator winding and the rotor case, and the magnetic circuit consists of the steel lamination.

The motor type to be discussed is a three-phase, squirrel cage induction motor as required by the contract. It has further been defined as being considered the prime mover for a centrifugal type load. This assumption is required since the starting torque required by the motor load has a direct influence on the rotor cage design and the machine size, refer to discussion of effect of temperature on performance. The scope of the program would have to be greatly expanded to cover all the various types of loads, and would contribute relatively small return since a thorough study of the assumed type of load fully illustrates the problems and their solutions. This assumption also enables the choice of a rated torque as a fixed percentage of the maximum generated torque, or breakdown torque. The value used is that the breakdown torque is 170% of the rated torque. This is a commonly used number for general aero-space applications and allows for "normal" variations in voltage and frequency of approximately 10% on voltage and ±5% on frequency.

The study has been conducted for motors ranging from a stator lamination O.D. of 1.16" to 4.91" with operating speeds of approximately 5,400, 10,000, and 20,000 rpm. A detailed computer print-out and analysis of a sample motor has been included as an example of the various items discussed and for illustration. The complete results of the computer study are too voluminous for for inclusion, particularly since they add little of value per se, their function being to serve as the basis for the output versus volume curves.

The sample motor is the same basic size and speed as that used for the bearing tests and discussed in Progress Report No. 5. The lamination geometry and windings have been changed as the result of the heat dissipation study, the electro-magnetic volume is identical however. It has been chosen for expansion since it closely approximates the specified package weight of two pounds, it is near the middle of the volumes studied, and is the median speed of the units studied.

The geometry of the lamination determines the torque generation capability and the losses of a given volume of copper and iron. The losses in the copper and iron must be limited such that the temperature rise is within the bearing and insulation system limits at the fluid condition which results in minimum heat dissipation. The limit for the subject systems has been established as 350°F, and in the specific case of this study the heat dissipation capability of helium at 70°F and 10 psia establishes the torque available from a given volume rather than strictly electro-magnetic limits. This is actually the usual limiting factor for motors except possibly those that operate in exclusively a cryogenic atmosphere.

The heat dissipation limit therefore means that the electro-magnetic design can not be treated independently, but must be interrelated with the heat dissipation study. Indeed, for maximum output from a given volume, the two analyses, electro-magnetic and heat dissipation, must be maximized simultaneously, not independently.

The mathematical analysis, however, can not be treated as a direct maximization of two simultaneous differential equations since these equations do not exist. The algebraic complexity involved in determining torque and losses from lamination dimensions is excessive, and prohibitive to writing such a differential equation. The problem was therefore approached from the industry standard method of cut and try, based upon experience guided first choices. This approach is ideally suited to the use of a digital computer, which provides optimization akin to that of maximizing differential equations, by virtue of the ability to rapidly compute successively smaller incremental changes in parameters. This digital technique is the arithmetic equivalent to the process of differentiation.

The problem is to vary the lamination dimensions so that the losses are equal to the heat dissipation, with power absorbed by the fan commensurate with the torque generated. With this in mind, a program was written to determine the heat dissipated and the horsepower consumed by the fan. The motor program is described later in this section and the heat dissipation program is described in another section. Both programs were put on a General Electric Digital Computer, Model No. 205 located at the Borg-Warner Corporate Research Center located in Des Plaines, Illinois.

It must be noted here that this idealized approach was modified somewhat as will be described in the ensuing discussions. A term used throughout the remainder of this section should also be defined:

"Active Material" or "Active Volume" - An induction motor consists of two laminations, a stator and a rotor, which are made of electrical sheet steel and contain slots for windings. These laminations are stacked, and windings are inserted in the slots. The cylindrical volume determined by the O.D. and stack length is referred to as the active material or active volume of a motor. It is within this volume that torque is generated, and in this volume only. The stator end turn extension, for example, does not provide torque generation but is simply the portion of the circuit which carries current from one slot to the next proper slot. As such, there is no torque generated in this part of the circuit, but there is a copper loss. It is this active volume, plus the losses in extraneous circuits such as the end turns, which is analyzed. The total motor weight can then be approximated by adding a factor for bearings, housing, shaft, et cetera, based on an empirical envelope density which varies with motor size, and is based upon experience.

6.2.1 Motor Computer Program

The motor computer program, since it is a digital approach, consists of assuming lamination dimensions, and then computing the motor performance. From this performance the maximum torque for the assumed geometry is available as well as the losses at "rated load." (The rated load is determined as a fixed percentage of this maximum torque as described under motor type.) The losses may then be compared to the heat dissipated for an assumed fluid path, and the fan horsepower compared to the rated load to ascertain that it is not excessive. The lamination dimensions may then be reassumed if the balance is not correct, and the fluid path and fan horsepower also altered.

The program input consists of the O.D. and I.D. of the stator and rotor laminations, the number of slots in each, the depth below slot and average tooth width, (dimensions which establish the magnetic circuit cross section), the rotor end ring dimensions, the rotor bar and end ring material resistivities, the number of poles, and factors which describe the type of winding.

The computer then calculates copper (slot) areas, magnetic circuit cross section, and the number of turns required for a pre-determined magnetic density. The computer then stops and prints-out sufficient information that the operator may choose an existing wire size for winding rather than an idealized wire size. This applies to both the stator winding and the rotor cage.

With this additional input the computer then proceeds and calculates the motor performance. The motor performance consists of torque generated, current and power input, power output, losses in various portions of the circuit, efficiency and power factor at various speeds such that the data can be used to plot a complete motor performance curve. The magnetic circuit densities are also printed out as a check although they should be balanced in view of the method of choosing input parameters described later.

An additional input is empirical modifications which are correction factors to equations used to calculate such parameters as leakage reactance, Corrections are also included so that the performance is computed at the cryogenic temperature and the maximum motor temperature deemed feasible for the bearing and insulation systems. This same maximum temperature is of course used in the heat dissipation study.

This approach was modified to the extent that one performance was calculated for each of the study volumes, the heat dissipation study optimized, and the final torque generated was ratioed from the existing calculated torque and loss. This modification is justified within the range of ratios used, since the accuracy is within the scope of the program and consistent with the accuracy of the other calculations involved in this study.

The computer input sheet for the lamination parameters is included as Figure 6.2-1 and has the values used for the sample motor. Figure 6.2-2 is a brief explanation of the symbols used. The computer output sheet for steps 1 and 2 are included as Figure 6.2-3. The output of step 2 is the input to the performance calculation, and a typical performance output is included as Figures 6.2-4 and 6.2-5 for winding temperatures at +350°F and -452°F.

He Motor Study - 3-Phase Motor-Computer Input Sheet
Lamination and Winding Calculations

Stator Lamination

O.D.′	2.312
D′	1.312
ATW′	.197
r_b	.060
r_t	.030
S_p	12
e′	.093
d′	.025
W	1.00
F	.950
p	4
Δ	.0092
f_s	.020
DBS′	.189

Winding

a	1
∝	1
K_p	.892
K_e	1.5
P_{cs}	1.33
P_{cz}	1.25
P_{ce}	0.94
Q	.0905
ACT	2
Y	1.5
K_W	.866
E	115
f	400
T_e	.20

Print-Out - Step 1

G_2	81,998
d_2	.0930
T′	56.14
K_p''	.8957
S.F.′	1.106
R_1	.3915
D_r''	1.1571

Input - Step 2

T	56
S_c	.00646
ρ	.0653
K_p	.896
K_r''	1.02

Rotor Lamination

D″	1.2935
D_i''	.500
d″	.0217
e″	.050
S_s	18
ATW″	.109

Temp. Corrections

K_{1h}	2.81
K_{1c}	.04
K_{bh}	3.73
K_{bc}	.45
K_{rh}	2.81
K_{rc}	.04

Print-Out - Step 2
(Use for Input to Perf. Calc.)

r_{1h}	10.0
r_{1c}	.142
r_{2h}	11.0
r_{2c}	1.3
X	18.6
X_o	89.4
F_{eh}	48.0
F_{ec}	60.0
K_p'''	.895

End Ring

D_{ir}	.715
l_b	1.25
S_r	.0534

Empirical Modifications

M_{Fec}	1.75
M_{Feh}	1.40
M_x	1.05
M_r	1.40
M_o	1.00

"Design" Tooth Density
B'_{ST} 93,000

NOTES
O.D. 2.312 Poles 4
Perf. Calc. Nos:
Hot 445
Cold 446
Project No. 116115A
Date 2/23/66 Sig. JWB

FIGURE 6.2-1

Explanation of Symbols Used on Computer Input Sheet for Lamination and Winding Calculations

FIGURE 6.2-2

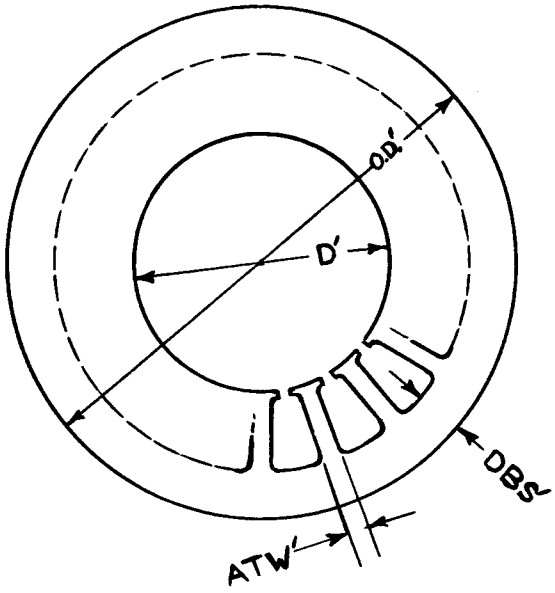

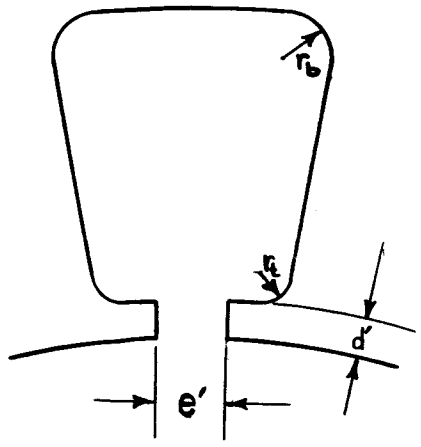

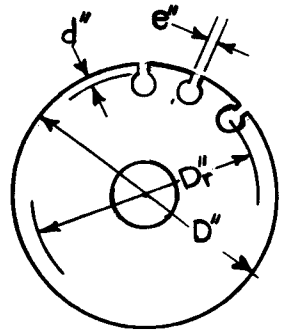

To be specified as input-

- $O.D.'$ - finished O. D.
- D' - I. D. of lamination
- ATW' - average tooth width, stator
- r_b - corner radius, slot bottom, stator
- r_t - corner radius, slot top, stator
- S_p - number of stator slots
- e' - stator slot opening
- d' - stator tooth tip thickness
- W - stator stack length
- F - stacking factor
- P - number of poles
- Δ - air gap
- f'_s - factor for slot constant, dependent upon slot wedge
- DBS' - depth below stator slot
- a - parallel circuits
- K'_p - assumed K_p
- K_e - end ring leakage constant
- P_{cs} - slot leakage pitch factor correction
- P_{cz} - zig-zag leakage pitch factor correction
- P_{ce} - end leakage pitch factor correction
- Q - skew leakage factor
- ACT - average coil throw in slots
- Y - factor for computing LMT (function of p)
- K_w - winding factor
- E - voltage per phase
- f - frequency
- α - coils per slot (= 1.0 or 0.500)
- T_e - end turn straight extension
- e'' - rotor slot opening
- d'' - rotor tooth tip thickness
- D'' - finished, O. D. of rotor
- D''_i - I. D. of rotor
- S_b - number of rotor slots
- ATW'' - rotor tooth width, neck
- D_{ir} - I. D. of end ring
- K''_r - end ring resistance correction
- l_b - length rotor bar
- S_r - end ring cross section in in^2
- K_{sh} - stator resistivity - hot
- K_{sc} - stator resistivity - cold
- K_{bh} - rotor bar resistivity - hot
- K_{bc} - rotor bar resistivity - cold
- K_{rh} - ring resistivity - hot
- K_{rc} - ring resistivity - cold
- M_{Fec} - multiplier for iron losses - cryogenic
- M_x - multiplier for leakage reactance
- M_r - multiplier for rotor resistivity
- M_{Feh} - multiplier for iron losses - hot
- M_b - multiplier for magnetizing reactance
- B'_{st} - assumed stator tooth density

PESCO POLYPHASE MOTOR DESIGN CALCULATIONS

INPUT DATA

2.3120	1.3120	0.1970	0.0600	0.0300
12.0000	0.0930	0.0250	1.0000	0.9500
4.0000	0.0092	0.0200	0.1890	
1.0000	1.0000	0.8920	1.5000	1.3300
1.2500	0.9400	0.0905	2.0000	1.5000
0.8660	115.0000	400.0000	0.2000	
1.2935	0.5000	0.0217	0.0500	18.0000
0.1090				
2.8100	0.0400	3.7300	0.4500	2.8100
0.0400				
0.7150	1.2500	0.0534		
1.7500	1.4000	1.0500	1.4000	1.0000
93000.0000				

G2	81998.	D2	0.0930
T	56.14	KP	0.8957
SF	1.106	R1	0.3915
DR	1.1571		

R1H	10.0
R1C	0.142
R2H	11.0
R2C	1.3
X	18.6
XO	89.4
FEH	48.0
FEC	60.0
KP	0.895

BSC	92858.	BST	93236.	BRC	55744.
BRT	100656.	BG	45839.	PHI	33345.

Computer Print-Out for Lamination and Winding Calculations
(Data for Sample Motor Included)

FIGURE 6.2-3

PESCO AC MOTOR COMPUTER CALCULATIONS

SLIP	TORQUE IN.LB	RPM	HP	I AMPS	EFF	PF	WATTS	VA	PRI LOSS	SEC LOSS	IRON LOSS	F W LOSS
0.30	0.01	11964.	0.001	1.257	0.73	23.90	104.	434.	47.4	0.0	48.0	7.5
0.60	0.06	11928.	0.012	1.259	7.94	25.77	112.	434.	47.6	0.1	48.0	7.4
1.00	0.14	11880.	0.026	1.262	15.89	28.24	123.	436.	47.8	0.3	48.0	7.4
1.30	0.20	11844.	0.037	1.266	20.88	30.05	131.	437.	48.1	0.5	48.0	7.3
1.60	0.25	11808.	0.047	1.270	25.19	31.83	139.	438.	48.4	0.7	48.0	7.3
2.00	0.33	11760.	0.061	1.276	30.10	34.16	150.	440.	48.8	1.1	48.0	7.2
2.30	0.38	11724.	0.071	1.281	33.25	35.86	159.	442.	49.2	1.4	48.0	7.2
2.60	0.43	11688.	0.080	1.287	36.03	37.53	167.	444.	49.7	1.8	48.0	7.1
3.00	0.51	11640.	0.093	1.296	39.24	39.69	177.	447.	50.4	2.4	48.0	7.1
3.30	0.56	11604.	0.103	1.303	41.34	41.26	186.	450.	51.0	2.9	48.0	7.0
3.60	0.61	11568.	0.112	1.311	43.21	42.79	194.	452.	51.6	3.4	48.0	7.0
4.00	0.68	11520.	0.124	1.323	45.39	44.76	204.	456.	52.5	4.2	48.0	6.9
4.30	0.73	11484.	0.133	1.332	46.83	46.19	212.	459.	53.2	4.8	48.0	6.9
4.60	0.78	11448.	0.142	1.341	48.12	47.58	220.	463.	54.0	5.4	48.0	6.8
5.00	0.85	11400.	0.153	1.354	49.63	49.36	231.	467.	55.0	6.4	48.0	6.8
5.30	0.90	11364.	0.162	1.365	50.63	50.65	239.	471.	55.9	7.1	48.0	6.7
5.60	0.95	11328.	0.170	1.376	51.52	51.89	246.	475.	56.8	7.9	48.0	6.7
6.00	1.01	11280.	0.181	1.391	52.58	53.48	257.	480.	58.1	9.0	48.0	6.6
6.30	1.06	11244.	0.189	1.403	53.27	54.63	264.	484.	59.1	9.9	48.0	6.6
6.60	1.11	11208.	0.197	1.415	53.90	55.73	272.	488.	60.1	10.8	48.0	6.5
7.00	1.17	11160.	0.207	1.432	54.62	57.14	282.	494.	61.5	12.1	48.0	6.5
7.30	1.21	11124.	0.214	1.445	55.10	58.15	290.	498.	62.6	13.1	48.0	6.4
7.60	1.26	11088.	0.221	1.458	55.52	59.13	297.	503.	63.8	14.1	48.0	6.4
8.00	1.32	11040.	0.231	1.476	56.01	60.37	307.	509.	65.4	15.5	48.0	6.3
8.30	1.36	11004.	0.238	1.490	56.32	61.26	315.	514.	66.6	16.6	48.0	6.3
8.60	1.41	10968.	0.245	1.504	56.60	62.11	322.	519.	67.9	17.8	48.0	6.3
9.00	1.46	10920.	0.253	1.523	56.91	63.20	332.	526.	69.6	19.3	48.0	6.2
9.30	1.50	10884.	0.260	1.538	57.10	63.98	339.	531.	70.9	20.5	48.0	6.2
9.60	1.55	10848.	0.266	1.553	57.26	64.73	347.	536.	72.3	21.7	48.0	6.1
10.00	1.60	10800.	0.274	1.572	57.43	65.68	356.	543.	74.2	23.4	48.0	6.1
10.30	1.64	10764.	0.280	1.588	57.53	66.36	363.	548.	75.6	24.7	48.0	6.0
10.60	1.68	10728.	0.286	1.603	57.61	67.01	371.	553.	77.1	26.0	48.0	6.0

#1

SLIP	TORQUE IN.LB	RPM	HP	I AMPS	EFF	PF	WATTS	VA	PRI LOSS	SEC LOSS	IRON LOSS	F W LOSS
11.00	1.73	10680.	0.294	1.624	57.67	67.84	380.	560.	79.1	27.8	48.0	5.9
11.30	1.77	10644.	0.299	1.639	57.70	68.43	387.	566.	80.6	29.2	48.0	5.9
11.60	1.81	10608.	0.305	1.655	57.70	68.99	394.	571.	82.2	30.6	48.0	5.9
12.00	1.86	10560.	0.312	1.676	57.68	69.71	403.	578.	84.3	32.5	48.0	5.8
12.30	1.90	10524.	0.317	1.692	57.65	70.23	410.	584.	85.9	34.0	48.0	5.8
12.60	1.93	10488.	0.322	1.708	57.60	70.72	417.	589.	87.5	35.4	48.0	5.7
13.00	1.98	10440.	0.328	1.730	57.52	71.34	426.	597.	89.7	37.4	48.0	5.7
13.30	2.02	10404.	0.333	1.746	57.44	71.79	432.	602.	91.4	39.0	48.0	5.6
13.60	2.05	10368.	0.337	1.762	57.35	72.22	439.	608.	93.1	40.5	48.0	5.6
14.00	2.10	10320.	0.343	1.784	57.21	72.76	448.	615.	95.5	42.6	48.0	5.5
14.30	2.13	10284.	0.348	1.800	57.09	73.15	454.	621.	97.2	44.2	48.0	5.5
14.60	2.16	10248.	0.352	1.817	56.97	73.52	461.	627.	99.0	45.8	48.0	5.5
15.00	2.21	10200.	0.357	1.838	56.79	73.99	469.	634.	101.4	48.0	48.0	5.4
20.00	2.68	9600.	0.408	2.111	53.58	78.04	568.	728.	133.7	77.3	48.0	4.8
30.00	3.30	8400.	0.440	2.612	45.15	80.63	727.	901.	204.7	142.2	48.0	3.7
40.00	3.60	7200.	0.412	3.027	36.59	80.36	839.	1044.	274.9	206.5	48.0	2.7
50.00	3.71	6000.	0.353	3.361	28.71	79.13	918.	1160.	338.9	265.3	48.0	1.9
60.00	3.70	4800.	0.282	3.629	21.63	77.59	972.	1252.	395.1	317.0	48.0	1.2
70.00	3.62	3600.	0.207	3.845	15.31	76.01	1008.	1327.	443.6	361.7	48.0	0.7
80.00	3.51	2400.	0.134	4.022	9.65	74.48	1033.	1388.	485.3	400.1	48.0	0.3
90.00	3.38	1200.	0.064	4.167	4.57	73.05	1050.	1438.	521.0	433.1	48.0	0.1
95.00	3.32	600.	0.032	4.231	2.23	72.37	1056.	1460.	536.9	447.8	48.0	0.0
98.00	3.28	240.	0.012	4.266	0.88	71.98	1059.	1472.	546.0	456.1	48.0	0.0
99.00	3.26	120.	0.006	4.277	0.44	71.85	1060.	1476.	548.9	458.8	48.0	0.0

MODEL NO.
CALC.NO. 445
FEB. 25,1966

E	115.000	PHI	3.000	RPM-SYNC	12000.000
R1-HOT	10.000	R2-HOT	11.000	X	18.600
XO	89.400	KP	0.895	FE LOSS	48.000
F AND W-SYNC		7.5			

FIGURE 6.2-4

Computer Print-Out, Sample Motor Performance, Windings at +350°F

aerospace equipment BORG WARNER

PESCO AC MOTOR COMPUTER CALCULATIONS

SLIP	TORQUE IN.LB	RPM	HP	I AMPS	EFF	PF	WATTS	VA	PRI LOSS	SEC LOSS	IRON LOSS	F W LOSS
0.30	0.45	11964.	0.086	1.335	48.39	28.80	133.	460.	0.8	0.2	60.0	7.5
0.60	0.95	11928.	0.180	1.439	66.05	41.03	204.	496.	0.9	0.9	60.0	7.4
1.00	1.60	11880.	0.302	1.628	76.06	52.69	296.	562.	1.1	2.3	60.0	7.4
1.30	2.07	11844.	0.388	1.795	79.96	58.51	362.	619.	1.4	3.9	60.0	7.3
1.60	2.51	11808.	0.470	1.974	82.44	62.50	426.	681.	1.7	5.8	60.0	7.3
2.00	3.06	11760.	0.571	2.222	84.50	65.80	504.	766.	2.1	8.8	60.0	7.2
2.30	3.44	11724.	0.640	2.409	85.49	67.21	559.	831.	2.5	11.4	60.0	7.2
2.60	3.79	11688.	0.703	2.595	86.17	68.00	609.	895.	2.9	14.2	60.0	7.1
3.00	4.21	11640.	0.778	2.837	86.74	68.33	669.	979.	3.4	18.2	60.0	7.1
3.30	4.49	11604.	0.826	3.011	86.99	68.20	708.	1039.	3.9	21.3	60.0	7.0
3.60	4.73	11568.	0.869	3.179	87.13	67.82	744.	1097.	4.3	24.5	60.0	7.0
4.00	5.01	11520.	0.916	3.391	87.17	67.03	784.	1170.	4.9	28.8	60.0	6.9
4.30	5.19	11484.	0.946	3.542	87.13	66.28	810.	1222.	5.3	32.0	60.0	6.9
4.60	5.34	11448.	0.971	3.685	87.03	65.44	832.	1271.	5.8	35.2	60.0	6.8
5.00	5.51	11400.	0.996	3.863	86.84	64.20	856.	1333.	6.4	39.5	60.0	6.8
5.30	5.60	11364.	1.010	3.988	86.66	63.21	870.	1376.	6.8	42.6	60.0	6.7
5.60	5.68	11328.	1.021	4.106	86.44	62.18	881.	1417.	7.2	45.6	60.0	6.7
6.00	5.75	11280.	1.030	4.253	86.12	60.79	892.	1467.	7.7	49.4	60.0	6.6
6.30	5.79	11244.	1.033	4.355	85.86	59.73	897.	1502.	8.1	52.2	60.0	6.6
6.60	5.81	11208.	1.033	4.451	85.58	58.67	901.	1535.	8.4	54.9	60.0	6.5
7.00	5.82	11160.	1.031	4.569	85.18	57.26	903.	1576.	8.9	58.4	60.0	6.5
7.30	5.82	11124.	1.026	4.652	84.87	56.21	902.	1605.	9.2	60.8	60.0	6.4
7.60	5.80	11088.	1.020	4.729	84.55	55.18	900.	1632.	9.5	63.1	60.0	6.4
8.00	5.77	11040.	1.010	4.825	84.11	53.83	896.	1665.	9.9	66.1	60.0	6.3
8.30	5.74	11004.	1.002	4.892	83.78	52.84	892.	1688.	10.2	68.2	60.0	6.3
8.60	5.70	10968.	0.992	4.955	83.43	51.87	887.	1709.	10.5	70.2	60.0	6.3
9.00	5.64	10920.	0.977	5.033	82.96	50.61	879.	1736.	10.8	72.7	60.0	6.2
9.30	5.59	10884.	0.966	5.087	82.61	49.69	872.	1755.	11.0	74.5	60.0	6.2
9.60	5.54	10848.	0.954	5.138	82.25	48.80	865.	1772.	11.2	76.2	60.0	6.1
10.00	5.47	10800.	0.937	5.201	81.76	47.64	855.	1794.	11.5	78.3	60.0	6.1
10.30	5.41	10764.	0.924	5.245	81.39	46.80	847.	1808.	11.7	79.8	60.0	6.0

SLIP	TORQUE IN.LB	RPM	HP	I AMPS	EFF	PF	WATTS	VA	PRI LOSS	SEC LOSS	IRON LOSS	F W LOSS
10.60	5.35	10728.	0.911	5.286	81.02	45.98	839.	1824.	11.9	81.3	60.0	6.0
11.00	5.27	10680.	0.893	5.338	80.52	44.93	827.	1842.	12.1	83.1	60.0	5.9
11.30	5.21	10644.	0.880	5.374	80.15	44.16	819.	1854.	12.3	84.4	60.0	5.9
11.60	5.15	10608.	0.866	5.408	79.77	43.42	810.	1866.	12.5	85.6	60.0	5.9
12.00	5.06	10560.	0.848	5.451	79.26	42.46	798.	1881.	12.7	87.1	60.0	5.8
12.30	5.00	10524.	0.835	5.481	78.89	41.76	790.	1891.	12.8	88.2	60.0	5.8
12.60	4.94	10488.	0.822	5.509	78.50	41.09	781.	1901.	12.9	89.2	60.0	5.7
13.00	4.86	10440.	0.804	5.544	78.00	40.22	769.	1913.	13.1	90.5	60.0	5.7
13.30	4.79	10404.	0.791	5.569	77.61	39.59	761.	1921.	13.2	91.4	60.0	5.6
13.60	4.73	10368.	0.779	5.593	77.23	38.98	752.	1930.	13.3	92.3	60.0	5.6
14.00	4.65	10320.	0.762	5.622	76.72	38.19	741.	1940.	13.5	93.4	60.0	5.5
14.30	4.59	10284.	0.749	5.643	76.34	37.61	732.	1947.	13.6	94.2	60.0	5.5
14.60	4.53	10248.	0.737	5.663	75.96	37.06	724.	1954.	13.7	95.0	60.0	5.5
15.00	4.46	10200.	0.721	5.688	75.45	36.34	713.	1962.	13.8	95.9	60.0	5.4
20.00	3.62	9600.	0.552	5.896	69.14	29.27	595.	2034.	14.8	104.1	60.0	4.8
30.00	2.57	8400.	0.342	6.059	57.29	21.31	445.	2090.	15.6	110.9	60.0	3.7
40.00	1.97	7200.	0.225	6.117	46.59	17.05	360.	2110.	15.9	113.6	60.0	2.7
50.00	1.59	6000.	0.151	6.144	36.94	14.42	306.	2120.	16.1	114.8	60.0	1.9
60.00	1.33	4800.	0.102	6.158	28.22	12.65	269.	2125.	16.2	115.5	60.0	1.2
70.00	1.15	3600.	0.066	6.167	20.27	11.37	242.	2127.	16.2	116.0	60.0	0.7
80.00	1.01	2400.	0.039	6.172	12.98	10.41	222.	2129.	16.2	116.3	60.0	0.3
90.00	0.91	1200.	0.017	6.175	6.26	9.65	206.	2130.	16.2	116.5	60.0	0.1
95.00	0.86	600.	0.008	6.176	3.07	9.34	199.	2131.	16.3	116.5	60.0	0.0
98.00	0.84	240.	0.003	6.177	1.22	9.16	195.	2131.	16.3	116.6	60.0	0.0
99.00	0.83	120.	0.002	6.177	0.61	9.10	194.	2131.	16.3	116.6	60.0	0.0

MODEL NO.
CALC.NO. 446
FEB. 25,1966

E	115.000	PHI	3.000	RPM-SYNC	12000.000
R1-HOT	0.142	R2-HOT	1.300	X	18.600
XO	89.400	KP	0.895	FE LOSS	60.000
F AND W-SYNC		7.5			

FIGURE 6.2-5

Computer Print-Out, Sample Motor Performance, Windings at -452°F

aerospace equipment
BORG WARNER

6.2.2 Active Volumes to be Studied

The use of the digital computer dictates that specific active volumes be studied, from which curves may be drawn, rather than a generalized equation being written. Indeed a study of the curves will indicate the difficulty of arriving at a generalized equation if curve-fitting techniques are employed. The basic problem is that torque generated is a function of volume, whereas heat transfer is a function of surface area, the former a cubic and the later a squared function of linear dimensions.

The basic frame used was the same as employed for the bearing test vehicle since it conforms closely to the 2-pound package specified by the contract. From this point greater and lesser volumes were chosen to provide a complete study. The linear dimensions of this frame were varied by a factor of $\sqrt[3]{2}$ which results in volumes varying by 2 to 1 when compared to the immediately adjacent volumes. In addition, it was decided to calculate the capability of each volume with 2, 4, and 8 pole windings. This will cover the range of the majority of applications and indeed in the smaller frames the 8 pole winding was dropped since it is impractical to get sufficient slots in the smaller diameters. With the specified frequency of 400 cps this results in approximate operating speeds of 20,000, 10,000, and 5,400 rpm.

The specific active volumes for which computations were made are shown in Table 6.2-6.

6.2.3 Basic Geometry of Laminations

In order to maintain consistency and minimize the number of trial and error calculations necessary, certain dimensions were based upon constant ratios, or figures of merit. The first such number is the ratio of stator I.D. to O.D., which is constant for each number of poles. As was done with all these figures of merit, the choice is based upon wide experience with aero-space motors for applications with similar heat transfer characteristics.

ACTIVE VOLUMES STUDIED AND SOME PERTINENT DIMENSIONS

O.D.′ (O.D. of stator lam.)	1.16	1.45	1.45	1.83	1.83	2.312	2.312	2.312	2.91	2.91	2.91	3.67	3.67	3.67	4.62	4.62	4.62
P (No. of poles)	2	2	4	2	4	2	4	8	2	4	8	2	4	8	2	4	8
W (Width of stack)	.500	.629	.629	.793	.793	1.00	1.00	1.00	1.26	1.26	1.26	1.59	1.59	1.59	2.00	2.00	2.00
V (Active volume - in^3)	.528	1.04	1.04	2.08	2.08	4.19	4.19	4.19	8.38	8.38	8.38	16.8	16.8	16.8	33.5	33.5	33.5
D′ (I.D. of stator lam.)	.520	.655	.826	.825	1.042	1.040	1.312	1.470	1.312	1.640	1.860	1.650	2.070	2.350	2.080	2.610	2.950
Sp (No. of stator slots)	6	9	12	12	12	12	12	24	12	18	24	18	24	36	18	36	36
Ss (No. of rotor slots)	11	14	18	17	18	17	18	29	19	28	29	29	34	47	29	46	47
Δ (Air gap)	.007	.008	.008	.009	.009	.010	.009	.009	.010	.010	.010	.011	.011	.011	.012	.012	.012
D′/O.D.′	.448	.451	.571	.452	.569	.450	.568	.636	.451	.563	.639	.450	.564	.640	.450	.565	.639

FIGURE 6.2-6

The second figure of merit is referred to on the computer sheet as R_1 and is the ratio of copper cross section to iron cross section in the stator lamination. This ratio is descriptive of the copper losses encountered for a given flux, or a given torque generation capability, and is again constant throughout the chosen volumes, but different for each choice of poles. This ratio varies with poles since horsepower is the product of torque and speed, and the losses are a function of power. The losses then vary with the speed whereas the electro-magnetic torque generation capability is more nearly independent of speed and a function of volume only. The value of R_1 varies from .3 to .9 over the range of poles studied.

The stator and rotor iron paths can be apportioned for each number of poles so that the flux density in each portion of the magnetic circuit is of the proper proportion. This is done by choosing DBS', DBS", ATW', and ATW" in the proper relationship, which again varies with the number of poles. With this proportionality in mind, it is then possible to choose one flux density and have the others of correct value. This value of flux density in turn results in a given flux, since the area has been also chosen, and it is this assumption which determines the torque generation capability of the assumed geometry. The value used is the stator tooth density which is assigned a value of 93,000 lines per square inch.

The value assigned to the flux density is typical of motors in general, both for aero-space applications and commercial uses. The magnetic portion of the active volume cannot be worked at higher densities with increased heat dissipation as can be done with the copper portions. This is due to the fact that the iron saturates magnetically and a small increase in density results in a prohibitively large increase in magnetizing current. The magnetizing current is out of phase with the torque producing current and results in a lower power factor and increased copper losses.

To summarize, the magnetic circuit is proportioned based upon the number of poles, and a dimension is assigned to the stator tooth width. This establishes the copper to iron ratio and hence, the losses. A magnetic flux density is assigned to the stator tooth which establishes the torque generation capability.

6.2.4 Windings

The term windings is used in this case to refer to both the stator coils and the rotor cage.

The stator winding is, of course, basically the three-phase, short pitch, distributed type encountered in most induction motors of this nature. Copper magnet wire is used.

The rotor cage is of the standard squirrel-cage type, however great care must be exercised in the choice of copper or copper alloy used for the rotor bars, as is discussed in the next paragraph.

6.2.5 Effect of Temperature on Performance

As noted in the discussion on magnetic materials the change in permeability encountered in a temperature range from +350°F to the cryogenic temperatures is an increase of only 3% which has no significant effect of performance or choice of densities. The iron loss increase at the cryogenic temperature is on the order of 25% which has a small effect on performance, however, this change is incorporated into the computer program. The magnetic property changes over the temperature range of this study therefore have only a small effect on performance.

The above statement is not true with regard to the conductivity of the electrical portion of the circuit.

The well known phenomena of extremely low resistance at cryogenic temperatures for most pure metal conductors, such as copper, is advantageous for the stator winding, but not for the rotor cage. The low stator resistance results in low copper losses and an increase in maximum torque generated. This same low resistance in the rotor circuit, however, would result in negligible starting torque. Copper alloys will easily provide the solution to this problem since they obey Mathiesson's rule which states that the difference in resistivity of a copper alloy compared to copper is essentially a constant as temperature varies. The solution however, introduces its own problem at the higher operating temperatures.

At the higher temperature, the greater resistance of the alloy will cause excessive slip and excessive losses. The design problem is then one of compromising to obtain the necessary starting torque at cryogenic temperatures while maintaining the best possible efficiency at the higher operating temperature. The obvious solution, that of a material of constant resistivity over the entire temperature range, is not presently available to the designer. The only relatively constant resistivity materials which could be found have resistivities of 20°C in the range of 35 to 45 micro-ohm-cm compared to that of copper which is 1.72 micro-ohm-cm. The use of the high resistance material would require rotor bars so large in diameter that the machine size would suffer drastically. If undersize high resistance bars are used, the maximum torque occurs at negative speeds (refer to equation 2 below) which is obviously not useable as motor power. The active volume is then very large to get the required load torque at a useable speed, and the motor efficiency is very low.

The effect of temperature on maximum torque and the speed at which this torque occurs are evident ay examining the following two equations.

The maximum torque developed by a polyphase machine is independent of rotor resistance but dependent upon stator resistance and can be expressed approximately as:

$$T_m = \frac{K}{N_s} \times \frac{(VK_p)^2 \times m}{2\left(\sqrt{r_1^2 + X^2} + K_p^2 r_1\right)}$$

where
- K — constant depending upon torque units, = 84.5 for torque in lb-in.
- N_s — synchronous speed
- V — line to neutral voltage
- m — number of phases
- r_1 — stator resistance per phase
- X — leakage reactance per phase
- K — ratio of magnetizing reactance to no load reactance

However, the speed at which the breakdown torque occurs is a function of rotor resistance and can be expresses as:

$$N_m = N_s - N_s \left[\left(\sqrt{\frac{r_2}{r_1^2 + X^2}} \right) \left(\sqrt{1 + \left(\frac{r_1}{X_o} \right)} \right) \right]$$

*(NOTE: The source of both equations is "Theory and Design of Small Induction Motors," Mc-Graw-Hill Book Company, Inc., Cyril G. Veinott)

To more completely illustrate and define these effects, the complete performance of the sample motor was computed at both the liquid helium operating temperature and the maximum operating temperature. The print-out data for this winding is shown on Figures 6.2-4 and 6.2-5. The pertinent results of these computations are summarized in curve form on Figures 6.2-7 through 6.2-10 and discussed in the next paragraphs.

Figure 6.2-7 is the speed-torque curve. The effect of temperature on the rotor resistance is immediately apparent in the change in slip $\frac{N_s - N_o}{N_s}$ at any torque between no-load and breakdown torque, and in the change of starting torque. These changes are minimized as much as possible by the choice of alloy. The actual resistivity used is based upon extrapolation from two known alloys to predict the resistivity of the necessary alloy. In the event that this particular performance is required, it may be possible to procure this predicted alloy, but if not then a further penalty would be required in the motor size and performance.

Figure 6.2-8 is a plot of power input and current versus torque load on the motor shaft. The most significant feature here is that the power input, for any given torque, is greater at the higher temperature while the output (Figure 6.2-7) is lower at any given torque. This is due, of course, to the greater I^2R losses at the higher resistances of the higher temperature. The iron losses however actually are slightly greater at the cryogenic temperature as noted previously. This increase in iron loss, however, does not approach the magnitude of the increased copper losses. This same effect is illustrated also in Figure 6.2-9 which is efficiency versus torque.

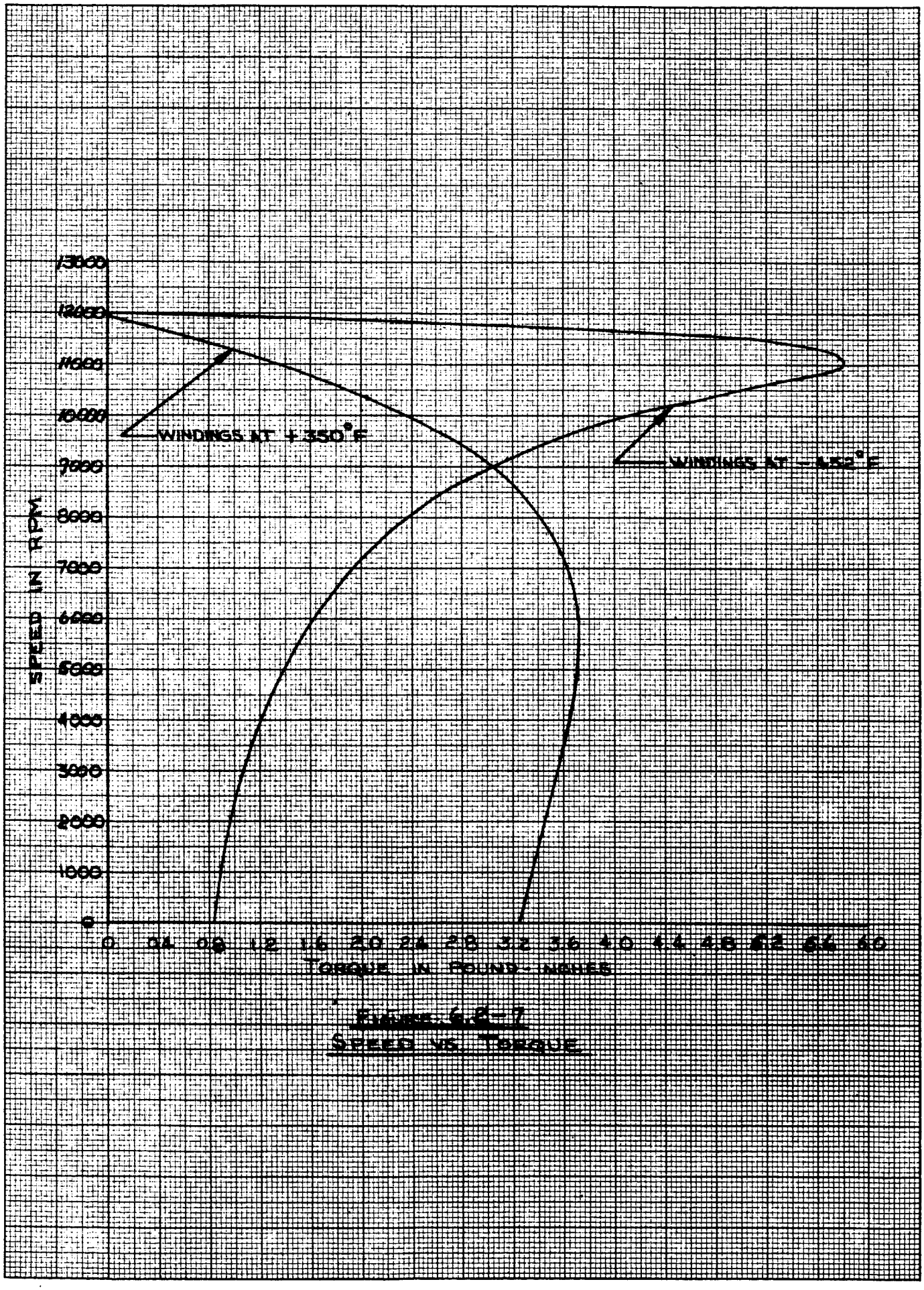

FIGURE 6.6-7
SPEED VS. TORQUE

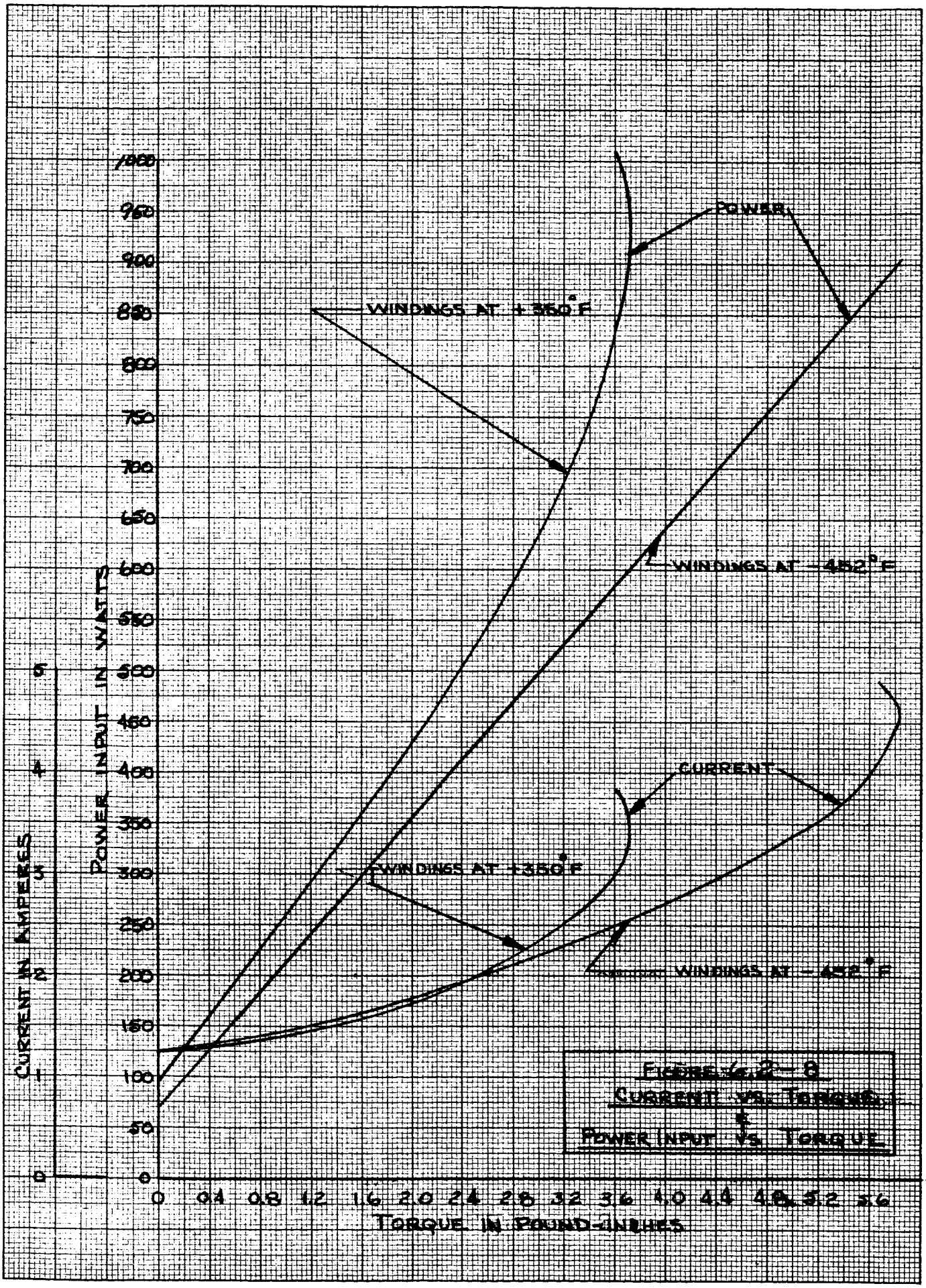

FIGURE 6.2-8
CURRENT VS. TORQUE
&
POWER INPUT VS. TORQUE

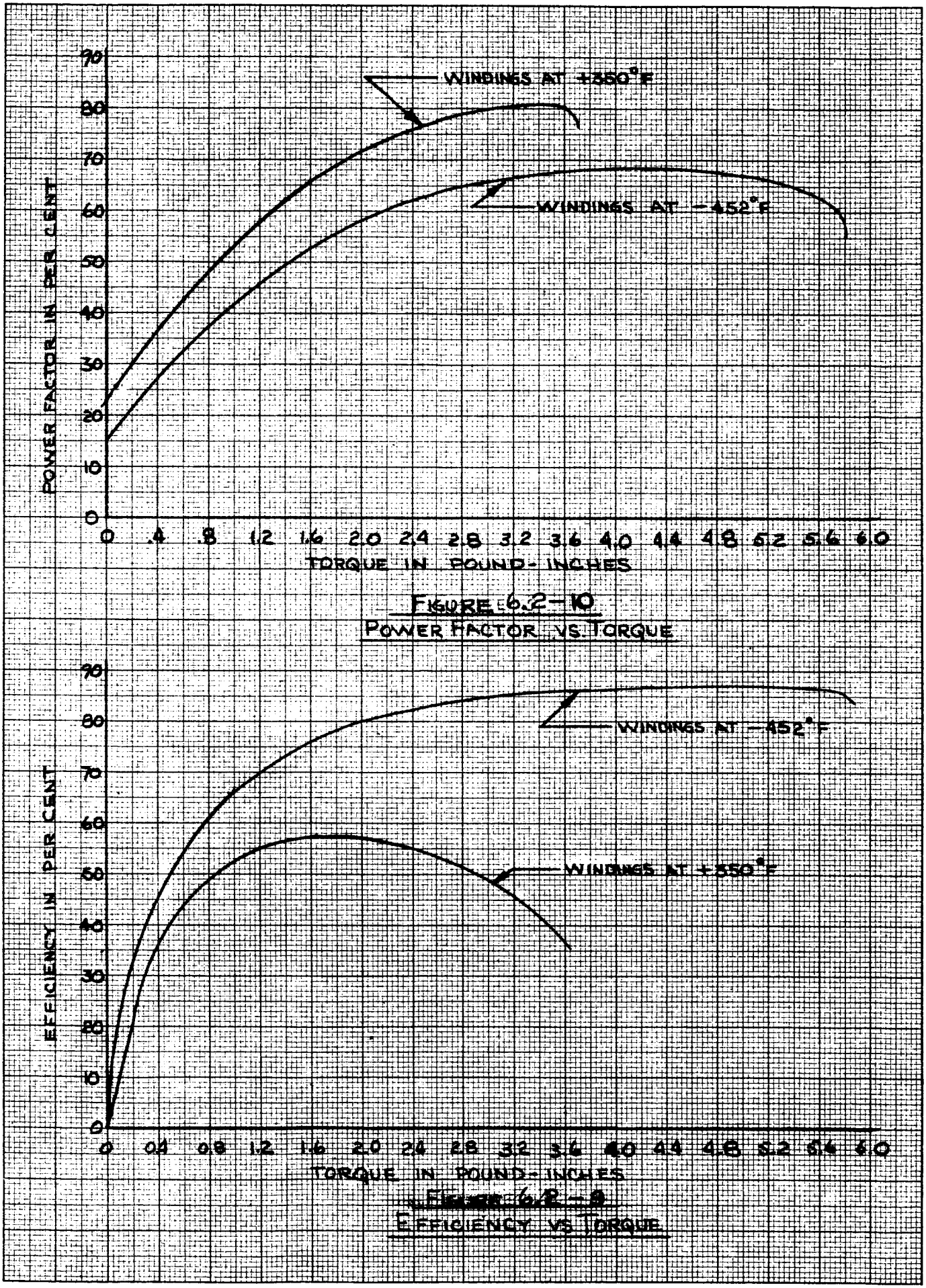

FIGURE 6.2-10
POWER FACTOR VS. TORQUE

FIGURE 6.2-9
EFFICIENCY VS TORQUE

KLUFFEL & ESSER CO.
18 X 25 CM.

Figure 6.2-10 is a plot of power factor versus torque, since the permeability of the silicon steel at the LHe temperature is only approximately 3% greater than at room temperature, the magnetizing reactance is essentially constant. The increased rotor resistance at high temperature, therefore, accounts for an improved machine power factor.

6.2.6 Insulation

The prime criteria for choosing insulation materials to operate in the specified ambient is not insulating properties but mechanical properties. Most insulators are as effective electrically, or slightly more so, at cryogenic temperatures as they are at elevated temperatures. The major problem encountered in cryogenic insulation systems is the mechanical problem associated with lack of flexibility, and, in the case of many plastic materials, their extreme brittleness.

The maximum operating temperature of 350°F used for design purposes in this study was based primarily upon thermal contraction problems associated with the bearings. For this temperature and the required life of 1000 hours, there are many insulations available and therefore the choice of materials is based almost solely on cryogenic performance. Many insulations, including formvar and common cotton sleeving have actually been operated successfully at cryogenic conditions, but aero-space applications require the utmost in reliability and the ability to withstand shock and vibration. These requirements rule out the use of materials which are brittle, although they might survive a simple, quiescent life test.

One further, general point is that the insulation characteristics required of 115/208 volt power motors are relatively unsophisticated. The emphasis on volume resistivity and dielectric constant required in instrumentation, high frequency, and high voltage systems is not evidenced in power motor applications. The major concern is the breakdown voltage, the absence of voids, the handleability, and ability to withstand the mechanical stresses. The breakdown voltage, of course, must be fairly high since power systems are subjected to transient surges, but sufficient thicknesses may be used to accommodate any reasonable value of volts/mill.

Two sources were employed in determining the materials to be used, a literature search defined earlier in the report and previous successful experience. The result is an insulation system of the following materials:

Slot Cells: Glass cloth impregnated with DuPont ML

Slot Separators: Glass cloth impregnated with DuPont ML

End Turn Insulation: Glass cloth impregnated with DuPont ML

Slot Wedge: Glass cloth laminate impregnated with Teflon

Magnet Wire Insulation: Glass serving impregnated with DuPont ML over ML film.

Lead Wire Insulation: Teflon or Teflon impregnated glass braid over Teflon

Varnish: DuPont Pyre ML

The success of Teflon at cryogenic temperatures is well known, and according to the work of K. N. Mathes of the General Electric Company, ML has equal or better flexibility than Teflon. ML is the copyrighted name for a polyimide manufactured by the E. I. DuPont de Neymours Company. This insulation system has been used in cryogenic units with great success.

It should be noted that the stator winding magnet wire is insulated by a film of ML over which is a glass serving impregnated with ML. This reduces the amount of copper in a given slot space to 67% to 89%, depending upon the wire size, of that possible with a film insulation only. There is a resultant decrease in the output from a given volume by virtue of the greater copper losses. However, the physical spacing provided by the glass provides much greater reliability in the event of film cracking due to thermal contraction stresses, vibration, et cetera. Some testing of ML film alone, and statistical reliability analyses may indicate in the future that the glass is not necessary, in which case a slightly greater output would be available from the volumes in this study. The extremely

thin build-up obtained with Pyre ML varnish (.0002" to .0005" per dip) and the minimization of corner builds tend to further substantiate this possibility. It should be borne in mind that the major mechanical problems are associated with the difference in thermal contraction rates of the insulation and metal parts of the system, and mechanical damage of handling prior to the temperature reduction.

In the September, 1963 issue of Electro-Technology an article by K. N. Mathes, Insulation Systems Engineer, Advanced Technology Laboratories, General Electric Company, entitled "Electrical Insulation at Cryogenic Temperatures" contained the following tabulated information.

Magnet Wire Flexibility in Liquid Helium
(Repeated Mandrel test on 0.0253", No. 22, insulated copper magnet wire)

FIGURE 6.2-11

Insulation	Insulation thickness in.	Mandrel diameter, in.	
		Failure	No Failure
Aromatic Polyimide (DuPont ML)	0.0014	1/8	1.8
Solution-coated TFE (DuPont Teflon)	0.0015	1/2	3/4
Terephthalic Polyester (G. E. Alkanex)	0.0014	3/4	1
Polyvinylformal (G. E. Formex)	0.0014	1	1-1/4
Suspension-coated polyimide (Nylon)	0.0007	1	1-1/4
Extruded TFE-fluorocarbon (Teflon)	0.014	1	1-1/4
Extruded plasticized polyvinylchloride	0.007	1-3/4	-

Average Electrical Breakdown Voltage for Insulated Wire
(Tests conducted on standard twisted-pair wire samples)

FIGURE 6.2-12

Wire Insulation	Values in volts for stated environment				
		Liquid			
	Air (23C, 296K)	Nitrogen (-196C, 97K)	Hydrogen (-253C, 20K)	Helium (-268.8C, 4.2K)	Vacuum (-268.8C, 4.2K)
Heavy polyvinylformal (G. E. Formex)	5,500	8,900	8,200	6,970	7,830
Heavy Polyester (Alkanex)	9,230	9,770	9,430	8,230	8,270
Heavy ML (Polyimide)	10,250	9.070	8,970	7,830	7,530
Suspension-coated TFE (Teflon)	6,070	7,700	8,230	6,300	7,400
Inorganic-bonded felted asbestos	1,000	3,770	3,270	2,000	3,470
Glass fiber with ML coating	2,100	11,250	-	1,320	7,970

USAF ZERO DEFECTS

aerospace equipment BORG WARNER®

In addition to the cryogenic phenomena observed and noted above, some further items deserve brief comment. Insulation, like many other materials, has a much greater resistance to compressive forces at cryogenic temperatures than at room temperature, the result is a much greater cut-through resistance at cryogenic temperature.

Mechanical properties are emphasized since electrical failures are often initiated by mechanical failures, and in any event the ultimate result is the same. While a thin film is relatively flexible at cryogenic temperatures because of the resultant low strain, when impregnated or bonded they assume the properties of a thicker material which may lead to deceptive conclusions. Electrical losses in most insulation materials at cryogenic temperatures are substantially lower than at room temperature, both for ionic conduction losses and dipole rotation (dielectric hysteresis) losses.

6.2.7 Conductor Materials

The effect of varying resistivity with temperature has been discussed in paragraph 6.2.5. Copper and copper alloys are generally stronger at cryogenic temperature than at room ambient and they maintain ductility. These factors combined with the structural integrity gained by heli-arc welding the bars to the rings, (fusing of the base metals) result in a minimum of mechanical problems in the cage structure. Therefore, this section has the single purpose of presenting some typical resistivity variations with temperature, and a tabulation to confirm the statement regarding strength.

The bulk of this purpose is accomplished through Figure 6.2-13, which is a plot of resistivity versus temperature for copper and a few copper alloys. Figure 6.2-14 is a plot of similar parameters but includes data on some of the constant resistivity alloys in addition to copper and a copper alloy to illustrate the magnitude of the bar size increase required to use a constant resistivity material, as discussed in paragraph 6.2.5 .

The Table in Figure 6.2-15 shown below is a tabulation of mechanical properties. This table is taken from an article in Engineering Design News entitled, "Properties of Copper Alloys at Cryogenic Temperatures" by C. L. Bulow, Chief Materials Engineer, Bridgeport Brass Company.

K&E 10 X 10 TO ½ INCH 46 1322
7 X 10 INCHES MADE IN U.S.A.
KEUFFEL & ESSER CO.

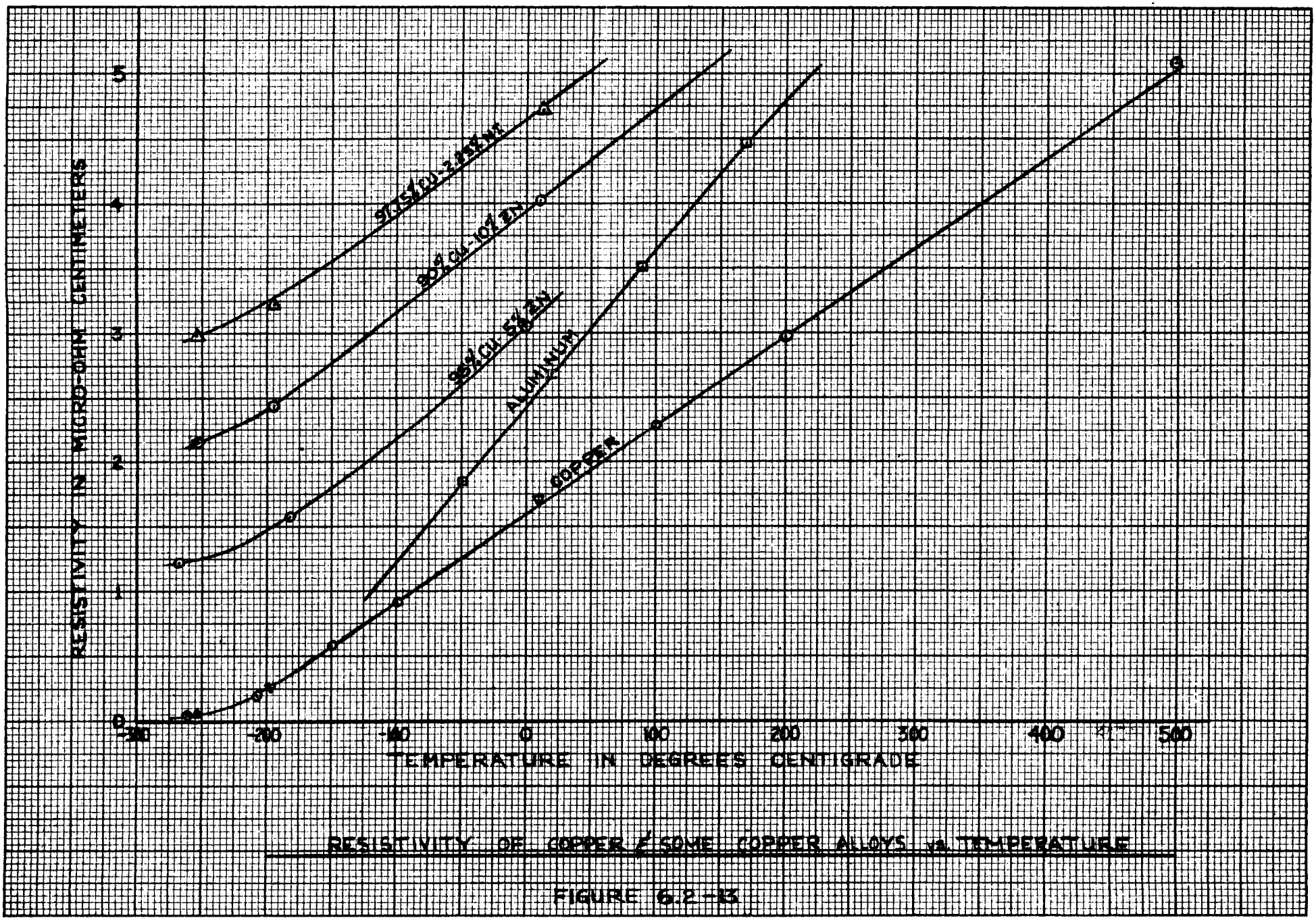

RESISTIVITY OF COPPER & SOME COPPER ALLOYS vs. TEMPERATURE

FIGURE 6.2-13

K+E 10 X 10 TO ½ INCH 46 1322
7 X 10 INCHES MADE IN U.S.A.
KEUFFEL & ESSER CO.

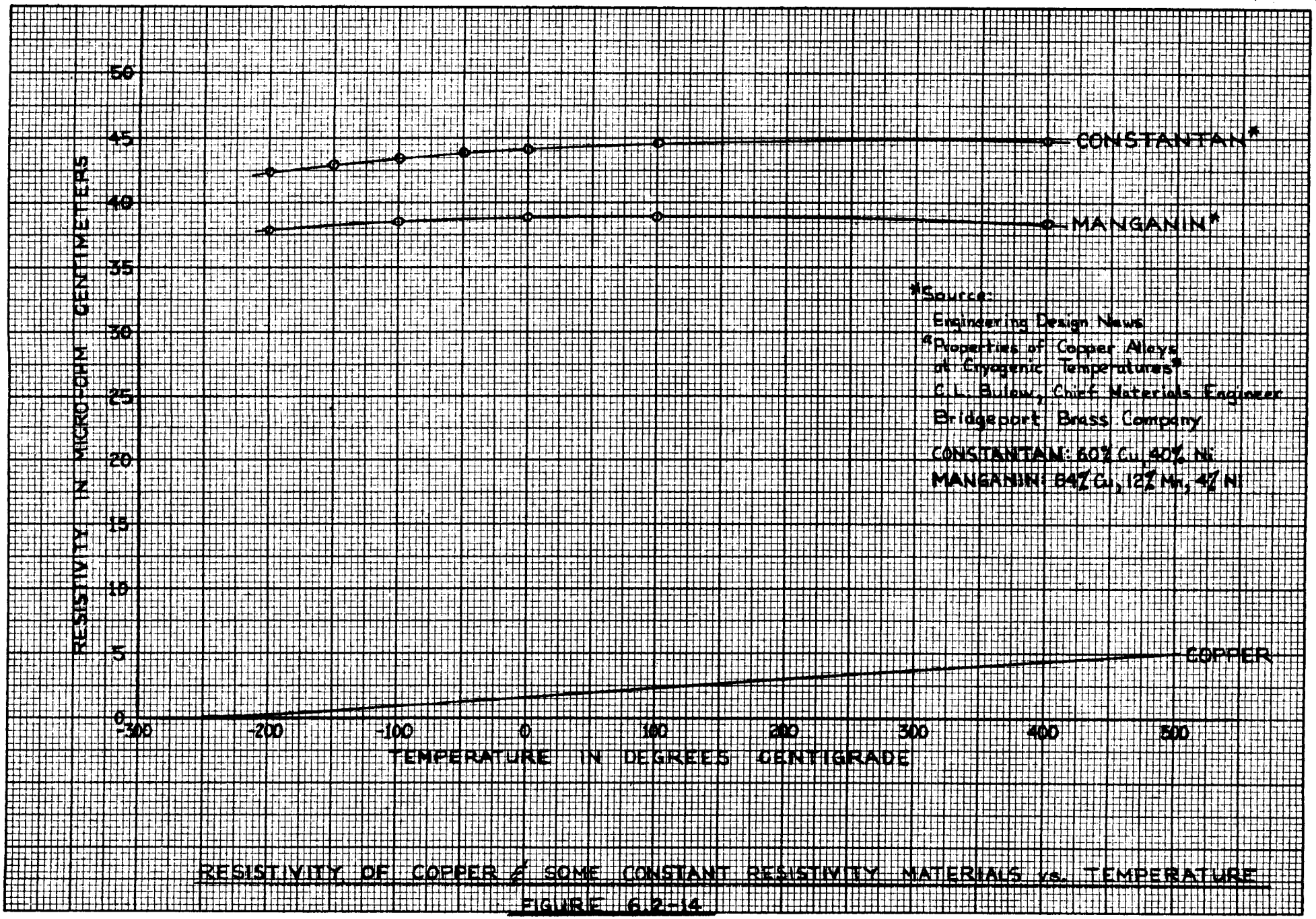

RESISTIVITY OF COPPER & SOME CONSTANT RESISTIVITY MATERIALS vs. TEMPERATURE

FIGURE 6.2-14

MECHANICAL PROPERTIES OF COPPER ALLOYS

Alloy	Composition Percent	Condition	Temperature	Tensile Strength (1000 psi)	Yield Strength (1000 psi)	Elonga tion Percent in 2 inches)	Impact Strength (ft-lbs)[a]	Modulus of Elasticity (psi x 10^6)
Aluminum Bronze	Al 7.31, Zn 1.02 Mn 0.44 Cu 91.1	Annealed rod	Room	77.3	26.7	26	24	
			-80C	82.7	27.1	31	24	
			-180C	96.1	29.2	29	20	
Beryllium Copper	Be2.56, Fe 0.034 Cu balance	Rod water quenched from 800C	Room	76.2	24.9	36	41	17
			-80C	86.7	29.1	38	40	21.6
			-180C	112.0	50.0	41	40	21.7
Beryllium Copper	Be2.56, Fe 0.034 Cu balance	Water quenched from 800C aged 2 hr.@ 300C	Room	187.0	125.0	2.6	2	21.4
			-80C	202.0	147.0	0.4	3	22.7
			-180C	214.0	155.0	3.0	3	20.6
70-30 Brass	Cu 70.0, Zn 30.0	Annealed rod	Room	51.0	28.2	49	66	16
			-80C	57.1	27.3	60	69	
			-180C	73.5	29.6	75	78	
67-33 Brass	Cu 67, Zn 33	Annealed rod	Room	56.9		50	14.4[b]	15
			-78C	61.2		50	16.9[b]	
			-183C	76.4		51	14.4[b]	
67-33 Brass	Cu 67, Zn 33	Cold-worked rod	Room	85.3		6	8.1[b]	15
			-78C	92.4		8	9.2[b]	
			-183C	03.0		10	9.4[b]	
Naval Brass	Cu 61, Zn 38 Sn 1	Rolled rod	Room	57.2		47		
			-183C	81.1		48		
Copper	Cu 99.985	Annealed rod	Room	31.4	8.6	48	43	
			-80C	35.5	10.1	47	44	
			-180C	50.8	11.5	58	50	
Copper electro-lytic		Cold-worked rod	Room	58.6	53.5	8.4		
			-78C	60.4	58.0	12.0		
			-183C	64.7	59.8	11.0		
Copper (OFHC)		Annealed square wire	Room	37		37		17
			-78C	44		40		
			-196C	57		42		
			-253C	72		45		
Copper (OFHC)		Harddrawn rod	Room	52.5	49	20		18.5
			-78C	57.2	55	20		19.7
			-196C	69	60	35		20.5
			-253C	76	62	55		21.2

a) Izod values, unless otherwise specified

b) Notched impact value, m - Kg/sq-cm

Figure 6.2-15

The effect of alloying copper has been expressed by Mathieson's Rule which states that the increase in resistivity due to a small concentration of another metal in solid solution is, in general, independent of temperature. (From Encyclopedia of Physics, edited by S. Flagge, Vol. XIV, Low Temperature Physics I, page 145.) This rule, although not inviolate as is normal, can be extremely useful in providing guide lines and leads for searches for materials of desired resistivity.

6.2.8 Magnetic Material

The magnetic properties of interest to a motor designer are permeability, total iron loss as a stacked structure, and inter-laminar resistance as it affects total iron loss.

It has been Pesco design practice for several years, based on data from complete motors, to increase the total machine iron loss by 25% at cryogenic temperatures (-297°F and below) as compared to the room temperature loss. The two references cited in the bibliography present data which tend to confirm this, however, the frequencies and magnetic densities cited are below the range employed in the study motors.

The permeability increases only 2 to 3% from room temperature to LH_2 temperature, a change which is insignificant, particularly since the variation in maximum permeability at room temperature from one heat to the next is greater than this. Refer to Figure 6.2-16 for a plot of the ratio of the saturation density at ambient temperature to the saturation density at absolute zero as a function of the ratio of ambient temperature to the Curie temperature.

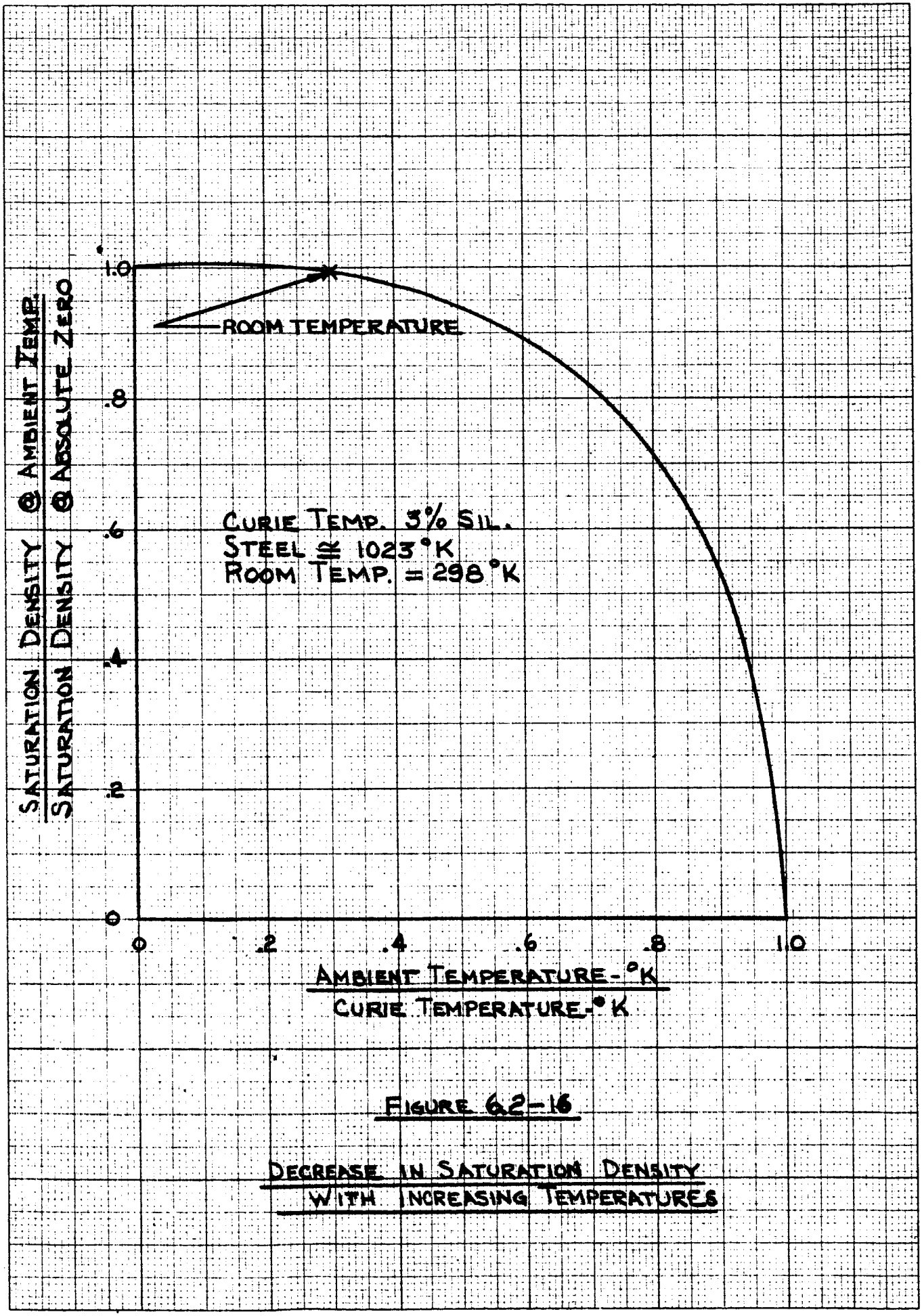

FIGURE 6.2-16

DECREASE IN SATURATION DENSITY WITH INCREASING TEMPERATURES

EUGENE DIETZGEN CO. MADE IN U. S. A.
NO. 340R-20 DIETZGEN GRAPH PAPER 20 X 20 PER INCH

6.2.9 Results of Electro-Magnetic Design Study

The purpose of this section is to summarize and present in curve form the results of the computer study of the active volumes tabulated in Figure 6.2-6.

The basic motor designs are for driving a load with the characteristics of centrifugal devices. This establishes two basic performance factors necessary to determine the lamination geometry and the windings, particularly the rotor cage materials. These performance criteria are:

1) The maximum or pull-out torque should be 1.7 times the rated torque to allow for "normal" variations in voltage and frequency.

2) The starting torque required by a centrifugal device is low.

The essential characteristic of centrifugal devices which leads to the above conclusions is that the torque required to drive the device is essentially proportional to the square of the operating speed.

The motor performance computations were then employed to determine the maximum torque generation capability of the active volume, the motor efficiency at a torque of 59% (1/1.7) of this value, and the starting torque at cryogenic temperatures.

The heat transfer computations must then be interrelated with the performance computations to ascertain that the heat transferred to the cooling fluid is equal to the motor losses, and that the power required to dirve the fan is a reasonable proportion of the generated power. It is obvious that this interrelation is a cut and try procedure and the results herein included are the culmination of this procedure, aided by extrapolation in some instances as the successive iterations closely approached the balanced condition. It should be noted that this is not an optimization study as such, but the basic concept was to determine the power available from an active volume operating in the specified ambient with reasonable efficiency with an emphasis on light weight.

A "reasonable fan horsepower" was defined as the horsepower required to drive the fan at the high density fluid condition (3000 psi) being equal to 10% of the rated horsepower at the worst cooling condition (10 psi). This actually results in a fan horsepower of slightly less than 10% of the 3000 psi condition horsepower since, by calculation, the temperature rise of the motor at this fluid condition is less than 30°F. The torque generation capability when the motor is at 100°F is greater than that when the motor is at 350°F by virtue of the lower copper resistance and is expressed by the equation in paragraph 6.2.5. The fan horsepower at the density of helium at 70°F and 10 psi is almost negligible, and since the fan is temperature compensated, the horsepower at cryogenic conditions is essentially disc friction, which although not negligible is no problem because of the increased motor output. The computations also included calculation of the specific speed of the fan and this value was kept within the range of values which indicate the feasibility of designing a fan to meet the required flow and pressure rise.

The final determination of the power available from a given volume was arrived at in the following manner after preliminary computations "homed-in" on the proper balance between motor losses, heat dissipation, torque generation, and fan horsepower.

The watts output of an electric motor can be expressed as:

$$W_o = \eta W_I$$

or $$W_o = W_I - W_L$$

where

W_o - power available at shaft in watts
η - efficiency as a decimal fraction
W_I - power input to motor in watts
W_L - motor losses in watts

these can be combined to result in:

$$W_o = \left(\frac{\eta}{1-\eta}\right) W_L$$

and since 1 horsepower = 746 watts, the power output from the motor (HP_o) operating in helium at 10 psia and 70°F can be expressed in horsepower as:

$$HP_o = \left(\frac{\eta}{1-\eta}\right)\left(\frac{W_L}{746}\right)$$

In order to maintain the assumed temperature rise, the motor losses (W_L) must be equal to the heat rransferred to the fluid (W_D, referred to as watts dissipated).

$$\text{i.e., } W_L = W_D$$

$$\text{(A)} \quad \therefore HP_o = \left(\frac{\eta}{1-\eta}\right)\left(\frac{W_D}{746}\right)$$

To complete the balance, the horsepower required to drive the fan (HP_f) in helium at 70°F and 3000 psia must be less than 10% of the above output,

$$\text{(B)} \quad \text{i.e., } HP_f \leq 0.1\ HP_o$$

It must be noted that equation A necessitates establishing electro-magnetic design to determine the motor efficiency for a design compatible with the load and ambient.

The results of this phase of the program are shown in Figure 6.2-17 which is a plot of continuous horsepower available from the motor when operating in helium at 70°F and 10 psia versus active volume. There are curves for operating speeds of 5,000, 10,000, and 20,000 rpm.

Three more curves are shown, which are the curves expressing the relationships necessary to arrive at the above horsepower. These curves are:

6.2-18 Motor Efficiency (η) versus Active Volume, operating in helium at +70°F and 10 psia.

6.2-19 Horsepower Consumed by Fan (HP_f) versus Active Volume, operating in helium at +70°F and 3000 psia.

6.2-20 Watts Dissipated (W_D) versus Active Volume, operating in helium at +70°F and 10 psia.

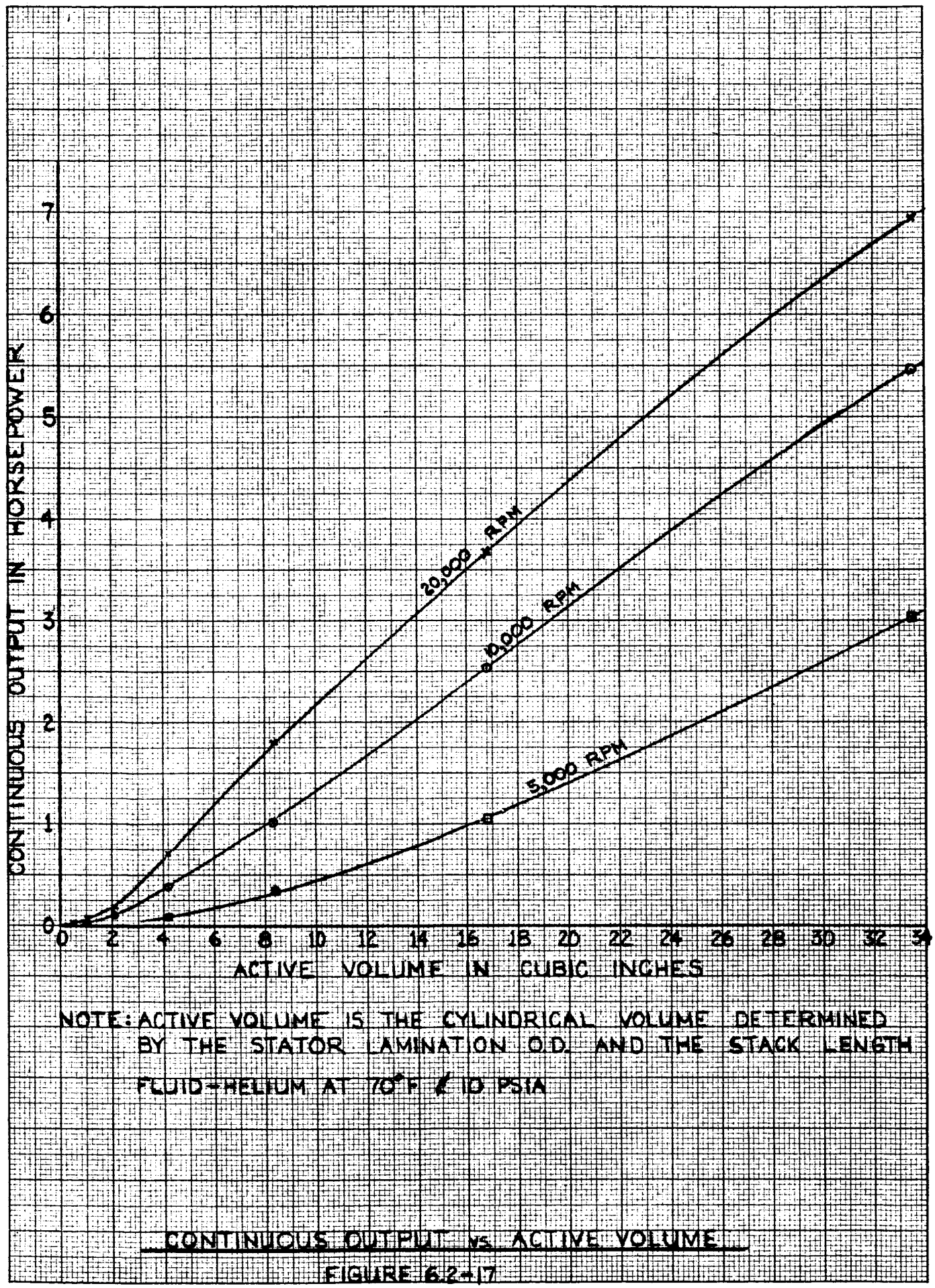

NOTE: ACTIVE VOLUME IS THE CYLINDRICAL VOLUME DETERMINED BY THE STATOR LAMINATION O.D. AND THE STACK LENGTH

FLUID - HELIUM AT 70°F & 10 PSIA

CONTINUOUS OUTPUT vs. ACTIVE VOLUME

FIGURE 6.2-17

KRUFFEL & ESSER CO.

7 X 10 INCHES MADE IN U.S.A.
KEUFFEL & ESSER CO.

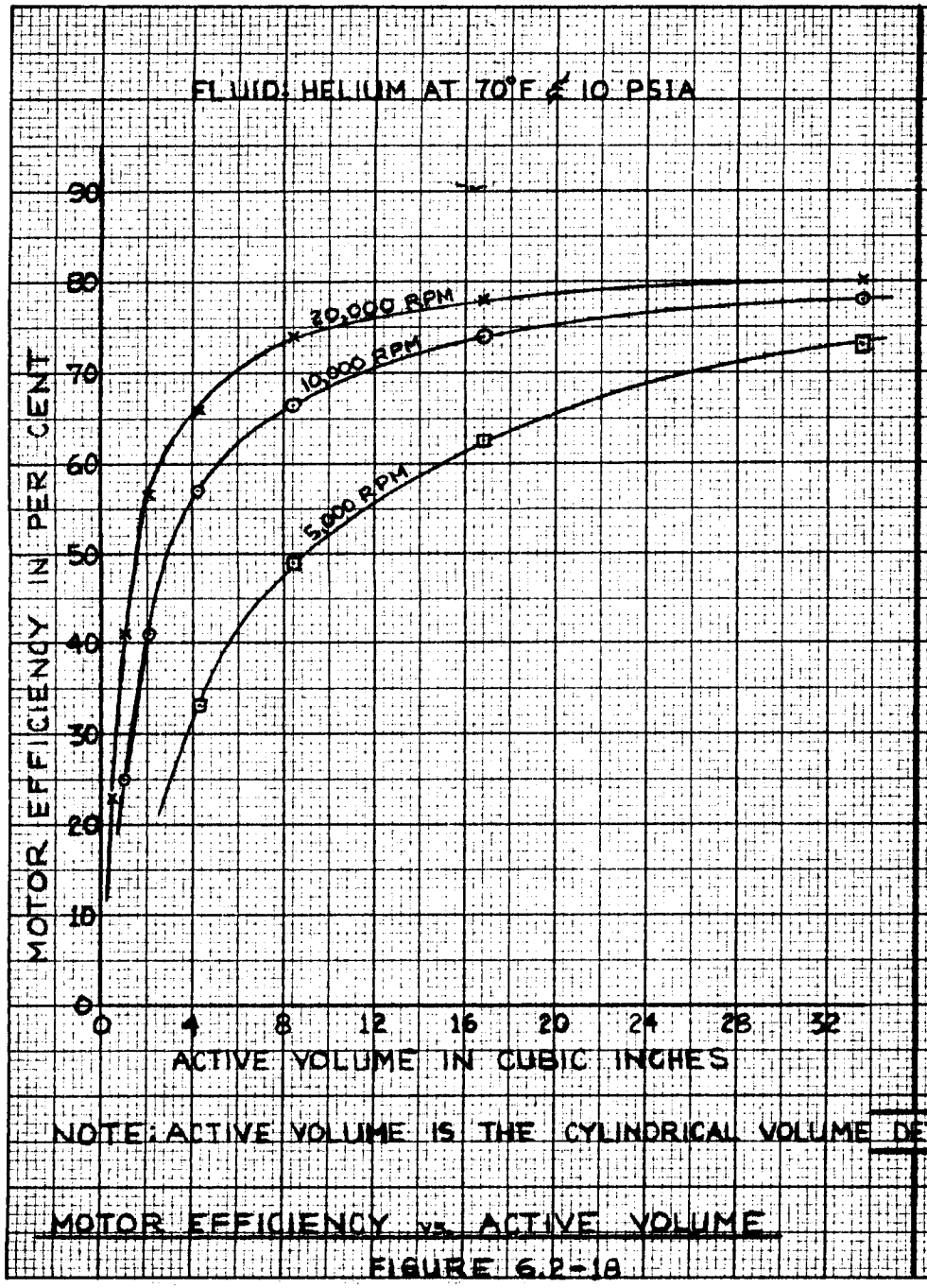

MOTOR EFFICIENCY vs. ACTIVE VOLUME

FIGURE 6.2-18

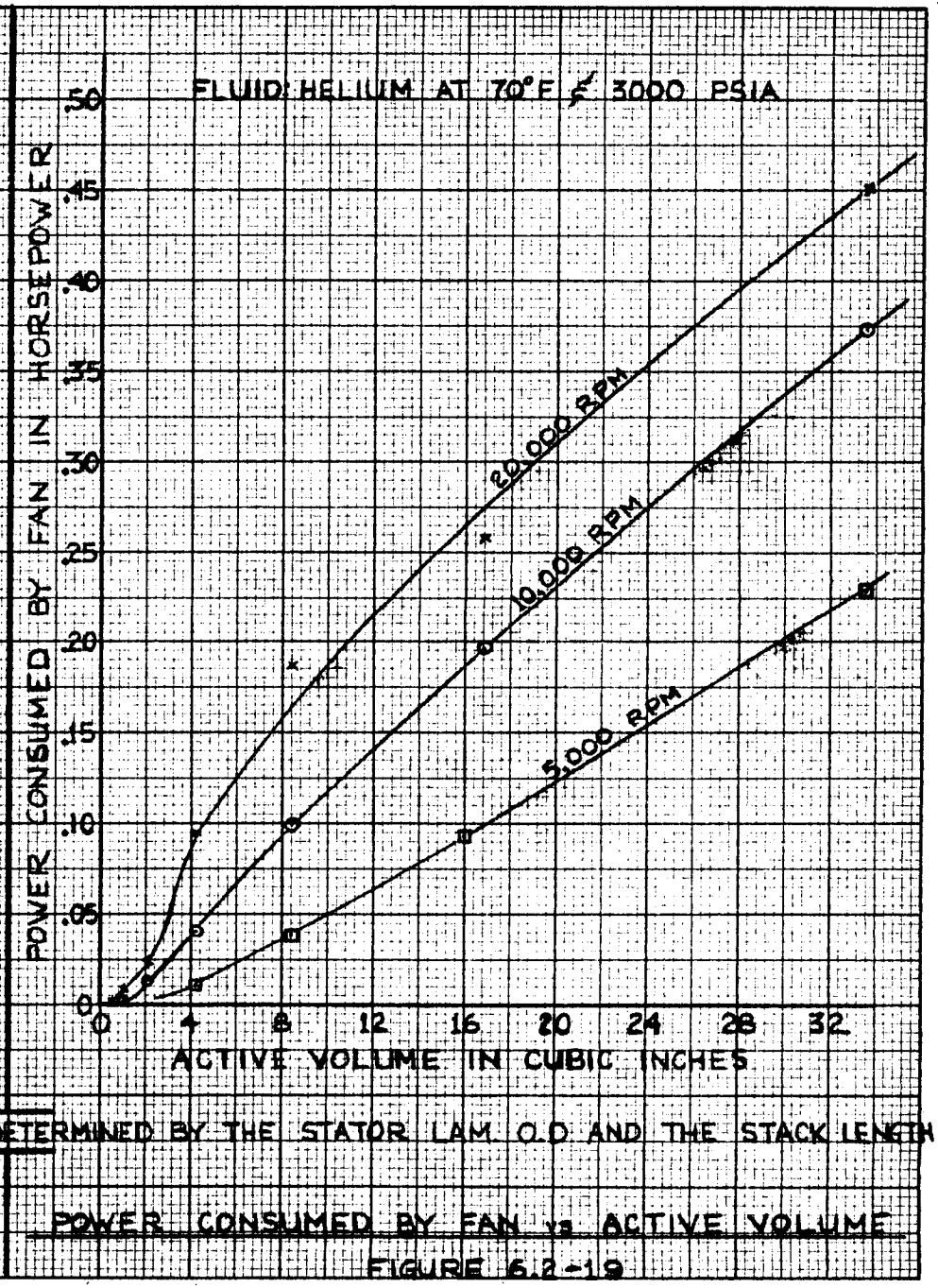

NOTE: ACTIVE VOLUME IS THE CYLINDRICAL VOLUME DETERMINED BY THE STATOR LAM. O.D AND THE STACK LENGTH

POWER CONSUMED BY FAN vs ACTIVE VOLUME

FIGURE 6.2-19

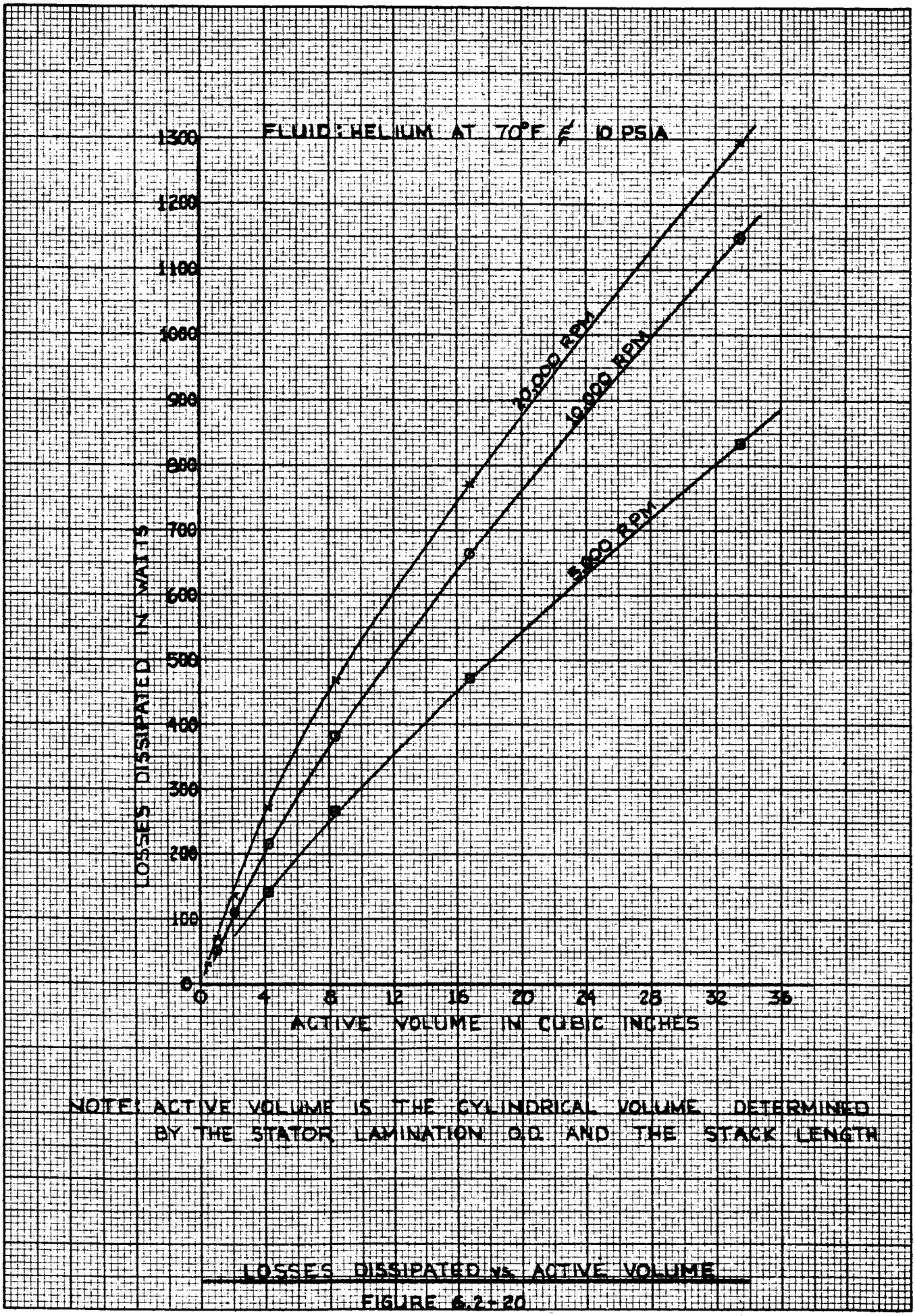

NOTE: ACTIVE VOLUME IS THE CYLINDRICAL VOLUME DETERMINED BY THE STATOR LAMINATION O.D. AND THE STACK LENGTH

LOSSES DISSIPATED vs. ACTIVE VOLUME

FIGURE 6.2-20

7 X 10 INCHES MADE IN U.S.A.
KEUFFEL & ESSER CO.

6.2.10 Other Factors Affecting Motor Design

This paragraph is a general discussion of the effect of the power supply on motor size and performance. The first part is a discussion concerning the three-phase sinusoidal power supply, then brief notes regarding two-phase operation of three-phase motors, and then operation from a quasi-square wave.

6.2.10.1 Variation of Voltage and Frequency, 3-Phase

The proportionalities listed below express the variation of certain performance parameters of 3-phase induction motors as voltage and frequency vary:

(1) Maximum Torque = $T_m \propto \frac{V^2}{f^2}$

(2) Flux = $\Phi \propto \frac{V}{f}$

(3) Synchronous Speed = $N_s \propto f$, independent of voltage

Equation (1) indicates that at reduced voltage and/or increased frequency, the maximum torque generated is reduced by the square of these parameters. It is obvious that the machine must be sized to produce the required torque at the worst combination of voltage and frequency. However, the magnetic curcuit must have sufficient cross section so that it is not saturated at maximum voltage, minimum frequency as indicated by equation (2). The first, obvious conclusion is that variation of voltage and frequency require an increase in machine size to provide adequate torque and to prevent over-saturation of the magnetic circuit.

Equation (3) shows that the synchronous speed, and normally the no-load speed, increases with frequency. The no-load speed usually increases slightly at higher voltages but must be lower than the synchronous speed by a slip sufficient to supply the motor's own no-load losses. The item of importance however is the speed at rated load which is not quite so obvious. As the voltage is increased at constant frequency, the slip at rated torque is reduced, but not in

direct proportion. The degree of change is dependent upon the initial slip and the ratio of maximum torque to rated torque. An increase in frequency results in an increase of no-load speed and a reduction in maximum torque and therefore the shape of the speed torque curve changes and the speed at rated torque may either increase or decrease. For most motor designs and their application, an increase in speed at rated torque may be expected. The net effect is, again, an increase in motor size.

The efficiency is also affected since the rotor losses are proportional to slip, the iron losses are approximately proportional to flux density squared and frequency to the 1.6 power, and stator copper losses are a function of current squared. The power factor is a function of the magnetic circuit density and the slip.

6.2.10.2 Operation of a 3-Phase Motor with One Phase Open (2-phase operation)

A three-phase motor will operate with one phase open, however, with a reduced maximum torque and starting torque capability. If the motor must deliver rated load at this power condition, it is apparent that it must be sized for this requirement and then will have an "over-capacity" with three-phase power. In addition, to the size increase necessitated by this requirement, the three-phase power factor and efficiency may also suffer since the rated torque is too far below the maximum torque. The motor is, in effect, operating lightly loaded which is probably not the load point for maximum efficiency. The maximum torque generated by a 3-phase motor when operating with one phase open, is approximately 50% of the 3-phase value.

A more detailed discussion of this operational mode can be found in the Society of Automotive Engineers' Aeronautical Information Report No. 34 prepared by Subcommittee A2M of SAE and issued November 15, 1957.

6.2.10.3 Quasi-Square Wave, 3-Phase, Voltage

The recent advances in solid state inverters have resulted in devices successfully applied to aero-space projects. The weight of these devices and their efficiency can be greatly improved if the output is not filtered. Since they are basically timed switching circuits, the output is simply the battery voltage connected to various circuit points, and to produce a sinusoidal output requires the weight and losses of a filter network. Motors have been operated on a conventional square wave, however if a 30° dwell time at zero voltage at the beginning and end of each half cycle is introduced, the resultant wave has been called a quasi-square wave. The line to line voltage then will be:

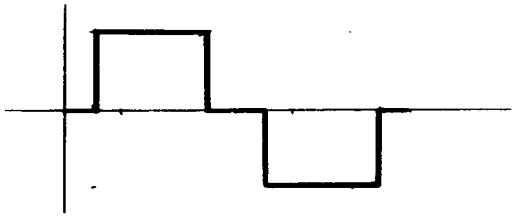

The first advantage of this wave form is that it contains no third harmonic, the most troublesome and largest magnitude harmonic of a square wave. Further, as established by Fourier Analysis and confirmed by test, the line to neutral voltage wave form is as follows:

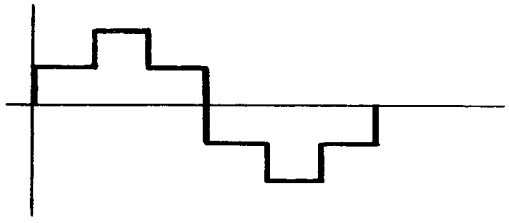

While it is true that the inverter has no neutral point, the motor windings see the line to neutral voltage when connected in the normal wye manner. The result is effective motor operation with essentially the same maximum torque generation capability as achieved on sine wave operation with slightly greater losses due to harmonics, a small order effect. In summary, three-phase motors have been operated effectively and successfully from quasi-square wave voltage power supplies.

6.3 Heat Rejection Study

When an efficient electric motor of relatively low power - up to about one horsepower, depending on motor speed and size - is to be operated in cryogenic helium liquid or dense gas, adequate cooling of the motor is not expected to constitute a serious problem. This is provided, however, that a small cooling flow of fluid is maintained past or through the motor either by gravity induced natural convection or by a very small pump or fan. This conclusion is based on Pesco tests and experiences with cryogenic electric motors operated in cryogenic hydrogen gas or liquid under a gravity force of one "g". However, in the absence of gravity forces, there would be no differences in specific gravity between the cold and heated fluids to induce natural convection. Thus, a small fan or other circulating device would be necessary in zero "g" cryogenic fluids, simply to insure that the motor and its bearings would not operate in a growing, poor heat conducting stagnant bubble or cloud of warming gas.

When the motor is in a cryogenic environment, a very high value of temperature rise from the cryogenic temperature to +350°F or higher, can be tolerated in the motor windings and rotor without extremely impairing motor performance. This pre-supposes that the rotor bars, stator windings, and insulation have been selected for wide temperature range of operation. However, it is always necessary to prevent large differential contractions or expansions, particularly between bearing inner race, balls, and outer race, which could internally preload the bearings excessively and cause their premature failure. A small flow of liquid or gas through the bearings is always necessary, primarily for this purpose.

In contrast, when the motor is to be operated in high temperature gas, three things occur which adversely affect motor cooling, as follows:

1) The resistance, hence I^2R losses in the motor conductors greatly increase with the increase in motor temperature. This decreases motor efficiency and increases the losses and heat which must be transferred to the gas. This also tends to be self-generating or "Bootstrapping." As the losses and temperature rise increase, the I^2R losses also increase, contributing in turn to even more heat generation and temperature rise, more I^2R losses, thus even more heat generation. Depending on cooling rates, this will continue until the insulation fails or rotor bars melt, or the motor reaches some high temperature balance with the heat rejection rate.

2) For a given gas pressure, as the temperature of the gas increases, its density decreases in about inverse proportion. This leads to a lesser mass of gas adjacent to the cooling surfaces, and lesser cooling rates. A greater volumetric flow of gas past the cooling surfaces is then required to preserve the initial heat balance and temperatures of the motor parts.

3) As the ambient gas temperature increases, less temperature difference can be permitted to exist between the motor and its coolant gas before excessive temperatures of the electrical insulation and conductors occur.

In order to maintain a heat balance at reasonable component temperatures a forced flow of the gas over the heat generating parts is required.

6.3.1 Effect of Fluid Density on Fan Performance

The main problem of cooling a motor by a fixed fan or blower is simply this: If the motor fan or blower is designed to give adequate cooling mass flow rates in the higher temperature, lower density gas, then the power drawn by this same fan or blower becomes excessive when it is operated in the lower temperature, much more dense fluid. This problem is discussed following.

Pump or fan design and performance is affected appreciably by fluid viscosity only when the viscosity becomes higher than about 10^{-2} poises. Both liquid and gaseous helium have extremely low viscosity; typically 2×10^{-4} poises and thus effects of viscosity, or changes in it are negligible for fan design. Consequently, the power required for operation of a given fixed blade fan or blower is directly proportioned to fluid specific weight and to the cube of the rpm, as given by (these relations are for fixed fan size and geometry):

Q	-	K_1N
P	-	K_2wN^2
Fan Power	-	$K_1K_2wN^3$

where:

Q	-	fan flow rate, in cfm
K_1 & K_2	-	design constants of the fan or blower
N	-	fan rpm
w	-	fluid specific weight pounds per cubic foot
P	-	pressure rise produced across the fan, which is converted to cooling gas velocity head and fluid friction in cooling passages.

As second order effects:

Because rotor bar resistance decreases at low temperature, the motor slip will be less and the motor rpm will be slightly higher at low motor temperatures than at higher temperatures, at a fixed motor torque or power output. However, offsetting this, the cooling gas at the lower temperatures is more dense and a cooling fan operated in the lower temperature gas will require more torque and horsepower from the motor. This additional loading will tend to cause the motor speed to decrease, thus tending to balance (or more than balance) the speed increase from lower rotor bar resistance.

Neglecting possible motor speed changes versus temperature and assuming a relatively constant speed; then for fixed fan speed geometry and size, the following applies:

Fan Flow Rate = Q = K_3 = (fixed, at constant rpm)

Fan Pressure Rise, P = K_4w = (proportional to gas sp.wt.)

Fan Power = K_3K_4w = (proportional to gas sp.wt.)

where: $K_3 = K_1N$, $K_4 = K_2N$ are constant and w is fluid specific weight, (e.g., pounds per cubic foot.

"Helium Specific Weight versus Temperature, showing the motor operating envelope" is shown in Figure 6.3-1.

The cooling fan may be required to operate with its inlet sucking through the motor windings, rather than with its discharge blowing through the windings, in order to meet a motor mounting requirement, secure proper flow into the inlet of the fan, or secure more uniform mass flow cooling rates. In this event, the cooling flows will be considerably warmed by the motor before passing through the fan, particularly in the low pressure, high temperature, least dense gas condition.

The resultant "Helium Specific Weight versus Temperature, showing Fan Operating Envelope" is shown in Figure 6.3-2. In this envelope, an 80°F temperature rise of the gas has been considered, from 530°R (70°F) to 610°R (150°F).

Some extremes of ambient helium specific weights to be considered are tabulated below:

He Temperature	Pressure, psia	He Specific Wt., w, lbs/ft^3
70°F (530°R)	10	.0068
70°F (530°R)	3000	1.9
-453°F (7°R)	3000	Approx. 15.0 (extrapolated from existing data)

As Examples:

Suppose a fan, designed to provide motor cooling, draws only 1% of the total power of the motor under low density conditions of 70°F, 10 psia and .0068 lbs/ft^3, the same fan will draw 1.9/.0068 x 1% or 280% of the rated power of the motor under 70°F, 3000 psi gas conditions of 1.9 lbs/ft^3, (an impossibly high fan load).

At -453°F, 3000 psia conditions of about 15 lbs/ft^3, the fan power required would be 15/.0068 x 1% = 2,250% of the rated output of the motor, (an even more impossible fan load).

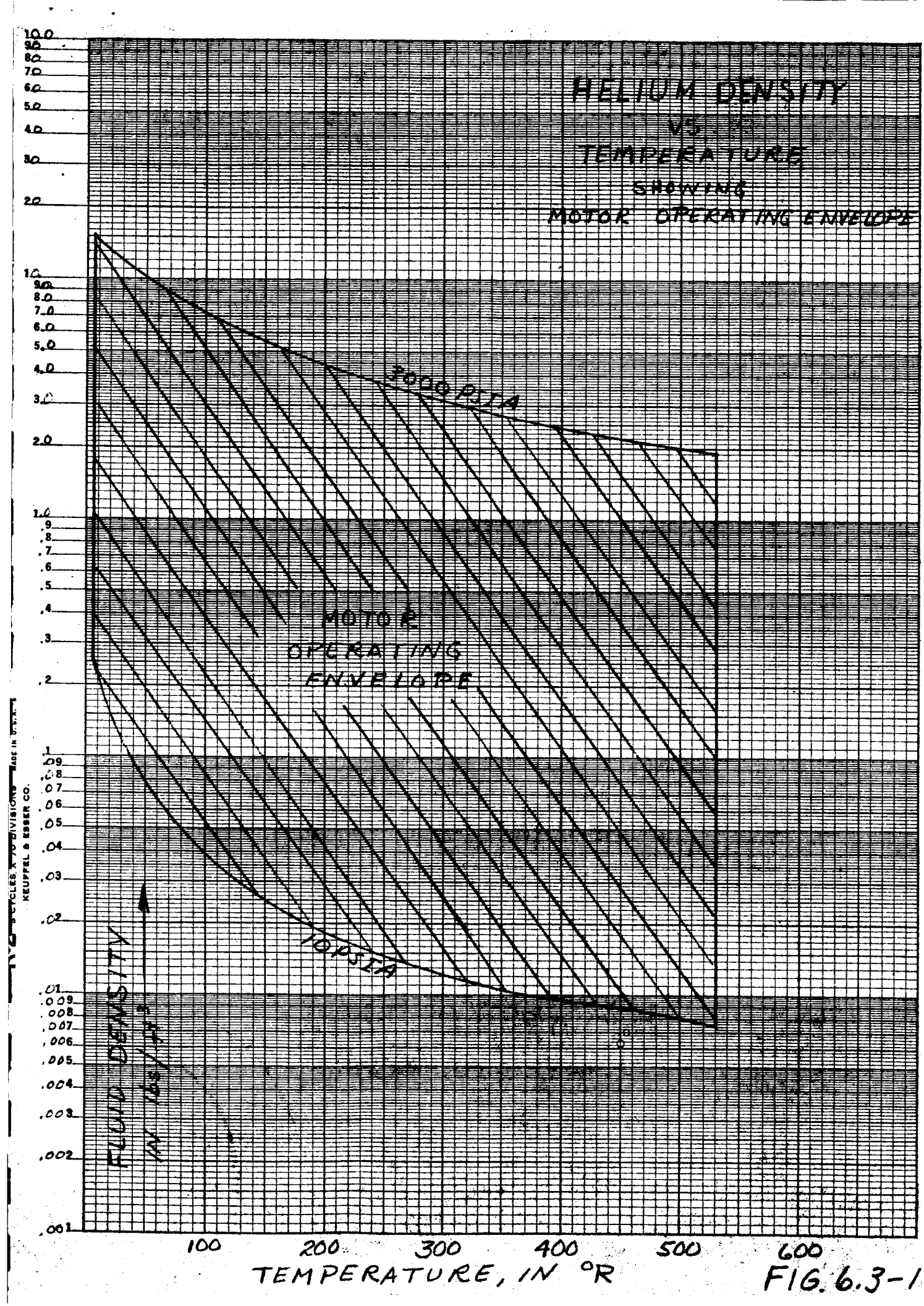
HELIUM DENSITY
VS.
TEMPERATURE
SHOWING
MOTOR OPERATING ENVELOPE
3000 PSIA
1025 PSIA
MOTOR
OPERATING
ENVELOPE
FLUID DENSITY, LB/CU FT
10.0
9.0
8.0
7.0
6.0
5.0
4.0
3.0
2.0
1.0
.9
.8
.7
.6
.5
.4
.3
.2
.1
.09
.08
.07
.06
.05
.04
.03
.02
.01
.009
.008
.007
.006
.005
.004
.003
.002
.001
100
200
300
400
500
600
TEMPERATURE, IN °R
KEUFFEL & ESSER CO.

FIG. 6.3-1

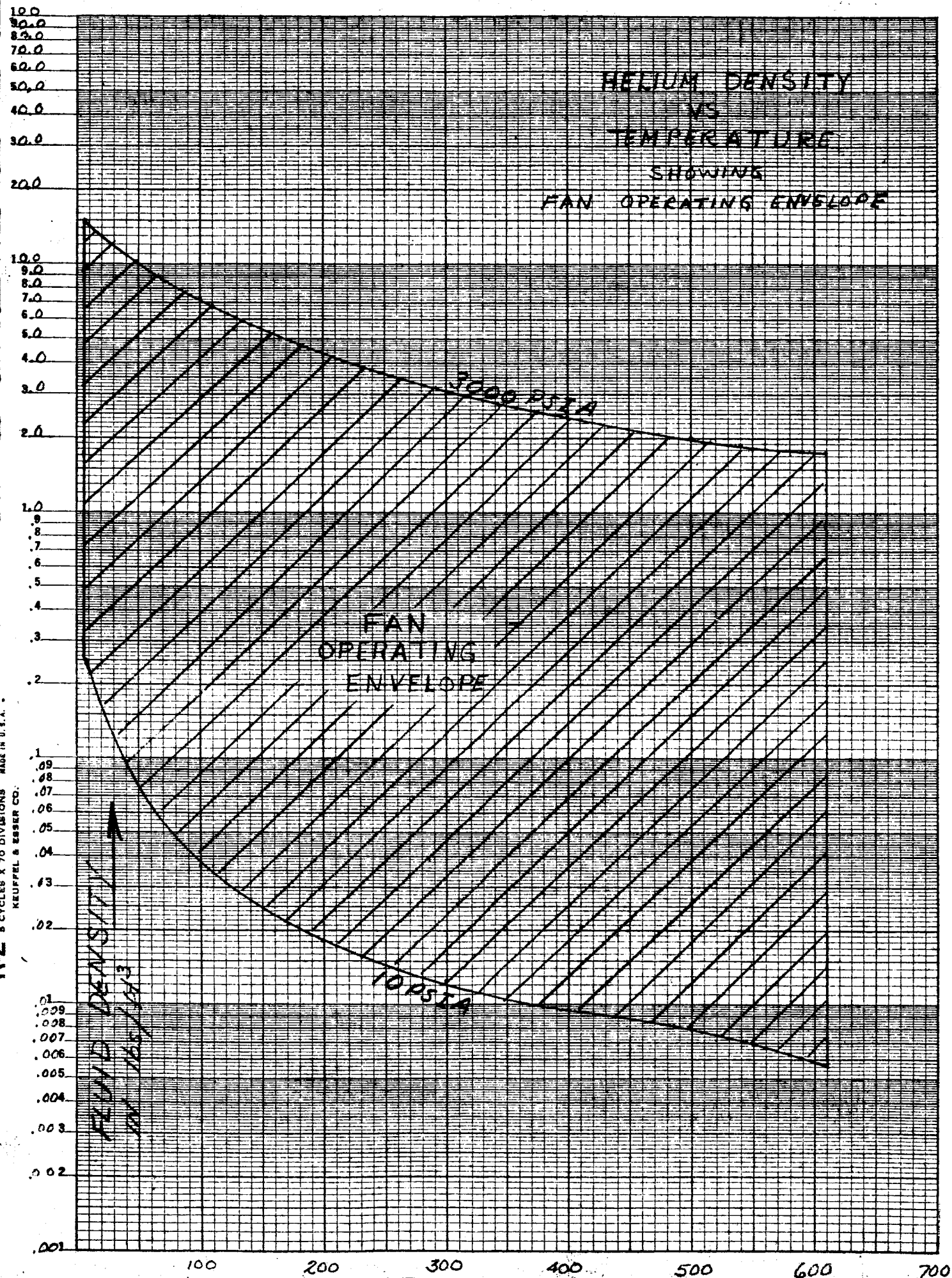
HELIUM DENSITY
VS
TEMPERATURE
SHOWING
FAN OPERATING ENVELOPE
FAN
OPERATING
ENVELOPE
2000 PSIA
1000 PSIA
100 PSIA
10 PSIA
1 PSIA
100
200
300
400
500
600
700
TEMPERATURE, IN °R
KEUFFEL & ESSER CO. MADE IN U.S.A.

FIG. 6.3-2

Thus, under the above dense fluid conditions, the fan would simply load the motor so extremely that the motor would never approach the required speed. It would operate at a very low speed approaching stall, with very low efficiency and high current simply from the load of a fan designed with only the least dense gas conditions in mind.

In contrast, a much smaller fan or blower can be designed to operate with a reasonably low value (say 10%) of total motor power output under the most dense fluid conditions (about 15 lbs/ft^3). The fan power requirement will be only .0068/15 x 10% = .00045 x 10% = 0045% of same motor output at 10 psia 70°F conditions. However, this fan will be so extremely small that its pressure rise to be converted to cooling velocity, and its cooling flow rate would be so extremely low in the 70°F 10 psia fluid condition as to provide almost negligible cooling effect.

Providing a fan or blower small enough so that it will not seriously overload the motor at the most dense fluid conditions where the motor requires least cooling, and which will still provide adequate cooling of the motor with higher temperature least dense gas constitutes a serious problem. It poses a serious limitation on the cooling, and hence, resultant power output that can be obtained from the motor under the least gas density conditions of highest temperatures and lowest gas pressures.

6.3.2 Compensating for Fluid Density Variations

One solution to this problem is to try to provide a variable fan, whose power consumption tends to remain more constant with fluid state changes. Its pressure rise or flow rate must therefore vary with either the gas temperature or density change, or both. At the low temperatures and high gas densities, where the cooling flow requirement is less, this variable fan would produce less flow and cooling velocity, and consume less power than otherwise would be required.

For considering this variable fan approach, more general expressions for the flow rate and power requirements of fans are given below; where the geometry and size are no longer fixed.

$$\text{Fan Flow Rate, } Q = K_1 D^3 N \times f_1 (B_2)$$

$$\text{Fan Pressure Rise, } P = K_2 D^2 N^2 \times f_2 (B_2)$$

$$\text{Fan Power Requirement} = K_1 K_2 D^5 N^3 \times f_1 f_2 (B_2)$$

where

K_1 and K_2 are fixed constants of the fan design which include area and flow rate conversion factors.

D = fan diameter

N = fan rpm

$f_1 (B_2)$ and $f_2 (B_2)$ = empirical functions of the fan blade width, discharge angle B_2, and blade camber. As the fan blade discharge angle, B_2, or blade camber is reduced, less flow, pressure rise and power consumption of the fan result.

Changing Fan or Blower Diameter "D"

Varying the effective fan diameter, "D", such as by telescoping or pivoting variable radius members, as a function of either fluid density or temperature, or both, presents mechanical complications and reliability problems. This is particularly true for a very small sized motor and the resulting small size, delicate mechanisms required. For a high rpm motor this method also presents extreme operating and reliability problems in balancing high centrifugal forces on the extendable or variable diameter members. Because of these mechanical and reliability problems on small motors, varying fan diameters is not further considered here. It could, however, be considered on larger and lower speed motors where the mechanisms required might be considerably larger and more rugged.

Varying RPM of the Fan or Blower

Varying the effective rpm of the fan or blower, in order to vary its cooling flow, pressure, and power requirements with density changes of the fluid, is a more feasible method for the very small or medium sized motor.

The use of variable reduction gearing or friction drives is not judged feasible because of excessive size, weight, complications and the wear of such mechanisms in the unlubricated state required for cryogenic operation.

However, the use of magnetic, hysteresis or eddy current, couplings as variable speed reducing methods between motor and its fan may be feasible and reliable. In this method the fan would have its own bearing and could be driven at reduced variable speed by an eddy current or hysteresis disc (or cup). Eddy current or hysteresis torque on the disc could be produced by a magnetic field in the form of a permanent magnet placed on the rotor shaft adjacent to the disc or cup. Alternatively, it might be produced by an extension of the magnetically revolving field of the stator opposite the O.D. of an induced current or hysteresis rotor, constituting in effect the addition of an auxiliary rotor for operation of the fan. The magnetic coupling and the size of the magnetic parts could be adjusted by design so that with the fan completely stalled or operated at low speed in highest density fluids, the maximum torque and power taken from the motor by the magnetic coupling would have a reasonably low value, say 5% of the motor output.

The torque on an output eddy disc, (or cup) is equal to the torque applied on the input revolving magnet. However, as the torque on the output is increased, the output rpm decreases in rough proportion. This occurs because some relative motion, or "slip" between the revolving magnetic field and induction disc is necessary to produce the induced eddy currents, and hence, induced torque.

With the fan operation in the higher temperature and lower density gas, the torque required by the fan will be quite low. The fan would then operate with little magnetic slip from motor rotor rpm, hence, at high speed, producing the high volumetric flow necessary for effective motor cooling in the higher temperature and lower density gas.

When the fluid temperature is low and pressure high, resulting in high fluid density, the higher torque required by the fan would produce more magnetic slip in the induction disc. The fan would then run at much reduced rpm and take lower torque than would be required for full speed. The fan torque varies as the square and power as the cube of its speed. The flow rate of the fan would also automatically decrease (being directly as the speed) to supply the lesser volumetric flow required for motor cooling by the dense gas.

For these conditions, the maximum torque and hence maximum power requirement on the motor could be adjusted by coupling design to be no more than say 5% of the motor power output.

However, the rpm slip, in the magnetic coupling represents a power loss that appears in the form of heat in its parts. It accordingly reduces over-all motor efficiency in fan operating conditions of high coupling slip.

Also, when the magnetic slip coupling would be flooded with liquid or high density helium, the circulation of dense fluid between its parts revolving at different speeds would cause them to be hydraulically coupled to each other in the manner of a hydraulic torque converter as well as magnetically. This hydraulic coupling would be due, not primarily to viscous shear (which would be negligible for helium gas or liquid) but primarily to a pumping-turbining effect from fluid circulated between parts. This hydraulic pumping and turbining follows the same hydraulic laws and relations as apply to the cooling fan or blower. That is, the hydraulic torque developed between the parts would be proportional to the square of their speed difference and directly to the fluid specific weight. Thus, as the fluid density increased, from lower temperatures or higher pressures, or the relative speeds of the parts increased, the hydraulic coupling and torque between parts would increase, tending to drive the fan faster and further load the motor, whereas it is the opposite effect that is desired.

Consequently, the effect of varying fluid density (and viscosity), with temperature and pressure changes of the fluid, in producing an additional variable hydraulic coupling would also have to be studied in the design of a magnetic, variable slip (variable speed) coupling. Beyond variable power loss, there is also the additional weight and envelope that would have to be considered for a magnetic slip coupling for a cooling fan, as follows:

The flux densities that can be used in a permanent magnet are considerably lower than in the permeable iron laminations of the motor proper. The permanent magnet also requires that the magnetic path be complete, in the form of the magnet additional magnets, or permeable iron, if its to be used effectively or efficiently. These represent additional weight and envelope. Also, if the torque or mechanical power to be put into the magnetic coupling is say 5% of the output of the motor, then the magnetic coupling device becomes in effect a very small and high slip "motor" with only 1/20th the output of the main motor. Consequently, it will have the inefficient use of materials and low efficiency associated with very small motors, requiring a higher ratio of weight and input to output power than for the main motor. The magnetic coupling device and fan operating at reduced speed will also require its own separate bearing, bearing support and added housing for its components, further adding to envelope and weight.

The result is that for a small motor where the magnetic coupling is to deliver 5% of the total motor power to the fan, the extra weight from the magnetic coupling device may be much greater than 5% of the motor weight. It may add a representative 20% to 40% to the weight of a small motor.

The same comments apply to the addition of an extra, small, high slip rotor with its own bearings for purposes of driving the fan only. The extra rotor along with an extra stator, or additional length of stator windings to excite it constitutes in fact the direct addition of a motor.

The usefulness of the variable slip magnetic fan coupling will then depend in part on the ratio of power the motor is required to deliver, (hence, ratio of cooling required), between the various temperatures and densities of the helium, and tradeoffs between weight, envelope, power consumption and the added complexity of the coupling.

For the above reasons, other simpler means of varying fan power and performance were also considered, including the use of thermostatically variable fan vane angles and camber.

Fan Blade Variable Discharge Angle

A useful method of controlling fan discharge flow, pressure rise and power requirement is to vary the blade discharge angle "B." A bimetallic or thermostatic element or strip may be used to vary angle "B" and camber as a function of fluid temperatures.

At low fluid temperatures where less motor cooling is required, the vane discharge angle "B" and camber would be reduced. The vanes would go "flat" to approach a disc configuration, produce less flow and pressure, and reduce power requirement in the more dense low temperature fluid.

A simple way of performing this is to make the fan vanes themselves out of bi-metallic strips. The fan vanes would be performed in arc at room temperature so that they become flat at liquid helium temperature. The fan then approaches a flat slotted disc, with lowered power requirements, low head rise and lowered flow rates in low temperature fluid where less cooling rate is required. See Figure 6.3-3 "Fan Assembly, Variable Pitch," where the blades are shown in this low temperature flattened condition.

As the cooling gas temperature increases, the vanes would then increasingly warp, increasing the vane camber, discharge angle, head rise and volumetric flow rate through the fan and motor.

To study feasibility of this concept, various bi-metallic sheet materials were obtained. Sample, single, fan vanes cut and preformed, and they as well as flat strip were tested in temperatures ranging from submersion in liquid nitrogen at -320°F to heated air at approximately +350°F.

The cryogenic tests were necessary since information available on the bi-metallic materials did not extend to the low temperatures of liquid nitrogen at -320°, much less liquid helium at approximately -450°F. Also, some of the alloys used in the bi-metallic sheet were not materials on which wide range contraction rates are available. The contracting or bending rates are often markedly non-linear with temperature and also depend on the thickness, relative thickness and methods of manufacture of the sheet.

Results of liquid nitrogen tests on some useful by-metallic materials are given later. For an example type of bi-metallic fan blade with the leading edge secured and fixed at zero degrees, and its trailing edge free to warp or move, per Figures 6.3-3 and 6.3-4, the fan trailing edge discharge angle "B" can be calculated with sufficient accuracy for preliminary design as twice the measured linear deflection, A, divided by the length "L" of the bi-metallic strip. This approximation is obtained by using the first two terms of the series expansion of the cosine of the vane discharge angle. This is justified because the bi-metallic strip forms a relatively small arc of a circle on temperature warping, illustrated in Figure 6.3-4.

USAF ZERO DEFECTS

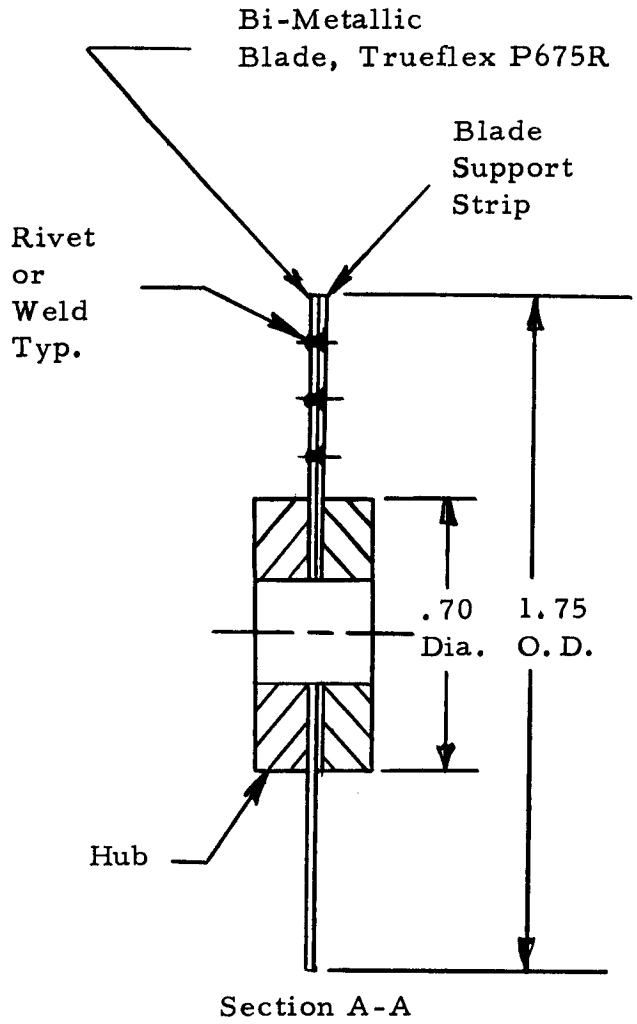

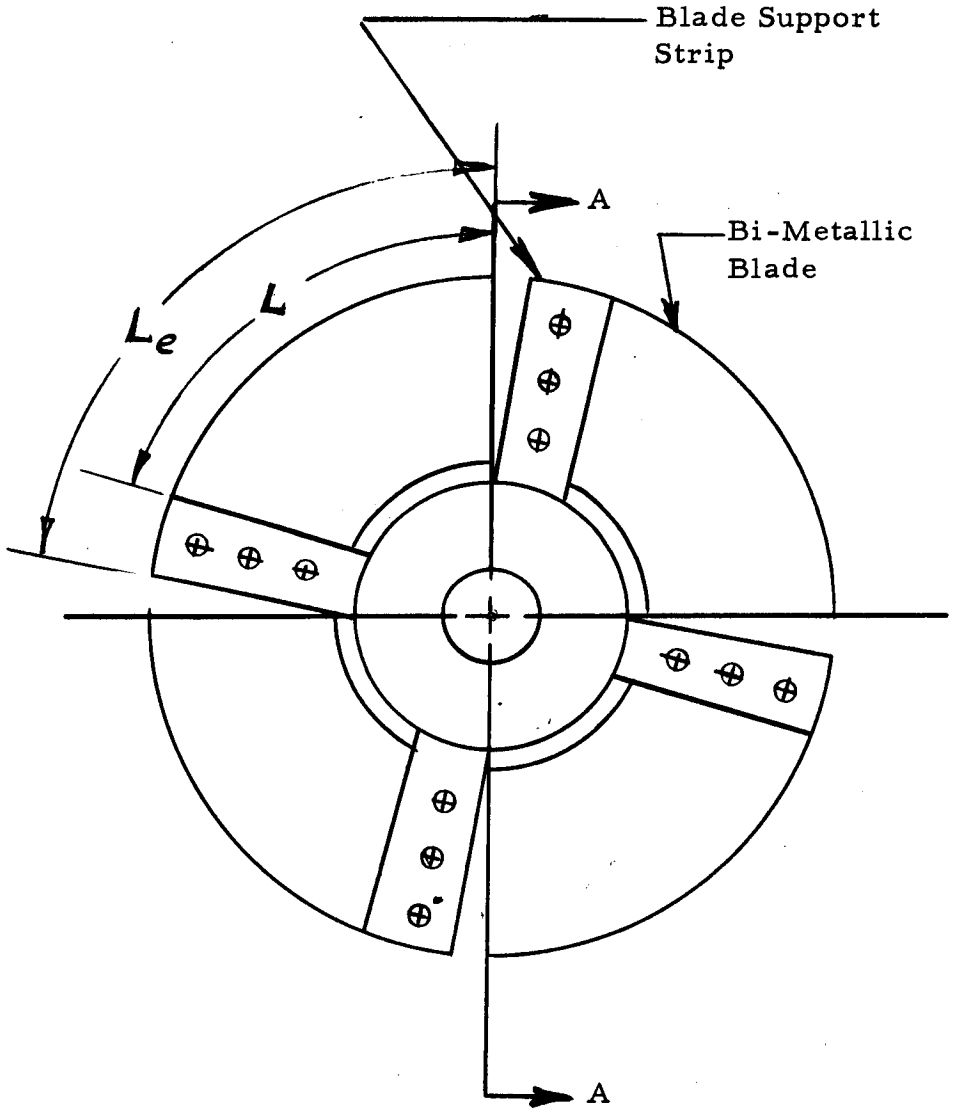

FAN ASSEMBLY
VARIABLE PITCH
2X SCALE

FIGURE 6.3-3

Pesco Products DIVISION OF BORG-WARNER CORPORATION

aerospace equipment BORG WARNER ®

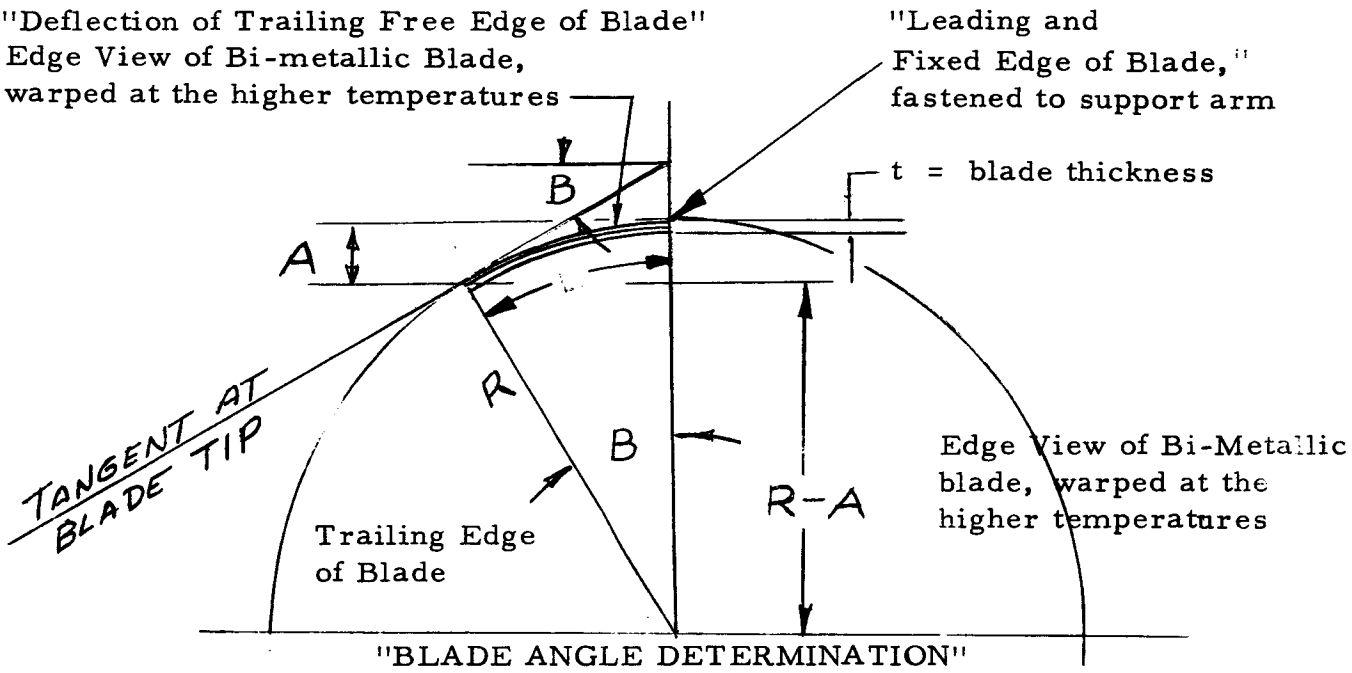

where B is expressed in radians, $\frac{L}{R} = B$, and $\frac{R - A}{R} = \text{Cos. } B =$

$$1 - \frac{B^2}{2!} + \frac{B^4}{4!} - \frac{B^6}{6!} + \frac{B^8}{8!} - \ldots$$

Where L and B are small compared with R, the terms $\frac{B^4}{4!} - \frac{B^6}{6!} + \ldots$ become negligible, so that:

$$1 - \frac{A}{R} = 1 - \frac{B^2}{2 \times 1}, \text{ or } \frac{A}{R} = \frac{B^2}{2}.$$

Substituting $R = \frac{L}{B}$, $\frac{BA}{L} = \frac{B^2}{2}$, $\frac{A}{L} = \frac{B}{2}$, or $\boxed{B = \frac{2A}{L}}$

Also, where curvature $\frac{1}{R}$ is assumed proportional to both the temperature difference (T_2-T_1) and inversely as thickness, t, $R = \frac{t}{K(T_2-T_1)}$ Where K is a function of the material. Substititing this in

$A = B \frac{L}{2} = \frac{L}{R} \times \frac{L}{2} = \frac{L}{2R}$, $A = \frac{K(T_2-T_1)L^2}{2t}$. The form of the expression given by Truflex is $A = \frac{.53F(T_2-T_1)L^2}{t}$, where $F = \frac{K}{2 \times .53}$.

The tests and calculations showed that the vane warpage on some samples would give suitable variations of blade discharge angle,"B" for fans for the helium motors. This was particularly true of the Truflex(1) bi-metallic material "P675R" in .015 and .010 total thickness which gave the greatest warpage. Variations of blade discharge angle B were from a value of B = 0° at -320°F (liquid nitrogen) to B = 35° at +350° (heated air), for a fan blade of 1.0 inch free circumferential arc "length," L. See Figure 6.3-3 and Figure 6.3-4. This 1.0 arc length when added to the small arc formed by the fan vane support arms, will provide a suitable four bladed fan with diameters from approximately 1.7 O.D. to 3.5" O.D. The corresponding fan blade "solidities" Le/S (discussed later) range from slightly less than 1.0 to about 0.5.

Bi-metallic materials are readily obtained only in a limited variety of alloy combination and sheet thicknesses. These, along with the vane length and configuration, determine the available blade warpage and its manner of response to temperature. Hence, the bi-metallic materials available determine in part, the fan characteristics available as a function of temperature.

Consequently, it may occur that the required fan performances over the temperature range cannot be obtained from the bi-metallic materials available by using a certain fixed fan geometry, such as a given number of blades and blade length.

However, it then becomes possible to vary the fan geometry over fairly wide ranges, (by varying number of fan blades, blade circumferential length, warpage, and "solidity") so that the desired fan characteristics can be closely approached by using bi-metallic materials readily available. These are discussed following.

(1) Tradename of Metals and Controls Division of Texas Instruments.

The bi-metallic blade tip deflection "A," is given by a manufacturer, "Truflex," as the following approximation:

$$A = \frac{0.53\ F\ (T_2 - T_1)\ L^2}{t}$$

where:

A = deflection of tip, from an initial flat configuration.

F = empirical material coefficient, determined by the alloys used in the bi-metallic strip and methods of manufacture

T_2 = final temperature, °F

T_1 = initial temperature, °F, (at which strip is flat)

t = thickness of strip

L = length of strip

On bending with a temperature change, an initially flat bi-metallic strip forms a segment of a true sphere. The curvature (1/Radius) is inversely proportional to the thickness of the strip. The curvature is also directly proportional to the temperature change over limited ranges of temperatures in which the material coefficient "F" is a constant. A straight line drawn on this initially flat surface then becomes an arc of a circle. The approximate expression for the deflection "A" is derived by using the first two terms of a series expansion for the cosine of the included angle expressed in radians, and by assuming the curvature is proportional to temperature, as given in Figure 6.3-4.

Some available bi-metallic materials have relatively constant values of F over limited temperature ranges. However, over the extreme ranges of temperature required by the helium motor fan, the coefficient, F, becomes markedly non-liner. "F" can also be expected to become extremely small with all materials at temperatures approaching that of liquid nitrogen or liquid helium, where residual thermal contractions and their differences become extremely small.

As an example; for .010 thick "Truflex" bi-metallic type "B_1" the value of F given (for the limited temperature range on which data was available) was $F = 123 \times 10^{-7}$. If this value of F is applied, however, to a temperature change of 400°F from +77°F to -323°F (liquid nitrogen) the according tip deflection, "A" of the 1.5 inch long strips of .010 type B-1 tested in LN would be calculated as:

$$A = \frac{(0.53)\,(123 \times 10^{-7})\,(400)\,(1.5)^2}{.010} = 0.586 \text{ in.}$$

However, the actual measured deflection of a 1.5 long strip of .010 thick B-1 material from approximately +77 to -323°F was only A = .297 inches.

This confirmed, as expected, that the bending became non-linear and decreased extremely at the lower temperature.

Consequently, in order to determine accurately the fan blade angles and fan performance obtainable at particular temperatures between about +350°F and -450°F, it will be necessary to measure the blade deflections for most useful bi-metals at a number of intervals in this temperature range. It would be even more useful to construct and test example fans using blades of the most promising bi-metals at temperature intervals to confirm their calculated performance. These were not possible in the limited time and funding of this contract.

For this fan feasibility study and preliminary design, the following linear temperature relation approximation was used:

$$F^1 = \frac{A^1_t}{0.53\,(T_2-T_1)L^2}$$

where a new average coefficient, F^1 was calculated using the actually measured deflection, A^1 as obtained from +77° to -323° tests in liquid nitrogen.

The resulting simplifying assumption of temperature linearity of of fan vane camber and discharge angle, made in absence of further experimental data, is obviously in appreciable error at intermediate or extrapolated temperatures. However, it is still useful for demonstrating feasibility and for preliminary design, particularly for the temperature extremes as tested.

For other temperatures, the fan vane deflection was thus calculated as linearly dependent on temperature, as:

$$A = \frac{0.53\ F^1\ (T_2-T_1)\ L^2}{t}$$

The resulting vane camber, "B" was calculated as

$$B = \frac{2A^1}{L} = 2 \times 0.53\ F^1\ (T_2-T_1)L^2 \text{ radians}$$

$$= B, \text{ radians} = 1.06\ F^1\ (T_2-T_1)L$$

using the cosine series approximation, previously noted.

The vane cambers expressed as degrees, as commonly used for propeller pump or fan calculations becomes:

B, degrees, = 57.3 x B in radians, or

$$\text{Vane camber, B, degrees} = \frac{60.6\ F\ (T_2-T_1)L}{T}$$

If the leading edge of a blade is fastened to its support arm to form an entrance angle, B, of zero degrees (from the plane of the arms, which is perpendicular to shaft), then the blade discharge angle B_2 = B, as follows:

$$B = (B_2-B_1) = (B_2-0) = B_2$$

A leading edge or entrance angle, B_1, of zero or nearly zero degrees is desirable only for the purpose of having the blades form a nearly flat disk as the blades become flat approaching liquid helium temperature for minimum fan power absorption in the more dense lower temperature fluid.

Some example experimental measurements of vane warp in liquid nitrogen, also calculated values of fan blade camber or B for other vane lengths and temperature differences, are given following, for reference and examples.

Example Experimental Results of Bi-Metallic Blade Warpage Tests in Liquid Nitrogen

(For the 1.5 inch blades tested, L = 1.5 and (T_2-T_1) 400°F, from +77°F to -323°F in (liquid nitrogen in all cases)

Truflex" Bi-Metal Material	Thickness	Strip Length	T_2-T_1 °F	Measured Deflection A, in.	Mean Coefficient, F for T_2-T_1 = 400°F
B_1	.015	1.5	400°	.25	78.7×10^{-7}
B_1	.010	1.5	400°	.296	62×10^{-7}
P675R	.015	1.5	400°	.312	100×10^{-7}
P675R	.010	1.5	400°	.531	111×10^{-7}

Example calc. for Truflex material B_1, .015 thick:

$$F^1 = \frac{Bt}{.53\,(T_2-T_1)L^2} = \frac{(.25)\,(.015)}{.53\,(400)\,(1.5)^2} = 78.7 \times 10^{-7}$$

Because of the short circumferential vane length, L, to produce warping, which would be available on a small fan, the material P675R, .010 inches thick appeared the most promising material for the purpose, because of its relatively high degree of warping ($F = 111 \times 10^{-7}$).

The resulting higher values of fan blade camber and discharge angle, B, are useful to produce the high volumetric flow rates required for the motor in the warm helium gas; while still giving the minimum feasible fan diameter and fan power consumption in the dense liquid.

As an example: for a temperature difference (T_2-T_1) of 523°F and a fan blade circumferential length of 1.0 inch, the fan blade camber, B will be:

$$B = \frac{1.06\ F\ (T_2-T_1)\ L}{t} \qquad \frac{(1.06)\ (111)\ (523)\ (1.0)}{010}$$

$$= .615 \text{ radians} = 35.4°$$

This is also its discharge angle B_2 if its entrance angle B_1 is made equal to zero.

This discharge angle should be adequate to produce an axial flow pump of about the highest ratio of flow rate to head, rise or power consumption, (i.e., highest value of N_s) which can be obtained without producing an undesirable region of pump or fan stalling or instability, as discussed later.

On these bases, the bi-metal pump or fan blades appear quite feasible for producing some motor cooling in the least dense high temperature gas, while still reducing the power consumption and required cooling, as needed, in the more dense liquid. The method would also be useful for producing a more uniform mass flow rate and load on the cryogenic motor where its sole load is to be apump or fan, such as for producing convection or destratification flows in a variable temperature fluid. It is therefore useful to discuss it in some detail.

Choice of Fan Type and Geometry

For purposes of most effective motor cooling, it was desired to obtain maximum feasible flow rates through the motor with the minimum pressure rise and resulting minimum fan power consumption. In particular here, this was also desired with a minimum impeller diameter in order to give minimum power consumption at the low temperatures, where little cooling is needed, the fluid is dense and fan power consumption is very critical.

These are achieved with a pump or fan of highest feasible N_s at high temperatures,

where:

$$N_s = \frac{nQ^{1/2}}{H^{3/4}}$$

and where:

n	-	pump or fan rpm
Q	-	pump or fan flow rate, gpm, at high temperature
H	-	pump or fan total head rise, in feet of fluid, including velocity head

N_s is simply a pump or fan design number, describing the pump or fan's geometrical proportions for best efficiency and most stable operation.

For N_s from about 9,000 to 17,000 the inlet diameter becomes equal to the discharge diameter and the hub diameter decreases with increasing N_s to increase the required flow area and decrease the pressure, the axial blade angles increase and the flow is predominantly axial. The impeller then becomes an axial propeller. This is the type of cooling fan selected, for maximum ratios of proportions for best efficiency and most stable operation.

For N_s = 500 to about 4000 (relatively low flow rates) an impeller is centrifugal. It uses increasing ratios of inlet diameter and discharge port width to impeller outside diameter as N_s increases. All flow passes through the same impeller diameter, its O. D.

For N_s of about 4000 to 9000, the impeller is best "mixed flow," (semi-centrifugal, semi-axial) with still further increases of inlet diameter. The required higher flow rates cannot be stably or efficiently turned a full 90°, in the short radial distance or vane length between inlet and outlet. Hence, vanes and discharge are inclined more axially to obtain a required vane length and flow discharge area. All fluid does not discharge from the impeller at the same diameter and thus, usually not at the same pressure.

For N_s from about 9000 to 17,000 the inlet diameter becomes equal to the discharge diameter and the hub diameter decreases with increasing N_s to increase the required flow area and decrease the pressure, the axial blade angles increase and the flow is predominantly axial. The impeller then, becomes an axial propeller.

This is the type of cooling fan selected, for maximum ratios of flow to head rise (for a given impeller diameter, and power consumption) as illustrated by the hydraulic expression for N_s.

Pumps or fans with N_s greater than 16,000 - 17,000 can be constructed but are usually inefficient, unstable, or both. Thus, better results (for higher ratios of flow to head rise and power consumption) can be obtained by operating N_s 16,000 pump or fan beyond its maximum efficiency flow rate.

For high N_s fans or pumps a hub to O.D. ratio of about .35 or .4 is the minimum practical for obtaining desired blade angle variation from hub to O.D. and constant axial velocity for high efficiency.

Fan-Pump Performance Calculation (Preliminary)

For an axial flow pump or fan, the performance at Best Efficiency Point (B.E.P.) can be calculated on the following basis:

Total Head Rise, in feet of fluid, including velocity head, $V^2/2g$, = $H = \frac{\psi u^2}{g}$ at B. E. P.

ψ is an empirical design constant, depending on N_s, and in turn on hub ratio, vane camber, angles and vane solidity.

u is the peripheral velocity of the impeller, preferably at a diameter representing a mean pressure. The root mean diameter,

$$Drms = \left(\frac{D_{oD}^2 \; D \quad D_{hub}^2}{2} \right)^{1/2}$$ is used below

since it rationally includes influence of the hub ratio.

The capacity at BEP can similarly be calculated as:

$$Q = KA_2V_{2a} = KA_2\phi u$$

A_2 is the discharge area. V_{2a} is the axial component of discharge velocity, which can be expressed as an empirical "capacity coefficient ϕ" times the rms peripheral velocity

K is a unit conversion factor. If Q is given in cubic feet per second, A_2 in square feet, and V_2 in feet per second, K is equal to unity.

If Q is given in gpm, V_2 in feet/second, and A_2 in square inches (usual for small pumps), then $Q = AV/0.321$.

For an example axial pump or fan designed for $N_s = 16,000$, the following values of ψ and ϕ versus B apply. They were used for calculating the example resultant pump-fan performance shown on Figure 6.3-5, as the bi-metallic fan vane camber and discharge angle, B, varied with the temperature. The values given are for a chosen hub/O.D. ratio of approximately 0.4.

Discharge Angle B, degrees	Head Coefficient ψ	Capacity Coefficient ϕ	Power Coefficient $\psi\phi$
40	.205	.58	.121
35	.188	.51	.0958
30	.17	.435	.074
25	.152	.368	.0559
20	.13	.295	.0383
15	.106	.225	.0238
10 *	.078	.156	(0.122 Ref.)*
0 *	.00	.00	----------*

The power coefficient $\psi\phi$ is useful here as a power comparison ratio. Because the fan efficiency remains relatively constant at appreciable values of B, the power expended by a given bi-metallic at a fixed rpm and fluid density will be about proportional to its discharge flow times its head rise, or $\psi\phi$.

* However, at the very low values of vane angles (*), (occurring at low fluid temperature), the pump efficiency will fall rapidly. It will equal zero at B = O°, where the impeller assumes the form of a slotted or "rough" flat disk. The power coefficient $\psi\phi$, which assumes a constant efficiency, then no longer applies.

USAF ZERO DEFECTS

aerospace equipment BORG WARNER®

ENGINEER: RUDDICK
TITLE: FAN VARIABLE PITCH FOR HE MOTOR

PESCO PRODUCTS DIVISION
BORG-WARNER CORP. BEDFORD, OHIO

MODEL: 2749 76-100
DATE OF TEST:

ESTIMATED PERFORMANCE, VARIABLE PITCH BLADES, HELIUM ENVIRONMENT - 3000 PSIA

D_o = 1.75 IN D_i = .70 IN

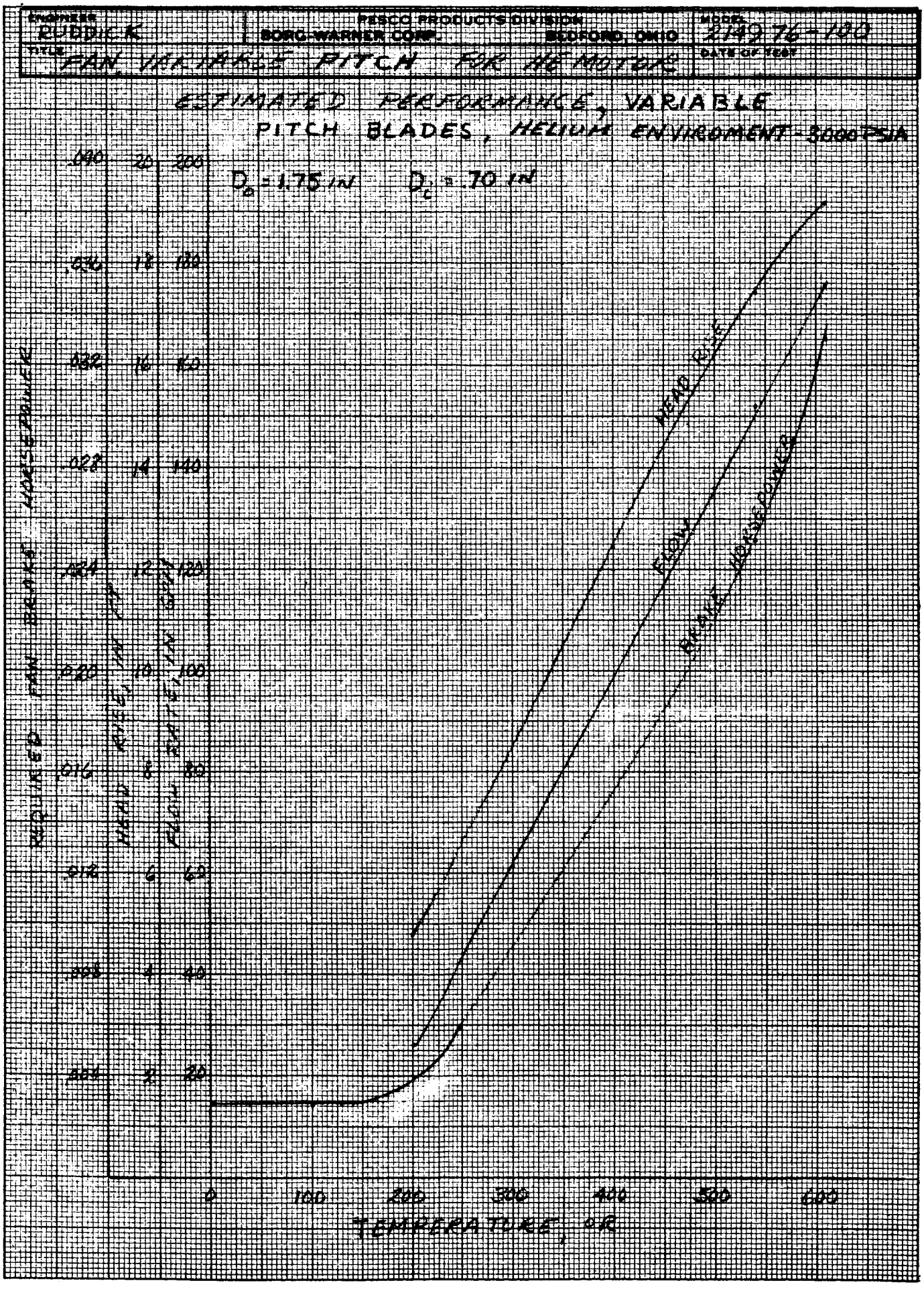

FIG. 6.3-5

For the minimum or zero vane angles, the fluid friction of a flat disk was calculated by conventional disk hydraulic power loss formula, using the fluid properties occurring at low temperature according to the method of Pfleiderer,

$$\text{bhp disk} = K_1 D^2 \quad \gamma u^3 = K_2 \gamma D^5 \quad n^3$$

K_1 or K_2 are empirically derived constants, depending on the Reynolds number derived from disk size, velocity, and fluid Kinematic viscosity under the various fluid conditions.

D	=	disk diameter
u	=	disk peripheral velocity
γ	=	fluid specific weight
n	=	disk rpm

For this purpose, the values of K_1 or K_2 for a smooth disk were multiplied by a figure of 2.0 to estimate the extra fluid losses produced by the radial slots in the "disk" and surface roughness of the blade support arms. There may be appreciable error in this estimate. The actual and critical BHP loss of some example fans with vanes in the flattened condition should be determined experimentally for greater accuracy. The flat vane disk losses will also depend somewhat on the separation of the vane surfaces from stationary walls and the cavity geometry. Consequently, for a given fan or motor, they will be determined most accurately by tests on the particular unit.

The calculated performance, by methods given, of an example fan with bi-metallic vanes at various temperatures in 3000 psia helium is presented in Figure 6.3-5. This is based on the 1.75 inch O.D. 4-bladed fan with solidity of about 0.95, and blades of "Truflex P675R," that was shown in Figure 6.3-3.

Below approximately 200°R, the blades become nearly flat to form a slotted disk and the power requirement becomes relatively constant, as shown on the "Estimated Fan Power Envelope," shown in Figure 6.3-6.

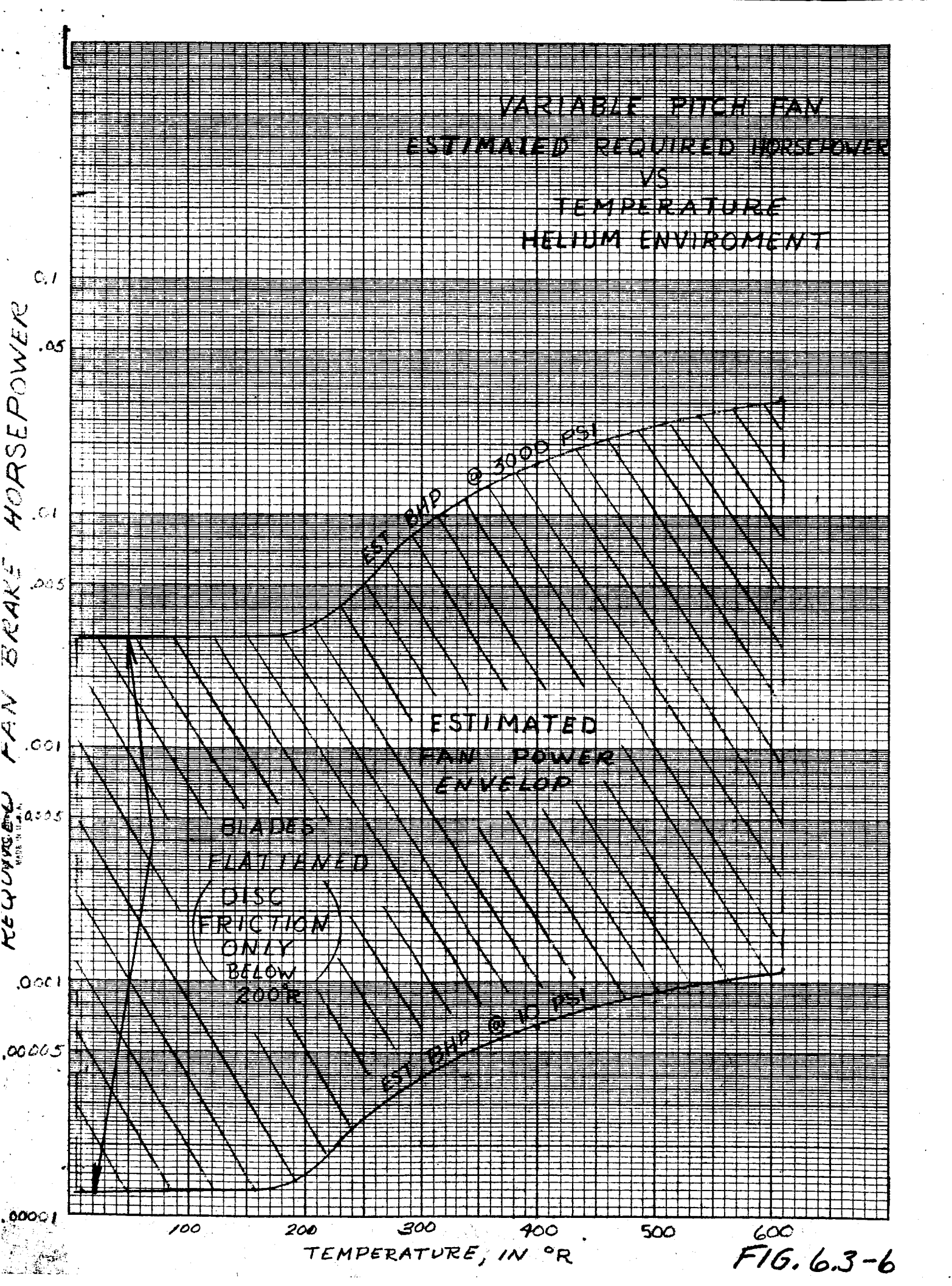
VARIABLE PITCH FAN
ESTIMATED REQUIRED HORSEPOWER
VS
TEMPERATURE
HELIUM ENVIROMENT
FAN BRAKE HORSEPOWER
0.1
.05
.01
.005
.001
.0005
.0001
.00005
.00001
EST BHP @ 300 PSI
EST BHP @ 10 PSI
ESTIMATED
FAN POWER
ENVELOP
BLADES
FLAT PLATED
DISC
FRICTION
ONLY
BELOW
200°R
100
200
300
400
500
600
TEMPERATURE, IN °R

FIG. 6.3-6

The estimated head capacity curve of this same fan with the blades in a high angle position at 610°R, is shown in Figure 6.3-7.

Note that the BHP curve shown, on Figure 6.3-7, is for the helium specific weight of 1.75 pounds per cubic foot. This would occur at 3000 psi at 610°R. For the BHP at other pressures and 610°R, the BHP's on the curve would have to be multiplied by the ratio of the specific weight at that pressure and 610°R to the 1.75 lbs/cu.ft. occurring at 3000 psi. The total head rise (static plus $V^2/2g$) given in feet of fluid being pumped and volumetric flow rate in cfm would remain as shown, regardless of fluid pressure and density, at 610°R. Only the mass flow rate and BHP would vary with density changes, so long as the temperature is maintained constant at 610°R. Head capacity and BHP relations for other temperatures and vane angles can be estimated similarly.

A cooling system flow resistance, when it is expressed in feet head loss, is almost independent of fluid density, but does depend on volumetric flow rate. The exact place where the fan will operate on its head capacity curve for a given temperature and vane angle depends solely on the flow resistance presented by the motor cooling path. This resistance of the flow path is determined by the configuration of the motor cooling path, primarily by its cross sectional area.

Consequently, in order to allow the fan to operate most efficiently, to provide a maximum cooling volumetric or mass flow rate with a minimum expenditure of fan power, it is necessary that the motor cooling flow path (particularly its cross sectional area), be sized according to available fan characteristics. It will be noted from Figure 6.3-7, that if the motor cooling path resistance is increased (by insufficient cross section area), not only will the cooling volumetric flow decrease, but also the BHP required by the fan will increase. An axial fan has an increasing BHP requirement as its flow rate is throttled toward shutoff.

ENGINEER RUDDICK | BORG-WARNER CORP. PESCO PRODUCTS DIVISION BEDFORD, OHIO | MODEL 2/14276-100
TITLE FAN, VARIABLE PITCH FOR MC MOTORS | DATE OF ISSUE 1/19/64

ESTIMATED PERFORMANCE CURVE AT MAX VANE CHAMBER AT 610°R
9600 RPM, 1.75 INCH O.D
.70 INCH HUB

$$N_s = \frac{(RPM)(CFM)^{1/2}}{(FH)^{3/4}} = \frac{9600 \times 23.5^{1/2}}{28.6^{3/4}} = 5200$$

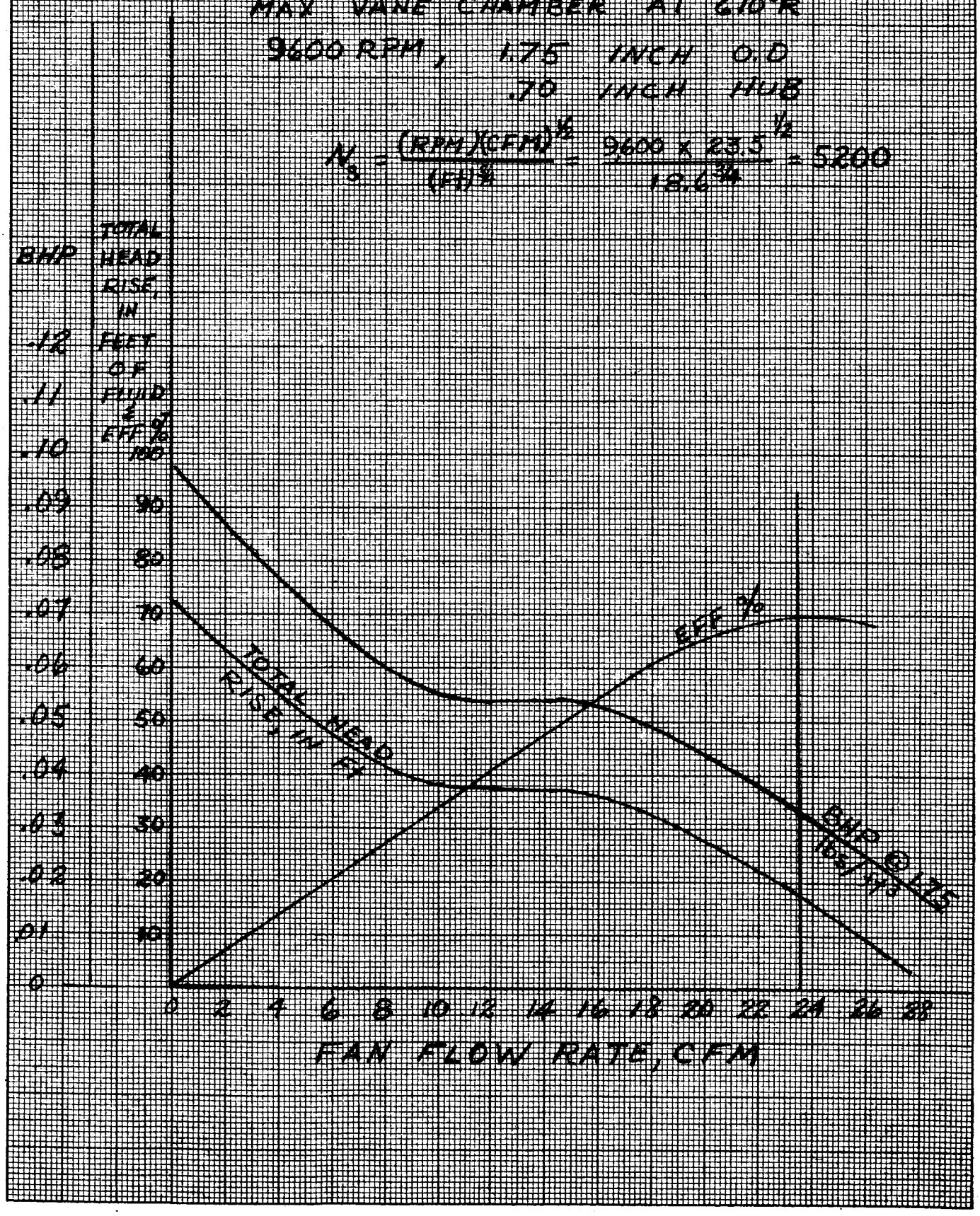

FIG. 6.3-7

Fans for Other Performance Requirements

For fans of other required performance rpm, or power requirements, the fan diameter or bi-metallic blade alloy and thickness can be changed according to the relations given. The geometry of the fan can be changed by varying the number of blades, blade length and resultant camber, or solidity, or by combinations of all of these.

Axial fan and pump blade solidity is the ratio of fan vane effective circumferential length, Le, to circumferential vane spacing S, (solidity = Le/S). It is a factor affecting fan flow rate, pressure rise, and power requirement; along with blade angles, blade camber, hub to O.D. ratio, diameter, and rpm.

As the solidity, or Le/S ratio is increased, from a usual minimum of about 0.4 to a practical maximum of about 1.1, both the pressure rise and power requirement of the axial fan will increase typically by a ratio of about 2 to 1.

Solidities of 0.6 to 0.7 give highest efficiencies for the usual axial flow fan or pump. However, the drop from optimum efficiency on further extending this range, from 0.4 to 1.0 is slight, typically 2% to 4%.

With an axial flow pump, maximum efficiency and optimum performance is obtained with a minimum feasible number of impeller blades. These are typically from 2 blades for low hub O.D. ratio at N_s = 16,000; to 6 blades for high hub ratios at N_s = 8000 - 9000. However, considerable variation from this is feasible with fans, to 20 blades or more, with little drop in performance so long as near optimum blade angles and solidity are maintained. An advantage sometimes occurs in increasing the number of blades while preserving the same blade solidity, angles, and performance, by correspondingly reducing axial blade length. This is, that the length of the fan and fan housing can be reduced, with envelope and weight savings, sometimes also with fabrication simplifications, but without much sacrifice in performance or simplicity.

For a minimum power consumption of a bi-metallic fan in low temperature dense fluid, the following also apply:

1. The blade support arms should be as thin (axially) as feasible, with rounded leading edges and tapered trailing edges. The riveting or brazing of blades to the arms should be as flat as feasible.

2. The blades should not interfere or overlap, to cause local projections, from a "flat disk," in the low temperature flattened conditions. This requires a blade solidity, Le/S of less than one.

3. The blade bi-metallic material, preforming and construction at room temperature should be such that the blades closely approach the form of a flat disk at the lowest temperatures. A slight residual waviness of the blades at the low temperatures is not considered important because of the presence and wake of the blade support arms.

This requires that the blade and support arm entrance angle, B_1, should also be nearly zero at low temperature so that a minimum blade waviness will remain between the leading and trailing edge at low temperatures.

However, because the leading edge of the blade proposed is attached to fixed arms, the blade entrance angle B_1 will remain fixed at a low angle at the higher temperatures, as the blade warpage, camber, discharge angle, flow, and pressure rise of the fan increase.

Normally, as the flow rate of a pump or fan increases, it is desirable to increase the blade entrance angle, B_1, in order to obtain a faborable inlet velocity triangle and reduce the fluid inlet turbulence. Fluid cavitation, pre-rotation and loss of head can otherwise occur.

Cavitation is not a problem in gas or super-critical fluid because there are no gross expansion or contraction of fluid possible in these, from liquid to vapor and vapor to liquid phases, to produce cavitation or its adverse effects.

The other adverse effects of insufficient B_1 are reduced because only a very limited portion of the vane entrance, namely, the vane support and bi-metallic strip immediately following it, have a zero angle. Thus, the limited area of low entrance angle will not have large effect in guiding the fluid compared with the rest of the vane. The residual inlet effects are reduced by rounding the vane-arm entrance. They can be further reduced by providing a small vane entrance angle B_1, that will be present at any temperature; then compensating for it at low temperature by providing a slight negative camber, so that the mean plane of the vanes will still be essentially flat at the low temperature.

6.3.3 Heat Transfer Calculation

The heat transfer rates in each of the flow paths, and then their sum, were calculated by computer.

The motor cooling flow path is shown in Figure 6.3-8 and consists of two annular paths in parallel. One is to the path of V_1, where the velocity V_1 was made constant by using a constant cross section area between the motor stator end turns (1), stator core (2), and the internally fluted motor housing (5). The second path is V_2 - V_3, consisting of two similar sections with velocity, V_2, between the stator end turns and bearing supports, and the narrow annulus V_3 which is the small "air gap" between the stator core (2), and the rotor (3).

The head and head loss across each of these paths is the head of the pump, and is the same. This head loss, in each of these paths, consist of the following: First, entrance contraction and re-expansion losses, usually amounting to about 0.5 $V^2/2g$, Second, "pipe friction" type losses which are the product of $V^2/2g$ times a friction factor which depends on the Reynolds Number, Third, exit losses which are approximately eqaul to $V^2/2g$. (In each case V is the local velocity.)

In the computer program, the head loss across each of these paths was equated and the relative flow rates in each path were found by a computer solution of the resulting quadratic equation, as noted in the outline of the computer program, appended.

A maximum feasible average motor temperature of +350°F was employed, on the basis that 350°F allowed feasible motor performance, also allowed possible local, higher temperature "hot spots" without motor failure.

THERMAL MODEL

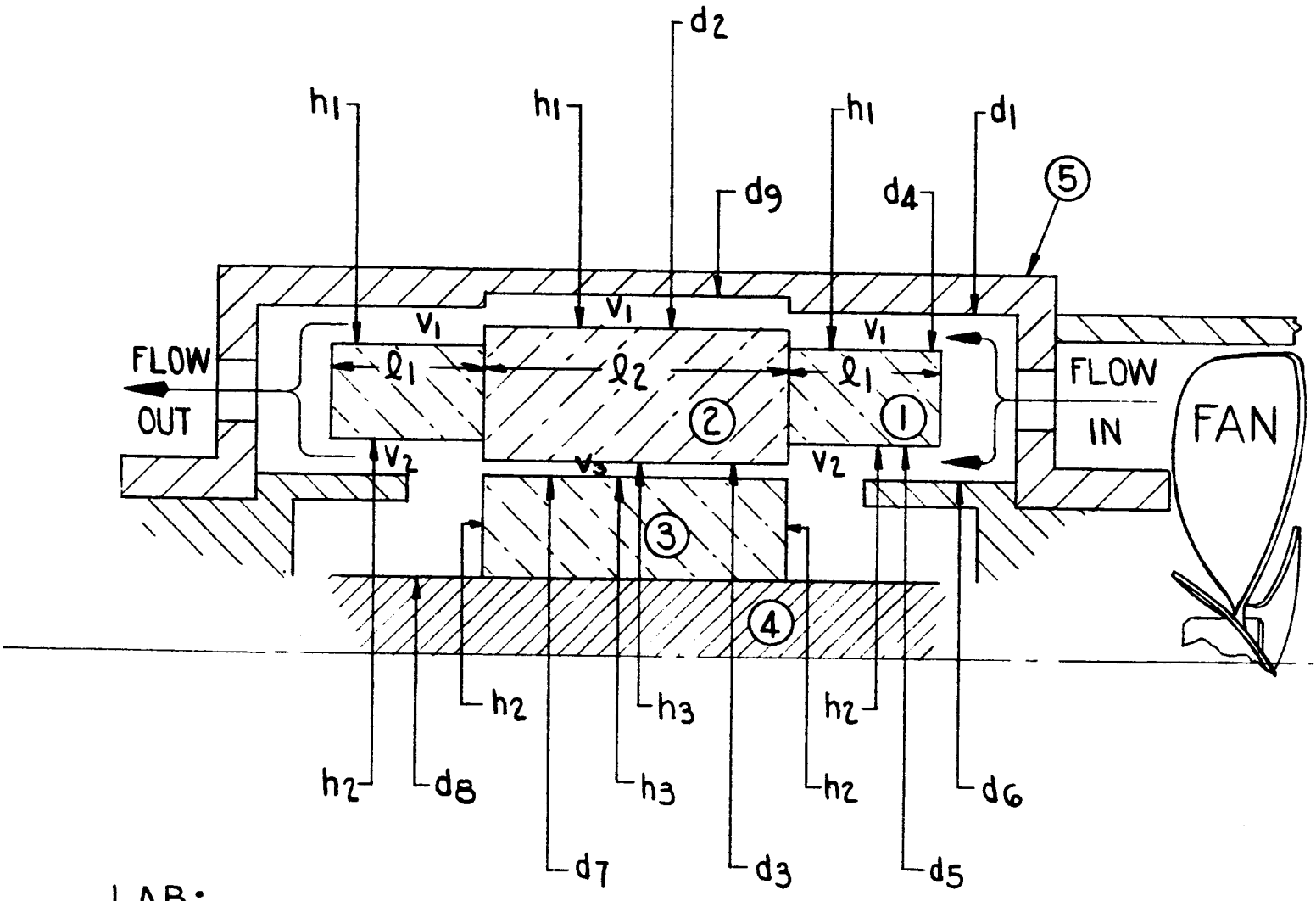

LAB:

1. STATOR WINDINGS
2. CORE
3. ROTOR
4. SHAFT
5. HOUSING

REF
- d_n → RESPECTIVE DIAMETERS
- l_n → RESPECTIVE LENGTHS
- V_n → RESPECTIVE VELOCITIES
- h_n → RESPECTIVE HEAT TRANSFER COEFFICIENTS

USAF ZERO DEFECTS

FIGURE 6.3-8

aerospace equipment BORG WARNER®

Maximum temperature and minimum fluid density conditions of 70°F and 10 psia were employed. Example calculations, which gave higher heat transfer rates and lower motor temperature with higher density fluid, proved that this 70°F 10 psia helium was the worst and critical fluid condition for motor cooling and output.

A selected and preliminary cooling mass flow rate was then fed into the computer, along with a certain value of housing diameter d_2.

The computer then calculated the following according to its programming:

a) The flow areas, flow division, volumetric flow velocity and head drop in the two parallel paths, according to inserted fluid properties the housing I. D., d_2, and consequent flow areas.

b) The heat transfer rate in watts, (according to the previously inserted mass flow rate and fluid properties, and the cooling velocities above). Conventional forced flow heat transfer formulas were employed along with the fluid properties inserted for the particular fluid, temperature, pressure, and density used.

c) Fan approximate N_s, (from above computed volumetric flow rate and head and a previously estimated and inserted motor fan rpm).

If the calculated fan N_s was below about 12,000, this indicated too high a pressure drop and fan head to match fan characteristics at BEP. A larger value of d_2 was then inserted (to increase flow area, flow rate and decrease pressure drop and head) until a suitable value of N_s was found.

Similarly, if the N_s was above about 16,000 (the maximum practicable for the fan) the diameter d_2 was decreased to decrease flow area and flow and increase the head, until the fan N_s value was in a range of 12,000 to 16,000.

d) The maximum fan horsepower was computed (according to above computed flow rate and required head), at the fluid density of 3000 psi and 70°F. This gives the highest and critical fan horsepower with the temperature sensitive bi-metallic fan proposes, (See Figures 6.3-5 and 6.3-6). The fan blade angle decreases to lower its horsepower at lower temperatures. The ratio of density at 3000 psi to that at 10 psi was multiplied by the BHP computed at 10 psia and 70°F conditions to obtain the BHP at 3000 psi and 70°F.

e) The motor performance was then computed by equating watts heat dissipated by the motor at 350°F rise, to watts removed by the cooling mass flow rate.

f) A fan to motor BHP ratio of about 10% was found to give about optimum motor performance in terms of highest BHP output within a useful range of over-all motor efficiency.

Thus if the horsepower drawn by the fan exceeded 10% of the motor BHP output, it indicated that an excessive product of cooling mass flow rate times pressure had been employed, that the fan required was drawing excessive BHP from the motor for good over-all efficiency.

g) The mass flow rate fed into the computer was reduced, and the above process repeated until an acceptable ratio of fan to motor horsepower was reached; achieving a maximum over-all horsepower output within an acceptable level of motor efficiency. An example final computer heat transfer print-out is enclosed as Figure 6.3-9.

INPUT DATA

2.620000	2.313000	1.039000	2.262000	1.070000
0.500000	1.021000	1.000000	1.000000	0.007030
1.250000	0.020500	0.000014	0.049610	0.086000
530.000000	880.000000	0.002790	178.000000	0.700000
20000.000000	0.500000	12.000000	0.024000	0.092000
17.000000	0.022000	0.049000		

OUTPUT DATA

A1	WP1	RH1	A2	WP2
1.37268	15.33726	0.08950	0.70285	4.93230
RH2	**A3**	**WP3**	**RH3**	**B**
0.14250	0.07394	10.34568	0.00715	12728.01250
C	**D**	**E**		
-48514.	4043150.	84179534.		
V1	**RE1**	**F1**	**M3**	**V2**
40.55905	617.47841	0.02591	0.00272	2.11222
RE2	**F2**	**M4**	**V3**	**RE3**
51.19950	0.31250	0.00007	20.07696	24.40935
F3	**DELTA P**	**HP**	**PR**	**H1**
0.65549	0.00108	0.00035	0.72108	10.15181
H2	**H3**	**Q1**	**T3**	**Q2**
0.86989	32.21890	1049.20023	613.55370	923.96514
FH	**NSP**	**Q2P**	**HPP**	
47.73041	14694.12050	270.72179	0.09514	

RESULTS FOR SECOND VALUE OF V

CF

Typical Computer Print-Out for Heat Transfer Rates

FIGURE 6.3-9

COMPUTER PROGRAM

Input Data

(1)	Inside diameter of the housing	d_1	inches
(2)	Outside diameter of the stator core	d_2	inches
(3)	Inside diameter of the stator core	d_3	inches
(4)	Outside diameter of the windings	d_4	inches
(5)	Inside diameter of the windings	d_5	inches
(6)	Outside diameter of the bearing sleeve housing.	d_6	inches
(7)	Outside diameter of the rotor	d_7	inches
(8)	Length of stator winding	l_1	inches
(9)	Length of stator core	l_2	inches
(10)	Density of fluid	ϱ	lbs/cft
(11)	Specific heat of fluid	C_p	BTU/lb°R
(12) or	Viscosity of fluid	μ	centipoises
(12 a) or	Viscosity of fluid	μ_1	lb/sec-ft
(12 b)	Viscosity of fluid	μ_2	lb/hr-ft
(13)	Thermal Conductivity of fluid	k	BTU/hr.ft°R
(14)	Initial temperature of fluid	t_1	°R
(15)	Motor temperature	t_2	°R
(16) or	Fluid mass flow	M_1	lb/sec
(16 a)	Fluid mass flow	M_2	gpm
(17)	Efficiency of the fan	η	
(18)	RPM of the motor	N	rpm
(19)	Shaft diameter	d_8	inches
(20)	Depth of stator slots	d'	inches
(21)	Width of stator slots	e'	inches
(22)	Number of stator slots	S_p	
(23)	Depth of rotor slots	d''	inches
(24)	Width of rotor slots	e''	inches
(25)	Number of rotor slots	S_s	inches

USAF ZERO DEFECTS

aerospace equipment BORG WARNER®

Input Data Adjustments for Inputs (12) and (16)

If input is given as (12)

Step A (12a) = (12) x .000672 $\frac{\text{lb}}{\text{sec-ft}}$

Step A$_1$ (12b) = (12) x 2.42 $\frac{\text{lb}}{\text{hr-ft}}$

or if input is given as (12a)

Step A (12b) = (12a) x 3600 $\frac{\text{lb}}{\text{hr-ft}}$

or if input is given as (12b)

Step A (12a) = (12b) x .000278 $\frac{\text{lb}}{\text{sec-ft}}$

If input is given as (16)

Step B (16a) = (16) x $\frac{1}{\rho}$ x 448.8 gpm = (16) x $\frac{1}{(10)}$ x 448.8 gpm

or if input is given as (16a)

Step B (16) = (16a) x .00223 x ρ = (16a) x .00223 x (10) lb/sec.

USAF ZERO DEFECTS

aerospace equipment BORG WARNER®

Output Data

Note (1) ≡ Input at 1 etc.

(Step 1) ≡ Output of Step 1 etc.

Between housing and stator windings -

(Step 1) Annular area $A_1 = \frac{\pi}{4}(d_1^2 - d_4^2) = \frac{\pi}{4}((1)^2 - (4)^2)$ sq.ins.

(Step 2) Wetted perimeter $WP_1 = (d_1 + d_4) = ((1) + (4))$ ins.

(Step 3) Hydraulic radius $r_{h1} = \frac{A_1}{WP_1} = \frac{\text{Step 1}}{\text{Step 2}}$ ins.

Between windings and bearing sleeve housing,

(Step 4) Annular area $A_2 = \frac{\pi}{4}(d_5^2 - d_6^2) = \frac{\pi}{4}((5)^2 - (6)^2)$ sq.ins.

(Step 5) Wetted perimeter $WP_2 = (d_5 + d_6) = \pi((5) + (6))$ ins.

(Step 6) Hydraulic radius $r_{h2} = \frac{A_2}{WP_2} = \frac{\text{Step 4}}{\text{Step 5}}$ ins.

Between Stator and Rotor

(Step 7) Annular area $A_3 = \frac{\pi}{4}(d_3^2 - d_7^2) + d'e'sp + d''e''S_s$ sq.ins.

$= \frac{\pi}{4}((3)^2 - (7)^2) + (20)(21)(22) + (23)(24)(25)$

(Step 8) Wetted perimeter

$WP_3 = (d_3 + d_7) + 2\,d'Sp + 2\,d''S_s$

$= \pi((3) + (7)) + 2\,(20)(22) + 2\,(23)(25)$ sq.ins.

Step 9 Hydraulic radius $r_{h_3} = \frac{A_3}{WP_3} = \frac{\text{Step 7}}{\text{Step 8}}$ ins.

Step 10 $(B) = \left[\frac{2\ell_1}{r_{h_2}} + \left(\frac{\ell_2}{r_{h_3}} + 1.5\right)\frac{A_2^2}{A_3^2} - 2\frac{A_2}{A_3} + 2\right]$

$= \left[\frac{2\,(8)}{\text{Step 6}} + \left(\frac{(9)}{\text{Step 9}} + 1\right)\frac{\text{Step 4}^2}{\text{Step 7}^2} - 2\frac{\text{Step 4}}{\text{Step 7}} + 2\right]$

Step 11 $(C) = \frac{2\ell_1 + \ell_2}{r_{h_1}} + 1 - (B)\frac{A_1^2}{A_2^2}$

$= \frac{2\,(8) + (9)}{\text{Step 3}} + 1 \text{ Step 10} \frac{\text{Step 1}^2}{\text{Step 4}^2}$

Step 12 $(D) = \frac{288\,M_1A_1}{\rho A_2^2} (B) = \frac{288\,(16)\,\text{Step 1}}{(10)\,\text{Step 4}^2}$ Step 10

Step 13 $(E) = \frac{-(144)^2M_1^2}{\rho^2 A_2^2} (B) = -\frac{(144)^2\,(16)^2}{(10)^2\,\text{Step 4}^2}$ Step 10

Between Housing and Stator Windings -

Step 14 Velocity $V_1 = \frac{-D \pm \sqrt{D^2-4CE}}{2C} = \frac{-\text{Step 12} \pm \sqrt{\text{Step 12}^2 - 4\,\text{Step 11}\,\text{Step 13}}}{2\,\text{Step 11}}$ ft/sec.

NOTE: Reject -ve values, use +ve values. If both the values are +ve, all the following output steps would have to be performed twice, and the steps recorded as Step 15 and Step 15a et cetera.

USAF ZERO DEFECTS

aerospace equipment BORG WARNER®

Step 15 Reynolds number $R_{e_1} = \frac{4 r_{h_1} \rho V_1}{12 \mu_1} = \frac{\text{Step 3} \cdot 10 \cdot \text{Step 14}}{3 \cdot 12a}$

Step 16 Friction Factor $f_1 = \frac{16}{R_{e_1}} = \frac{16}{\text{Step 15}}$ if Step 15 $< 10^3$

$= .016$ for $R_{e_1} =$ Step 15 $= 10^3$

$= .0086$ for $R_{e_1} =$ Step 15 $= 10^4$

$= .005$ for $R_{e_1} =$ Step 15 $= 10^5$

$= .0035$ for $R_{e_1} =$ Step 15 $= 10^6$

$= .0025$ for $R_{e_1} =$ Step 15 $= 10^7$

and linear interpolation in between.

Step 17 Mass flow $M_3 = \rho \frac{A_1}{144} V_1 = 10 \frac{\text{Step 1}}{144} \text{Step 14}$ lb/sec.

Between windings and bearing sleeve housing,

Step 18 Velocity $V_2 = \frac{144 M_1}{\rho A_2} - \frac{A_1}{A_2} V_1 = \frac{144 \cdot 16}{10 \cdot \text{Step 4}} - \frac{\text{Step 1}}{\text{Step 4}} \text{Step 14}$ ft/sec.

Step 19 Reynolds number $R_{e_2} = \frac{4 r_{h_2} \rho V_2}{12 \mu_1} = \frac{\text{Step 6} \cdot 10 \cdot \text{Step 18}}{3 \cdot 12a}$

Step 20 Friction factor f_2 = (Same procedure as for Step 16)

Step 21 Mass flow $M_4 = \rho \frac{A_2}{144} V_2 = 10 \frac{\text{Step 4}}{144} \text{Step 18}$ lb/sec.

USAF ZERO DEFECTS

aerospace equipment BORG WARNER®

Between Stator and Rotor

(Step 22) Velocity $V_3 = \frac{A_2 V_2}{A_3} = \frac{\text{(Step 4)}\ \text{(Step 18)}}{\text{(Step 7)}}$ ft/sec.

(Step 23) Reynolds number $R_{e_3} = \frac{4\, r_{h_3}\, \rho\, V_3}{12\, \mu_1} = \frac{\text{(Step 9)}\ \text{(10)}\ \text{(Step 22)}}{3\ \text{(12a)}}$

(Step 24) Friction factor f_3 = (Same procedure as for (Step 16))

(Step 25) Fluid pressure loss $\Delta p = \left(\frac{\rho f_1}{2 g_c}\right)\left(\frac{V_1^2}{r_{h_1}}\right)(2\ell_1 + \ell_2)\ \frac{1}{144}$

$= \frac{\text{(10)}\ \text{(Step 16)}\ \text{(Step 14)}^2\ (2\text{(8)} + 9)}{64.4 \times 144\ \text{(Step 3)}}$ psi

(Step 25a) Head to be developed by fan H

$= \frac{\Delta p \times 144}{\rho} + \frac{V_1^2}{2g}$

$= \frac{\text{(Step 25)} \times 144}{\text{(10)}} + \frac{\text{(Step 14)}^2}{64.4}$ ft.

(Step 26) HP required to drive the fan

$HP = \frac{M_1}{\eta \times 550}\left(\frac{\Delta p \times 144}{\rho} + \frac{V_1^2}{2g}\right)$

$= \frac{\text{(16)}}{\text{(17)} \times 550}\left(\frac{\text{(Step 25)} \times 144}{\text{(10)}} + \frac{\text{(Step 14)}^2}{64.4}\right)$ hp

(Step 27) Prandtl number for fluid $P_r = \frac{C_p \mu_2}{K} = \frac{\text{(11)}\ \text{(12b)}}{\text{(13)}}$

Heat Transfer Coefficients

Step 28 Between housing and stator windings h_1

$$h_1 = \frac{.023\, C_p \rho\, V_1 \times 3600}{(R_{e_1})^{0.2}\,(P_r)^{2/3}} \cdot \frac{82.8\,(11)(10)(\text{Step 14})}{(\text{Step 15})^{0.2}\,(\text{Step 27})^{2/3}} \quad \text{BTU/hr.ft}^2\text{°R}$$

Step 29 Between windings and bearing sleeve housing h_2

$$h_2 = \frac{.023\, C_p \rho\, V_2 \times 3600}{(R_{e_2})^{0.2}\,(P_r)^{2/3}} \cdot \frac{82.8\,(11)(10)(\text{Step 18})}{(\text{Step 19})^{0.2}\,(\text{Step 27})^{2/3}} \quad \text{BTU/hr.ft}^2\text{°R}$$

Step 30 Between the stator and the rotor

$$h_3 = \frac{.023\, C_p \rho\, V_3 \times 3600}{(R_{e_3})^{0.2}\,(P_r)^{2/3}} \left(\frac{\left[V_3^2 + \left(\frac{\pi d_7 N}{12 \times 60} \right)^2 \right]^{1/2}}{V_3} \right)^{0.8}$$

$$= \frac{82.8\,(11)(10)(\text{Step 22})^{0.2}}{(\text{Step 23})^{0.2}\,(\text{Step 27})^{2/8}} \left[(\text{Step 22})^2 + \left(\frac{\pi}{720}\,(7)(18) \right)^2 \right]^{0.4} \quad \text{BTU/hr.ft}^2\text{°R}$$

Step 31 Total heat picked up Q_1 (1st approximation)

$$Q_1 = 2h_1 \frac{\pi d_4 l_1}{144}(t_2 - t_1) + h_1 \frac{\pi d_2 l_2}{144}(t_2 - t_1)$$

$$+ 2h_2 \frac{\pi d_5 l_1}{144}(t_2 - t_1) + \frac{2h_2}{144}\,\frac{\pi}{4}\,(d_7^2 - d_8^2)(t_2 - t_1)$$

$$+ 2h_3 \frac{\pi d_7 l_2}{144}(t_2 - t_1) \quad \text{BTU/hr.}$$

$$= \left[(15) - (14) \right) \frac{\pi}{144} \left][\text{Step 28} (2\,④⑧ + ②⑨) + \text{Step 29} \left\{ 2\,⑤⑧ + \frac{1}{2} (⑦^2 - ⑲^2) \right\} + 2\,⑦⑨\ \text{Step 30} \right] \text{BTU/hr.}$$

Step 32 Final temperature of the fluid t_3

$$= \frac{Q}{3600 M_1 C_p} + t_1 = \frac{\text{Step 31}}{3600\,⑯\,⑪} + ⑭ \ ^\circ R$$

Step 33 Total heat picked up Q_2 (Corrected)

$$Q_2 = Q_1 \frac{(t_2 - \frac{t_1 + t_3}{2})}{(t_2 - t_1)} = \text{Step 31} \frac{(15) - \frac{⑭ + \text{Step 32}}{2}}{(15) - (14)} \text{ BTU/hr.}$$

Step 34 Specific Speed $N_s = \frac{N (M_2)^{1/2}}{H^{3/4}}$

$$= \frac{⑱\,⑯a^{1/2}}{\text{Step 25a}^{3/4}}$$

Computational Explanations

$$M_3 = \frac{\rho A_1}{144} V_1 \text{ lb/sec.}$$

$$M_4 = \frac{\rho A_2}{144} V_2 = \frac{\rho A_3}{144} V_3 \text{ lb/sec.} \quad \therefore A_2 V_2 = A_3 V_3$$

Total mass flow, $M_1 = M_3 + M_4 = \frac{\rho}{144}(A_1V_1 + A_2V_2)$ lb/sec.

$\Delta h = \Delta h$ for two flows (no assumptions)

$$\frac{f_1 \ell_1 V_1^2}{2g_c r_{h_1}} + \frac{f_1 l_2 V_1^2}{2g_c r_{h_1}} + \frac{f_1 \ell_1 V_1^2}{2g_c r_{h_1}} + \underbrace{\frac{V_1^2}{2g_c}}_{\text{vel. head}}$$

$$= \frac{f_2 \ell_1 V_2^2}{2g_c r_{h_2}} + \underbrace{\frac{V_3^2 - V_2^2}{2g_c} + \frac{.5V_3^3}{2g_c}}_{\text{contract. loss}} + \frac{f_3 l_2 V_3^2}{2g_c r_{h_3}} + \underbrace{\frac{V_2^2 - V_3^2}{2g_c} + \frac{(V_3 - V_2)^2}{2g_c}}_{\text{exp. loss}}$$

$$+ \frac{f_2 \ell_1 V_2^2}{2g_c r_{h_2}} + \underbrace{\frac{V_2^2}{2g_c}}_{\text{vel. head}}$$

assume $f_1 = f_2 = f_3$ in the 1st instant.

$$V_1^2 \left(\frac{2\ell_1 + l_2}{r_{h_1}} + 1 \right) = \frac{2l_1 V_2^2}{r_{h_2}} \quad \frac{l_2 V_3^2}{r_{h_3}} + 1.5\, V_3^2 - 2\, V_2 V_3 + 2\, V_2^2$$

$$= \frac{2l_1 V_2^2}{r_{h_2}} + \left(\frac{A_2}{A_3} V_2\right)^2 \left(\frac{l_2}{r_{h_3}} + 1.5\right) - 2V_2 \left(\frac{A_2}{A_3} V_2\right) + 2V_2^2$$

$$= \left(\frac{2l_1}{r_{h_2}} + \frac{l_2}{r_{h_3}} \cdot \frac{A_2^2}{A_3^2} + 1.5 \frac{A_2^2}{A_3^2} - \frac{2A_2}{A_3} + 2 \right) V_2^2$$

$$= \underbrace{\left[\frac{2l_1}{r_{h_2}} + \frac{A_2^2}{A_3^2} \left(\frac{l_2}{r_{h_3}} + 1.5 \right) - 2 \frac{A_2}{A_3} + 2 \right]}_{(B)} \left(\frac{144\, M_1}{\rho A_2} - \frac{A_1 V_1}{A_2} \right)^2$$

USAF ZERO DEFECTS

aerospace equipment BORG WARNER®

$$V_1^2 \left(\frac{2l_1 + l_2}{r_{h_1}} + 1 \right) = (B) \left(\frac{144 M_1}{\rho A_2} - \frac{A_1 V_1}{A_2} \right)^2$$

$$= (B) \left(\frac{(144)^2 M_1^2}{\rho^2 A_2^2} - \frac{288 M_1 A_1 V_1}{\rho A_2^2} + \frac{A_1^2 V_1^2}{A_2^2} \right)$$

$$V_1^2 \left(\frac{2l_1+l_2}{r_{h_1}} + 1 - (B) \frac{A_1^2}{A_2^2} \right) + \frac{288 M_1 A_1 V_1}{\rho A_2^2} (B) - \frac{(144)^2 M_1^2}{\rho^2 A_2^2} (B) = 0$$

$$(C) = \frac{2l_1 + l_2}{r_{h_1}} + 1 - (B) \frac{A_1^2}{A_2^2}$$

$$(D) = \frac{288 M_1 A_1 V_1}{\rho A_2^2} (B)$$

$$(E) = - \frac{(144)^2 M_1^2}{\rho^2 A_2^2} (B)$$

and

$$V_1 = \frac{-(D) \pm \sqrt{(D)^2 - 4 (C) (E)}}{2 (C)}$$

USAF ZERO DEFECTS

aerospace equipment BORG WARNER®

6.4 Effects of Fluids

The fluid present in the motor must be considered for its electrical, thermal, and physical behavior.

For purposes of this study only, helium has been considered to any great degree, however, some general relationships can be offered and the listed characteristics can be evaluated from existing data. The more common cryogenic fluids, LOX, LH_2, LN_2 and LHe are compared below for the various factors which could affect their use.

The dielectric properties of these fluids compared to air are listed below:

Fluid	Air	O_2	N_2	H_2	He
Dielectric Strength rms volts/mill (gas @ 1 atmos.)	56	53.2	65	48.6	
Dielectric Constant (gas @ 1 atmos.)	1.0006	1.0005	1.00052	1.00025	1.000065
Dielectric Constant (liquid 1 atmos.)		1.142	1.443	1.227	1.048

Although there are variations, none of these values cause any particular problem especially for induction motors and since conductive paths are normally insulated with dielectric materials such as glass and/or teflon.

Thermally each fluid must be evaluated in its specific application for both its ability to conduct and absorb heat and the power required to establish the necessary flow and pressure.

Physically the fluid, whether liquid or gas, presents losses due to frictional drag on rotating parts. This basic loss can be considered in two parts; disk friction due to the ends of the motor rotor and cylinder losses realized at the rotor O.D. in the air gap area.

The basic accepted relationship for fluid losses is -

$$HP = K\, w\, N^3 D^5$$

where K = Operational function based on Reynolds number

w = Fluid density

N = rpm

D = rotor diameter

Since K involves both the Reynolds number and friction factors due to surface conditions, an accurate theoretical approach is questionable especially for the transition and turbulent flow conditions.

Using the basic equation and connecting terms the fluid loss is expressed in watts as -

$$W = (K_1 + K_2)\ \frac{w}{g}\ N^3 D^5$$

where K_1 is the disk friction coefficient

K_2 is the cylinder friction coefficient

g acceleration of gravity ft/sec^2

w fluid density lbs/ft^3

N rpm

D diameter of rotor ft.

The K_1 and K_2 coefficients are taken from curve Figure 6.4-1 plotted against the Reynolds number where the Reynolds number

$$N_R = 2620 \frac{ND^2}{v \times 10^5}$$

and v = Kinematic viscosity ft^2/sec other parameters same as above. As noted on the curve, a broad band represents K_2 and must be interpreted as a function of the rotor length to rotor radial clearance ratio $\frac{b}{c}$.

It should be noted that this curve is a result of a theroetical analysis modified by limited test data. Therefore, it can be used to obtain approximate values only. In the turbulent range similarity to published data for pipe flow has been used to estimate the shapes of the curves. To establish a reliable fluid loss prediction method friction factors must be clearly defined and considerable test work should be accomplished.

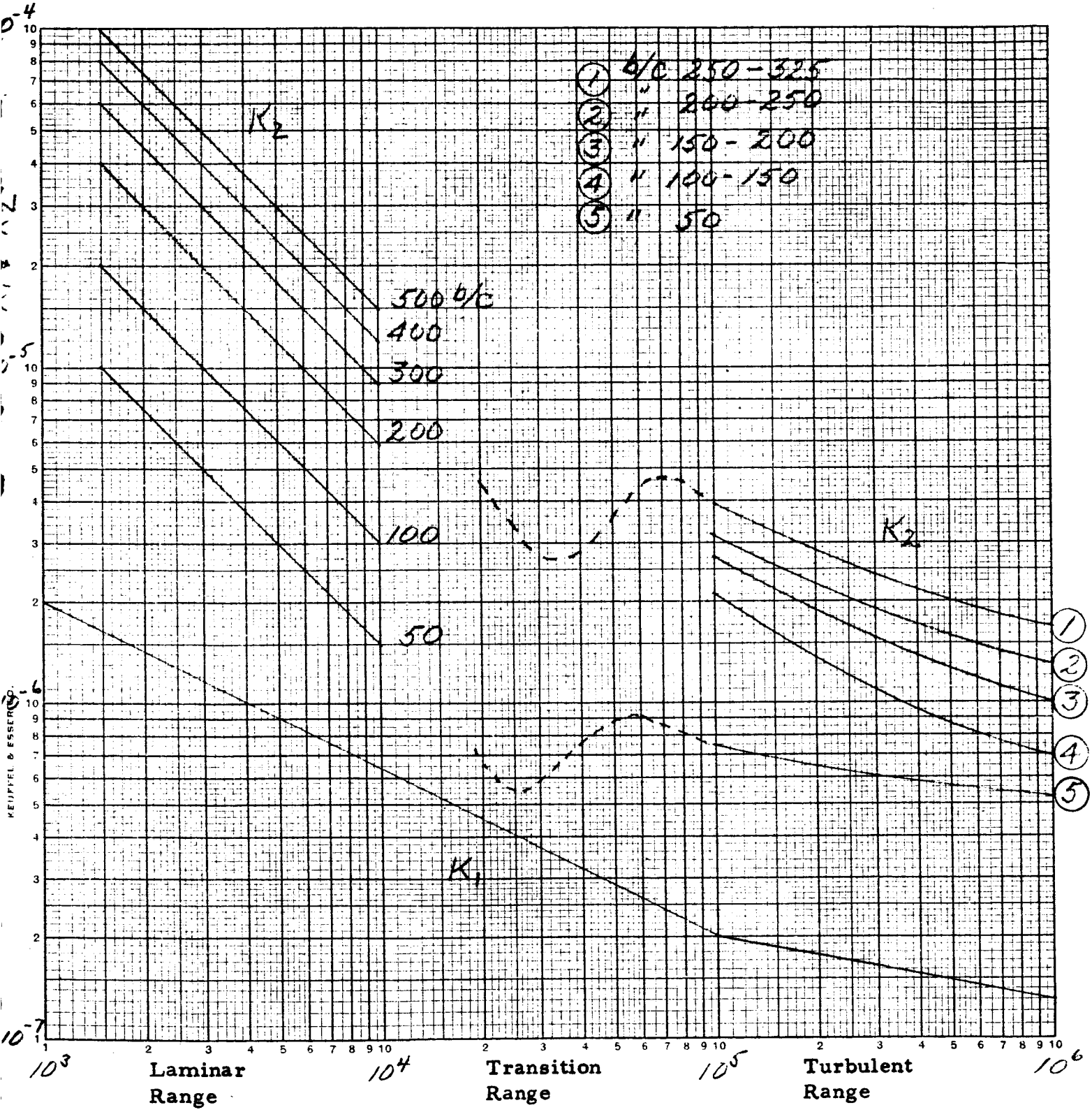

N_R (Reynolds Number)
Fluid Loss Coefficients

FIGURE 6.4-1

6.5 Test Description and Results

6.5.1 Test Scope

The purpose of this test was to determine if a particular set of bearings could operate over a temperature range of from -425°F to +300°F for a minimum operation time of ten hours at each ambient in order to verify the integrity of the bearing design and mounting arrangement.

6.5.2 Test Description

Two prototype motors, weight 2 lbs. -7 ozs. with instrumentation and leads, were assembled using Barden SR4ABSS bearings. See Figures 6.5-1 and 6.5-2 for assembled and detailed views. Copper-constantan thermocouples were inserted in the bearing sleeves and iron-constantan thermocouples were inserted in the stator core, windings, and rotor-stator gap, as is shown in the instrumentation schematic, Figure 6.5-3. Each unit was mounted to a flange, designed specifically for this test, and placed in the test dewar in a horizontal position (see Figures 6.5-4 and 6.5-5). A two-phase test was performed on each unit, at no load condition. Phase A was in helium gas at room ambient pressure and temperature and Phase B was in liquid hydrogen at ambient pressure and -425°F, each phase with ten hours run time. For the first unit, the sequence was Phase A, then Phase B. For the second unit, the sequence was reversed, this being done to see if the direction of temperature change could affect the bearing performance. Each phase had 50 on-off cycles performed during the last two hours. Parameter data was recorded every five minutes during the first hour, every fifteen minutes during the next seven hours, and for all on-off cycles. The on-off cycle times were ten seconds long. The following parameters were monitored during the test:

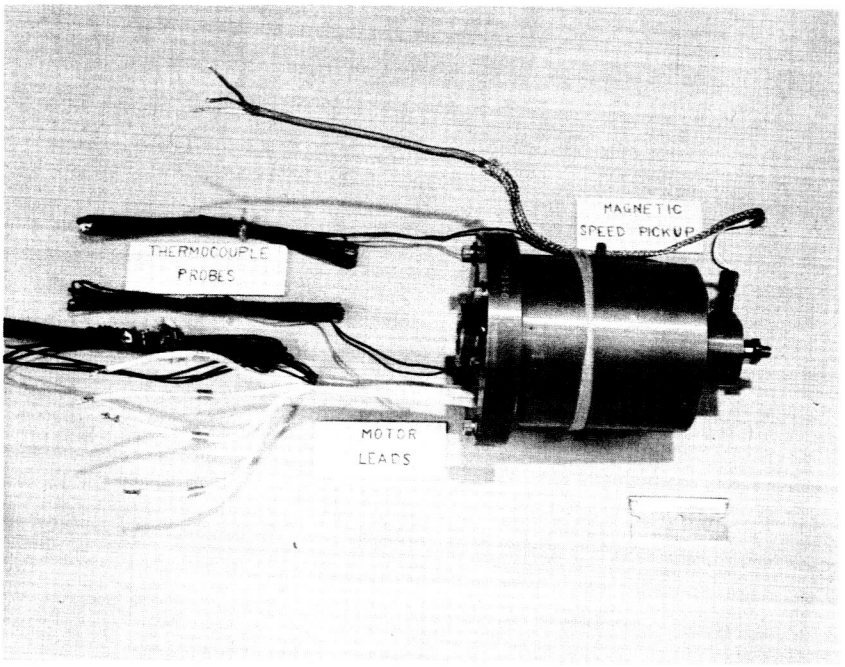

Test Motor
Figure 6.5-1

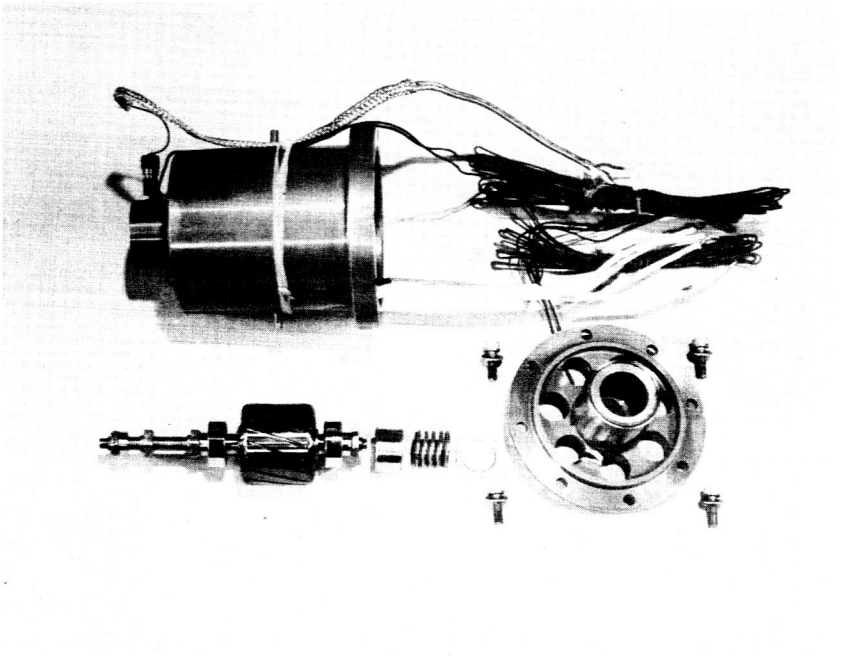

Test Motor - Disassembled
Figure 6.5-2

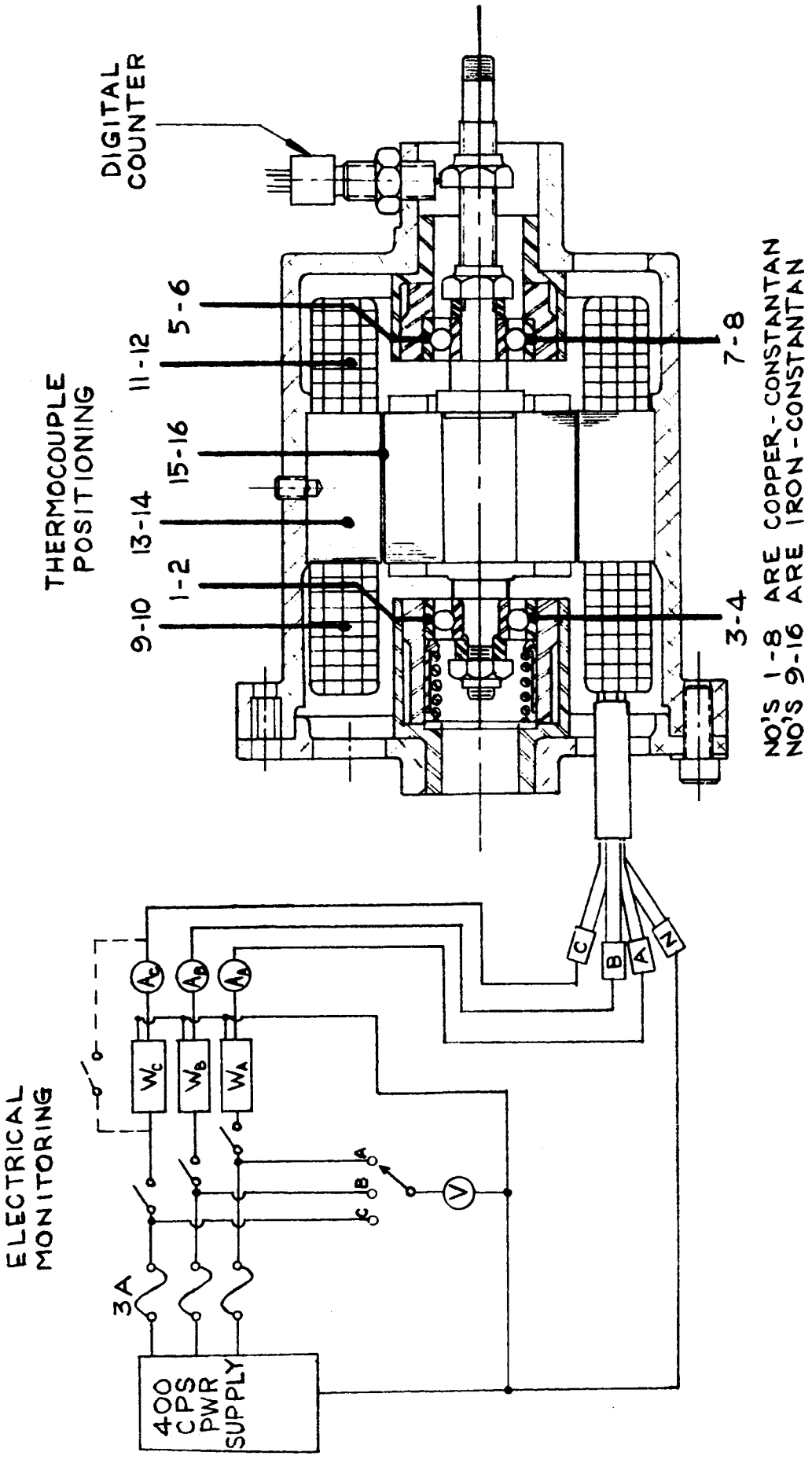

Instrumentation Schematic

FIGURE 6.5-3

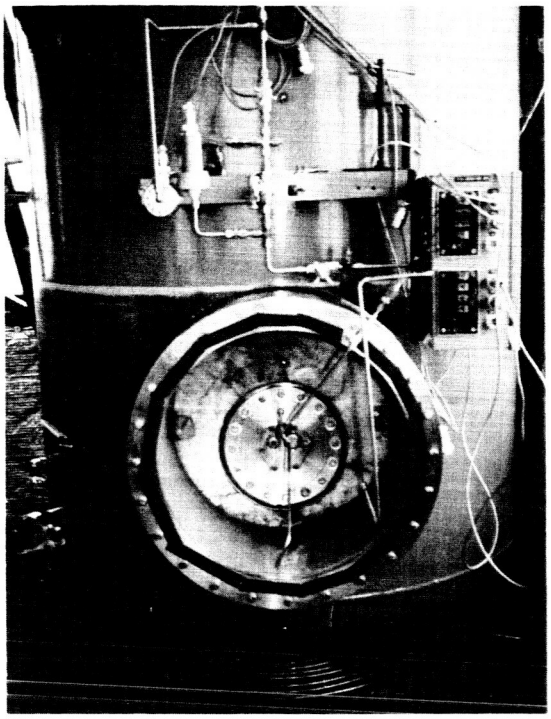

Test Dewar - Flange Mounted
Figure 6.5-4

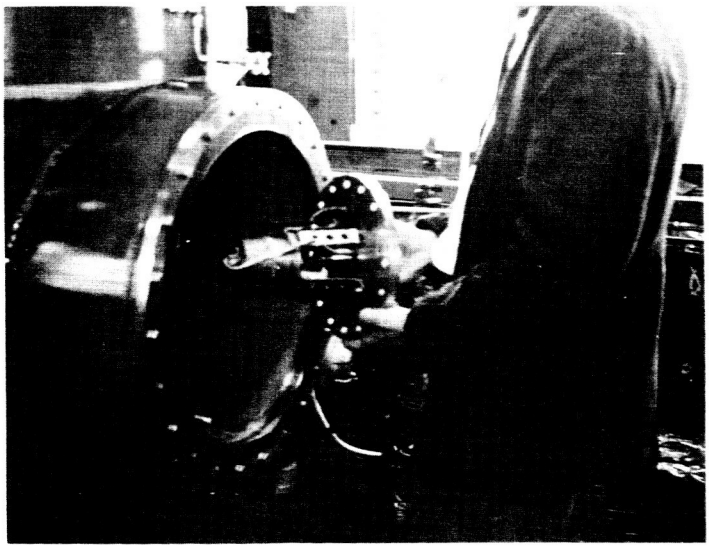

Horizontal Mounting
Figure 6.5-5

a) Phase voltage (L-N)
b) Phase current
c) Phase wattage
d) Core and windings temperatures
e) Bearing temperatures
f) Speed
g) Spin down time
h) Dewar pressure

6.5.3 Test Results

6.5.3.1 First Test Unit

6.5.3.1.1 Phase A (Gaseous Helium)

Phase voltages (L-N) were held constant at 120 volts. This in turn established the bearing temperatures at 180°F to 185°F and the stator core, windings, and air gap temperatures at 200°F to 205°F upon reaching equilibrium. Phase currents were balanced in the range of 0.8 to 0.85 amperes. Phase wattages were unbalanced and one phase reading was low with respect to the other two. Verification of balanced windings was made by comparing winding resistance, insulation resistance, and dynamic run checks before and after testing. The following comments are given as possible explanations for the unbalanced wattage readings:

1. Since this is a low power unit with a low power factor (less than 0.5), wattage readings are difficult to monitor, and

2. The instrumentation is a remote system with the test cell located some distance from the instrumentation, thus having many soldered connections between the wattmeter transducer and the output point.

The speed was constant at 11880 rpm. Reference to Figures 6.5-6a and 6.5-6d through i give a detailed analysis of the reduced data for this phase of testing.

BORG WARNER **Pesco Products**
DIVISION OF BORG-WARNER CORPORATION

CRYOGENI
TEST

HELIUM MOTOR Unit

Unit Ser. No. 1
Date of Test 2-22-66
Ltr. No. 608

TIME	SEQUENCE OF EVENTS
	2-22-66 RUN B5-2-38
07:45	START DEWAR EVACUATION
11:15	STOP DEWAR EVACUATION
11:20	AMBIENT HELIUM PURGE
11:35	START OF PHASE A
12:37	STOP - 62 MIN.
13:10	START
13:20	STOP - 10 MIN.
13:50	START
14:00	STOP - 10 MIN.
14:20	START
16:00	STOP - 1HR - 40 MIN.
	2-23-66 RUN: B5-2-3
09:15	RESUME PHASE A
14:30	STOP - 5HR - 15 MIN.
14:33	START ON-OFF CYCLES (10 SEC.
16:00	STOP - COMPLETED 19 CYCLES -
	2-24-66 RUN B5-2-4
08:20	RESUME PHASE A
09:20	STOP - 1HR
09:25	START - ON-OFF CYCLES (10 SEC.
10:06	STOP - COMPLETED 10 CYCLES - 1M
10:30	START - ON-OFF CYCLES (10 SEC.
11:48	STOP - COMPLETED 21 CYCLES -
13:18	START
13:54	STOP - END PHASE A - 34

C LABORATORY
LOG SHEET

Sr. Tech. BOB DOLSEN
Test Cell B5-2
Aux. Drive —
Test Cell Amb. Temp. 70 °F
Barometric Press. — " Hg
Pump Fluid HELIUM GAS

UN

	ACCUM. RUN TIME	Time of Data Point	Dewar Press. PSIG	Pur Sta
	1 HR. 2 MIN			
	1HR-12 MIN			
	1HR-22 MIN			
	3HR- 2 MIN			
9				
	8HR- 17 MIN			
EACH CYCLE)				
3 MIN.- 20 SEC.	8HR- 20MIN- 20 SEC.			
0				
	9HR- 20 MIN- 20 SEC.			
EACH CYCLE)				
IN- 40 SEC	9HR- 22 MIN-			
EACH CYCLE)				
3 MIN- 30 SEC.	9HR- 25 MIN- 30 SEC			
IN— 30 SEC.	10 HR			
		2		

FIGURE 6.5-6 a

Type of Test BEARING Sheet 1 of 3

Unit Ser. No. 1 Date 2-22-66

Run No. 85-2- Phase A Thru

Total Running Time 10 HR ~~Min.~~ ~~Sec.~~

Technicians DOLSEN, PEDACI, STILES

Total Seal Leakage — Cu. In.

IT SEAL DATA

np Seal Leakage tic-Cu In/Min.	Pump Seal Leak. Dyna. - Cu In/Min	Mtr. Cover Seal Leak. Cu In/Min.	External Leak. Cu In/Min.

BORG-WARNER **Pesco Products**
DIVISION OF BORG-WARNER CORPORATION

CRYOGEN
TEST

HELIUM MOTOR Unit

Unit Ser. No. 1
Date of Test 2-25-66
Ltr. No. 608

	TIME	SEQUENCE OF EVENTS
		2-25-66 RUN B5-2-
	08:45	START DEWAR EVACUATION
	09:20	STOP DEWAR EVACUATION
	09:25	AMBIENT PRESSURE CHECK
	09:30	START LH_2 FILL
	09:50	START PHASE B
	10:50	STOP - 1HR
	11:05	START
	12:50	FILL LH_2
	15:35	STOP 4HR - 30 MIN
	15:45	DUMP LH_2

C LABORATORY
LOG SHEET

Sr. Tech. BOB DOLSEN
Test Cell 85-2
Aux. Drive —
Test Cell Amb. Temp. 70 °F
Barometric Press. — " Hg
Pump Fluid LIQUID HYDROGEN

UNI

	ACCUM. RUN TIME	Time of Data Point	Dewar Press. PSIG	Pump Stat
41				
			10	
	1 HR			
			0	
			0	
	5HR-30MIN			
	2			

FIGURE 6.5-6 b

Type of Test BEARING EVALUATION Sheet 2 of 3
Unit Ser. No. 1 Date 2-25-66
Run No. 85-2- Phase B Thru
Total Running Time 10 HR ~~Min.~~ ~~Sec.~~
Technicians DOLSEN, PEDACI, STILES

Total Seal Leakage — Cu. In.

SEAL DATA

Seal Leakage c-Cu In/Min.	Pump Seal Leak. Dyna. - Cu In/Min	Mtr. Cover Seal Leak. Cu In/Min.	External Le Cu In/Mir

Pesco Products
DIVISION OF BORG-WARNER CORPORATION

CRYOGEN
TEST

HELIUM MOTOR Unit

Unit Ser. No. 1
Date of Test 2-28-66
Ltr. No. 608

	TIME	SEQUENCE OF EVENTS
		2-28-66 RUN B5-2-42
	07:50	START DEWAR EVACUATION
	08:40	STOP DEWAR EVACUATION
	08:45	AMBIENT LEAK CHECK
	08:50	START LH_2 FILL
	09:20	START PHASE B
	11:15	FILL LH_2
	11:50	STOP 2HR - 30 MIN
	12:00	START - ON-OFF CYCLES (10 SEC
	13:37	STOP 8 MIN - 33 SEC
	13:38	START
	15:30	STOP 1HR - 51MIN - 27 SEC
	14:17	FILL LH_2
	15.50	DUMP LH_2

IC LABORATORY
LOG SHEET

Sr. Tech. BOB DOLSEN
Test Cell B5-2
Aux. Drive —
Test Cell Amb. Temp. 70 °F
Barometric Press. — " Hg
Pump Fluid LIQUID HYDROGEN

	ACCUM. RUN TIME	Time of Data Point	Dewar Press. PSIG
			10
	8 HR		
EACH CYCLE)			
	8 HR 8 MIN - 33 SEC.		
	10 HR		
			2

FIGURE 6.5-6 c

Type of Test BEARING EVALUATION Sheet 3 of 3
Unit Ser. No. 1 Date 2-28-66
Run No. 85-2- Phase B Thru —
Total Running Time 10 HR ~~Min.~~ ~~Sec.~~
Technicians
DAESEN, PEDACI, STILES

Total Seal Leakage — Cu. In.

UNIT SEAL DATA

Pump Seal Leakage Static-Cu In/Min.	Pump Seal Leak. Dyna. - Cu In/Min	Mtr. Cover Seal Leak. Cu In/Min.	External Le Cu In/Min

PESCO PRODUCTS DIVISION
BORG-WARNER CORPORATION

HE

PHASE A HELIUM GAS	START	RUN 85-2-38		
DATA POINTS - HR:MIN	:05	:10	:15	:20
DEWAR PRESS - PSIG	0	(CONSTANT FOR E		
VOLTAGE - L-N				
PHASE A	120			
PHASE B	120			
PHASE C	120			
CURRENT - AMPS				
PHASE A	.87	.87	.87	.86
PHASE B	.96	.91	.90	.90
PHASE C	.86	.86	.86	.84
WATTAGE - WATTS				
PHASE A	33.5	41.5	41.5	40.5
PHASE B	46	42.5	42.3	41.5
PHASE C	39	39.6	39	37.5
SPEED - RPM	11880 ± 5 RPM			
SPIN DOWN TIME - MIN				
FREQUENCY - CPS				
TEMPERATURES - °F				
FRONT BEARING	55	86	113	133
REAR BEARING	55	83	112	129
FRONT WNDG TURNS	55	108	134	152
REAR WNDG TURNS	56	107	134	152
STATOR CORE	55	108	134	134
AIR GAP	56	105	132	150

++ INSTRUMENTATION TROUBLE - BELL

LIUM MOTOR TEST DATA

:25	:30	:35	:40	:45	:50	:55
NTIRE TEST)						
.85	.85	.85	.85	.85	.85	.85
.89	.89	.89	.89	.89	.89	.89
.84	.84	.82	.82	.82	.82	.82
40	40	40	40	40	40	40
41.5	40.5	40.5	40.4	40.3	40.3	40.3
37.5	37	37	36.8	36.8	36.8	36.8
		400 ± 1 CPS				
148	156	165	171	174	177	179
141	152	161	165	171	174	176
167	176	184	189	192	196	197
166	176	184	189	191	195	197
167	176	184	189	192	196	197
165	175	182	187	191	194	196

WATTMETER TRANSDUCER REMOVED FROM

V

FIGURE 6.5-6 d

1:00	1:15	1:30	1:45	2:00	2:15	
	128					
.85	.86	.71	.62	.66	.64	
.89	.90	1.00	.93	.90	.86	
.82	.85	.83	.90	.87	.85	
40	17.5	17.5	14.5	0 ##	0 ##	
40.3	20	20	20	0 ##	0 ##	
36.8	37.5	21.5	21.5	0 ##	0 ##	
:04						
182	90	91	132	86	139	
179	89	89	131	86	138	
200	92	93	133	95	156	
199	92	93	134	95	155	
200	92	94	134	96	156	
199	91	94	94	155	179	
SYSTEM						

PESCO PRODUCTS DIVISION
BORG-WARNER CORPORATION

PHASE A HELIUM GAS	STOP RUN B5-2-38			
DATA POINTS - HR.MIN	2:30	2:45	3:00	3:1
VOLTAGE - L-N	120	←	→	120
PHASE A	120	←	→	120
PHASE B	128	120	120	122
PHASE C				
CURRENT - AMPS				
PHASE A	.64	.64	.64	.74
PHASE B	.86	.86	.86	.93
PHASE C	.85	.85	.85	.84
WATTAGE - WATTS				
PHASE A	0##	0##	0##	17
PHASE B	0##	0##	0##	5
PHASE C	0##	0##	0##	26
SPEED - RPM	11880	←	→	1188
SPIN DOWN TIME - MIN			:04	
FREQUENCY - CPS	← 400 ± 1 CPS		→	←
TEMPERATURE - °F				
FRONT BEARING	163	174	179	63
REAR BEARING	171	175	178	63
FRONT WNDG TURNS	189	195	196	64
REAR WNDG TURNS	189	195	196	64
STATOR CORE	191	195	196	66
AIR GAP	189	194	195	65

INSTRUMENTATION TROUBLE - BEL

START RUN B5-2-39

3:30	3:45	4:00	4:15	4:30	4:45	5:00
121						
.74	.67	.67	.71	.73	.67	.67
.86	.87	.87	.86	.84	.86	.87
.81	.80	.80	.80	.80	.80	.80
10	5	5	7.5	10	5.5	5.5
20.5	26	26.5	23.5	20.5	25	26
			400±1 CPS			
131	163	174	180	182	182	182
131	163	173	177	180	180	180
149	179	190	195	197	198	198
147	177	189	194	196	196	196
150	181	192	197	199	200	200
148	179	190	195	197	198	19

WATTMETER TRANSDUCER REMOVED

FIGURE 6.5-6 e

5:15	5:30	5:45	6:00	6:15	6:30	
.67	.71	.71	.76	.74	.74	
.87	.86	.90	.84	.84	.86	
.80	.80	.80	.80	.80	.80	
5.5	10	7.5	11.5	11.5	11.5	
26	21.5	26	20	20	20	
182	182	182	184	186	186	
180	180	180	182	182	182	
198	198	198	200	201	201	
196	196	196	198	200	200	
200	200	200	201	203	203	
198	198	198	200	200	200	

ROM SYSTEM

PESCO PRODUCTS DIVISION
BORG-WARNER CORPORATION

PHASE A HELIUM GAS				
DATA TIME - HR:MIN	6:45	7:00	7:15	7:3
VOLTAGE - L-N	121			
PHASE A	120			
PHASE B	122			
PHASE C				
CURRENT - AMPS				
PHASE A	.74	.74	.74	.7
PHASE B	.84	.84	.84	.8
PHASE C	.80	.80	.80	.8
WATTAGE - WATTS				
PHASE A	17			
PHASE B	11.5	11.5	12	12
PHASE C	20	20	20	20
SPEED - RPM	11880			
SPIN DOWN TIME - MIN				
FREQUENCY - CPS	←		400 ± 1	CPS
TEMPERATURES - °F				
FRONT BEARING	186			
REAR BEARING	182			
FRONT WNDG TURNS	201			
REAR WNDG TURNS	200			
STATOR CORE	203			
AIR GAP	200			

			19 ON-OFF CYCLES (10 SEC RUN EA				
7:45	8:00	CYCLE 1	2	3	4	5	
		121					
		120					
		122					
.71	.71	.84	.74	.60	.60	.60	
.85	.86	.46	.84				
.80	.80	.77					
		13.5	15,5	13.5	13.5	13.5	
8	8	20	13.5	11.5	11.5	11.5	
21.5	22	15	22.5	20	20	20	
		11880					
	:04	:04	:04	:04	:04	:04	
					LINEAR	DEC	
					"		
					"		
					"		
					"		
					"		

FIGURE 6.5-6 f

CH)					
6	7	8	9	10	11
60	.60	.60	.60	.87	.60
13.5	13.5	13.5	13.5	15.5	13.5
11.5	10	10	11.5	20.5	11.5
21.5	20	20	13.5	20	13.5
04	:04	:04	:04	:04	:04
00 ± 1 CPS					
EASE IN		TEMPERATURE			
"	"	"			
"	"	"			
"	"	"			
"	"	"			
"	"	"			

PESCO PRODUCTS DIVISION
BORG-WARNER CORPORATION

PHASE A HELIUM GAS				
DATA TIME - HR-MIN	CYCLE 12	13	14	15
VOLTAGE — L-N				
PHASE A	121			
PHASE B	120			
PHASE C	122			
CURRENT - AMPS				
PHASE A	.87	.87	.6	.87
PHASE B	.84			
PHASE C	.81			
WATTAGE - WATTS				
PHASE A	15	15.5	14	
PHASE B	20	21	11.5	20
PHASE C	18.5	20	13.5	15
SPEED - RPM	11880			
SPIN DOWN TIME - MIN	:04	:04	:04	:04
FREQUENCY - CPS				400 ±
TEMPERATURES - °F				
FRONT BEARING		LINEAR	DECREASE	
REAR BEARING		"	"	
FRONT WNDG TURNS		"	"	
REAR WNDG TURNS		"	"	
STATOR CORE		"	"	
AIR GAP		"	"	

STOP RUN 85-3-39				START RUN 85-2-		
16	17	18	19	8:15	8:30	8:45
				120		
				120		
				122		
.87	.87	.87	.87	.87	.84	
				.86	.82	.81
				.82		
				16.5		
				20		
15	13.5	13.5	13.5	13.5		
				11880		
:04	:04	:04	:04			
/ CPS				400 ± 1 CPS		
IN TEMPERATURE				64	134	168
"	"			64	134	167
"	"			64	153	186
"	"			64	151	183
"	"			64	153	186
"	"			64	152	185

FIGURE 6.5-6 g

40	31 ON-OFF CYCLES (10 SEC RUN EACH)				
9:00	CYCLE 20	21	22	23	24
	120				
	120				
	122				
	.84				
.81	.83				
	.82				
	16.5				
	20				
	13.5				
	11880				
	:04	:04	:04	:04	:04
			400 ± 1 CPS		
180	LINEAR DECREASE IN TEMP				
177	"		"	"	"
200	"		"	"	"
200	"		"	"	"
200	"		"	"	"
200	"		"	"	"

PESCO PRODUCTS DIVISION
BORG-WARNER CORPORATION

PHASE A HELIUM GAS				
DATA TIME - HR:MIN	CYCLE 25	26	27	2
VOLTAGE - L-N				
PHASE A	120			
PHASE B	120			
PHASE C	122			
CURRENT - AMPS				
PHASE A	.88			
PHASE B	.83	.86		
PHASE C	.82			
WATTAGE - WATTS				
PHASE A	16.5			
PHASE B	20.0			
PHASE C	13.5			
SPEED - R.P.M	11880			
SPIN DOWN TIME - MIN	:04	:04	:04	:0
FREQUENCY - CPS	←			
TEMPERATURE - °F				
FRONT BEARING	←			
REAR BEARING	←			
FRONT WNDG TURNS	←			
REAR WNDG TURNS	←			
STATOR CORE	←			
AIR GAP	←			

28	29	30	31	32	33	34	35
4	:04	:04	:04	:04	:04	:04	:04
				400 ± 1 cps			
			LINEAR	DECREASE	IN	TEMPER	
			"	"		"	"
			"	"		"	"
			"	"		"	"
			"	"		"	"
			"	"		"	"

FIGURE 6.5-6 h

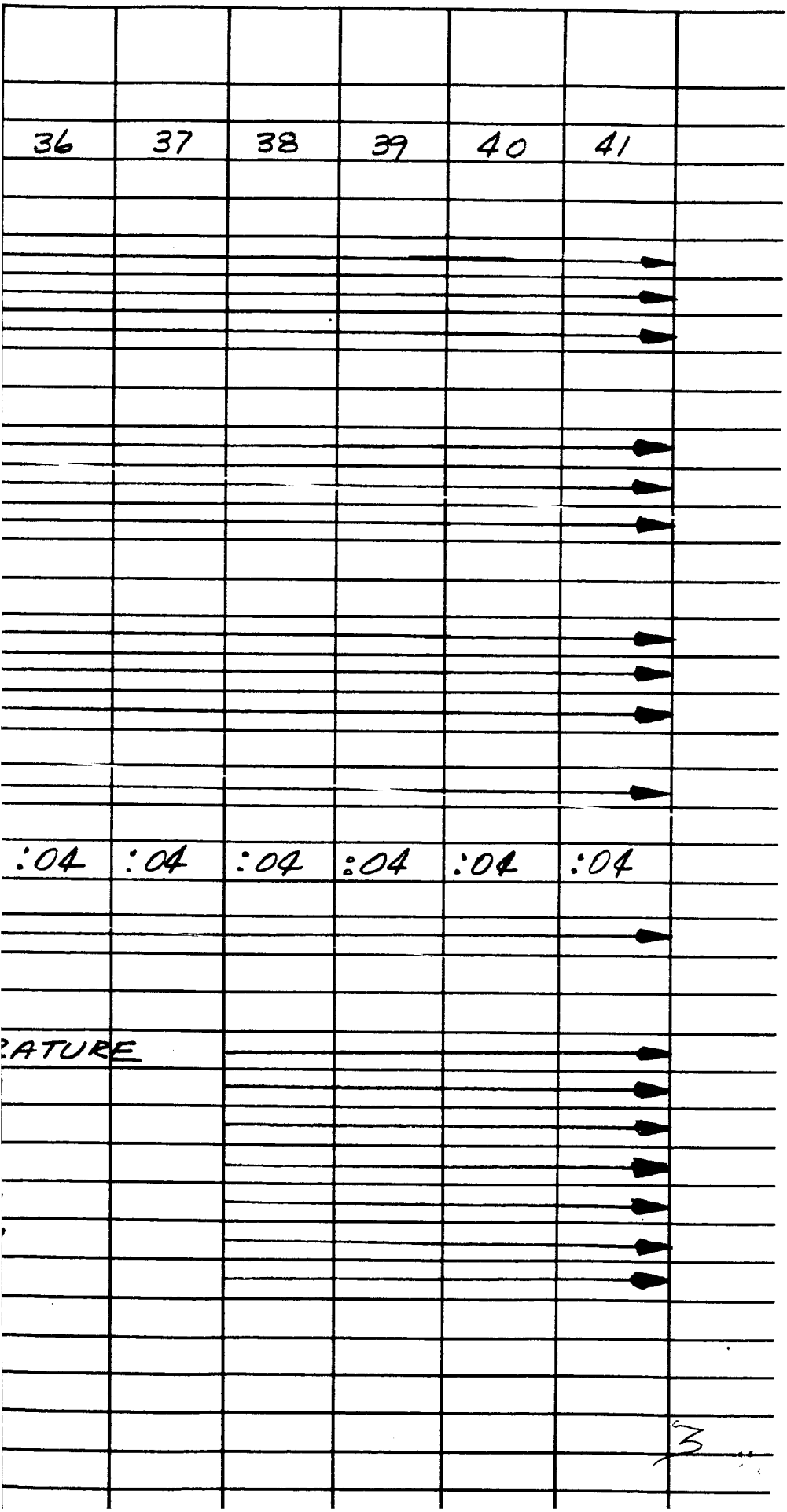

PESCO PRODUCTS DIVISION
BORG-WARNER CORPORATION

PHASE A HELIUM GAS			
DATA TIME - HR:MIN	CYCLE 42	43	44
VOLTAGE - L-N			
PHASE A	120		
PHASE B	120		
PHASE C	122		
CURRENT - AMPS			
PHASE A	.88		
PHASE B	.86		
PHASE C	.82		
WATTAGE - WATTS			
PHASE A	16.5		
PHASE B	20		
PHASE C	13.5		
SPEED - RPM	11880		
SPN DOWN TIME - MIN	:04	:04	:04
FREQUENCY - CPS	←		
TEMPERATURES - °F			
FRONT BEARING	←	LINEAR DECRE	
REAR BEARING	←	"	"
FRONT WNDG TURNS	←	"	"
REAR WNDG TURNS	←	"	"
STATOR CORE	←	"	"
AIR GAP	←	"	"

1

45	46	47	48	49	50	9:30	9:4
						120	
						120	
						122	
						.87	.84
						.86	.83
						.82	.82
						13.5	
						20	
						13.5	
						11880	
:04	:04	:04	:04	:04	:04		
400±1 CPS							400±
ASE IN TEMPERATURE						73	137
"	"	"				73	137
"	"	"				76	156
"	"	"				76	147
"	"	"				76	15(
"	"	"				76	153

FIGURE 6.5-6 i

END PHASE A

5 10:00

.95

.83

.82

cps

174

173

192

190

192

191

PESCO PRODUCTS DIVISION
BORG-WARNER CORPORATION

PHASE B LIQUID HYDROGEN	START	RUN: B5-2-		
DATA TIME - HR:MIN	05	10	15	
VOLTAGE - L-N				
PHASE A	120			
PHASE B	120			
PHASE C	120			
CURRENT - AMPS				
PHASE A	1.08			
PHASE B	1.09			
PHASE C	.99			
WATTAGE - WATTS				
PHASE A	6			
PHASE B	27.5			
PHASE C	13.5			
SPEED - RPM	11880			
SPIN DOWN TIME - MIN				
FREQUENCY - CPS				
TEMPERATURE - °F				
FRONT BEARING	-425			
REAR BEARING	-425			
FRONT WNDG TURNS	-425			
REAR WNDG TURNS	-425			
STATOR CORE	-425			
AIR GAP	-425			

HELIUM MOTOR TEST DATA

41							
20	25	30	35	40	45	60	55

400 ± 1 cps

FIGURE 6.5-6 j

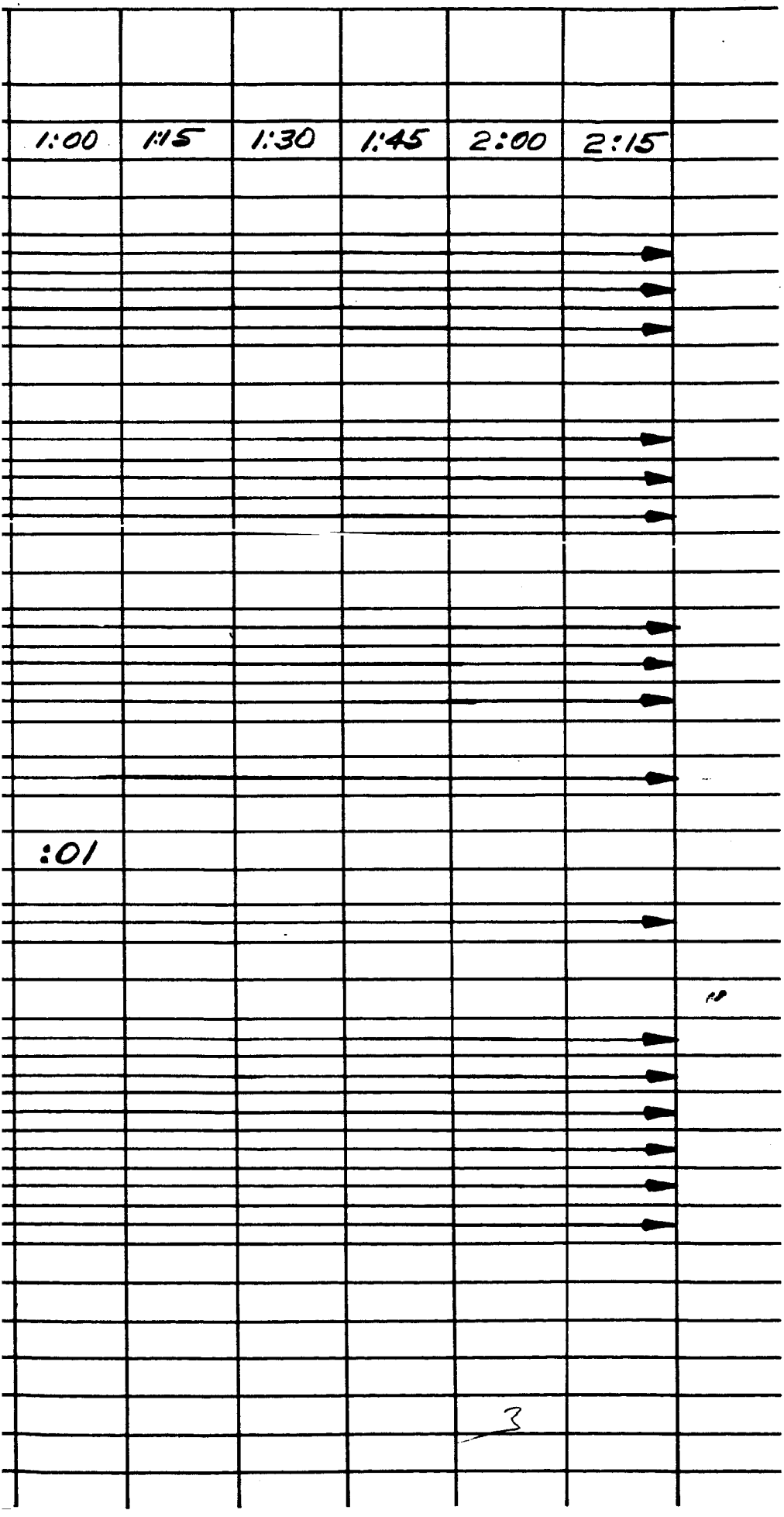

PESCO PRODUCTS DIVISION
BORG-WARNER CORPORATION

PHASE B / LIQUID HYDROGEN				
DATA TIME - HR:MIN	2:30	2:45	3:00	3
VOLTAGE - L-N				
PHASE A	120			
PHASE B	120			
PHASE C	120			
CURRENT - AMPS				
PHASE A	108			
PHASE B	1.09			
PHASE C	.99			
WATTAGE - WATTS				
PHASE A	6			
PHASE B	27.5			
PHASE C	13.5			
SPEED - RPM	11880			
SPIN DOWN TIME - MIN				
FREQUENCY - CPS				
TEMPERATURE - °F				
FRONT BEARING	-425			
REAR BEARING	-425			
FRONT WNDG TURNS	-425			
REAR WNDG TURNS	-425			
STATOR CORE	-425			
AIR GAP	-425			

STOP RUN B5-2-4

:15	3:30	3:45	4:00	4:45	5:00	5:15	5:3

:01

400 ± 1 CPS

✓

FIGURE 6.5-6 k

START RUN B5-2-42

5:45	6:00	6:15	6:30	6:45	7:00
122					
120					
122					
1.09					
1.07					
1.00					
7.5					
27.5					
13.0					
11880					
		400 ± 1 cps			
-425					
-425					
-425					
-425					
-425					
-425					

PESCO PRODUCTS DIVISION
BORG-WARNER CORPORATION

PHASE B LIQUID HYDROGEN			
DATA TIME - HR:MIN	7:15	7:30	7:45
VOLTAGE - L-N			
PHASE A	122		
PHASE B	120		
PHASE C	122		
CURRENT - AMPS			
PHASE A	1.09		
PHASE B	1.07		
PHASE C	1.00		
WATTAGE - WATTS			
PHASE A	7.5		
PHASE B	27.5		
PHASE C	13.0		
SPEED - RPM	11880		
SPIN DOWN TIME - MIN			
FREQUENCY - CPS	←	400 ± 1 c	
TEMPERATURE - °F			
FRONT BEARING	-425		
REAR BEARING	-425		
FRONT WNDG TURNS	-425		
REAR WNDG TURNS	-425		
STATOR CORE	-425		
AIR GAP	-425		

50
ON-OFF CYCLES (10 SEC RUN EACH)

8:00	CYCLE 1	2	3	4	5	6	
	122						
	120						
	122						
	1.09						
	1.07						
	1.00						
	7.5						
	27.5						
	13.0						
	11880						
:01	:01	:01	:01	:01	:01	:01	:0
DS						400	
	-425						
	-425						
	-425						
	-425						
	425						
	-425						

FIGURE 6.5-6 1

7	8	9	10	11	12	13

PESCO PRODUCTS DIVISION
BORG-WARNER CORPORATION

PHASE B LIQUID HYDROGEN			
DATE TIME - HR:MIN	CYCLE #	15	16
VOLTAGE - L-N			
PHASE A	122		
PHASE B	120		
PHASE C	122		
CURRENT - AMPS			
PHASE A	1.09		
PHASE B	1.07		
PHASE C	1.00		
WATTAGE - WATTS			
PHASE A	7.5		
PHASE B	27.5		
PHASE C	13.0		
SPEED - RPM	11880		
SPIN DOWN TIME - MIN	:01	:01	:01
FREQUENCY - CPS			
TEMPERATURE - °F			
FRONT BEARING	-425		
REAR BEARING	-425		
FRONT WNDG TURNS	-425		
REAR WNDG TURNS	-425		
STATOR CORE	-425		
AIR GAP	-425		

17	18	19	20	21	22	23	
:01	:01	:01	:01	:01	:01	:01	:
				400 ± 1 CPS			

FIGURE 6.5-6 m

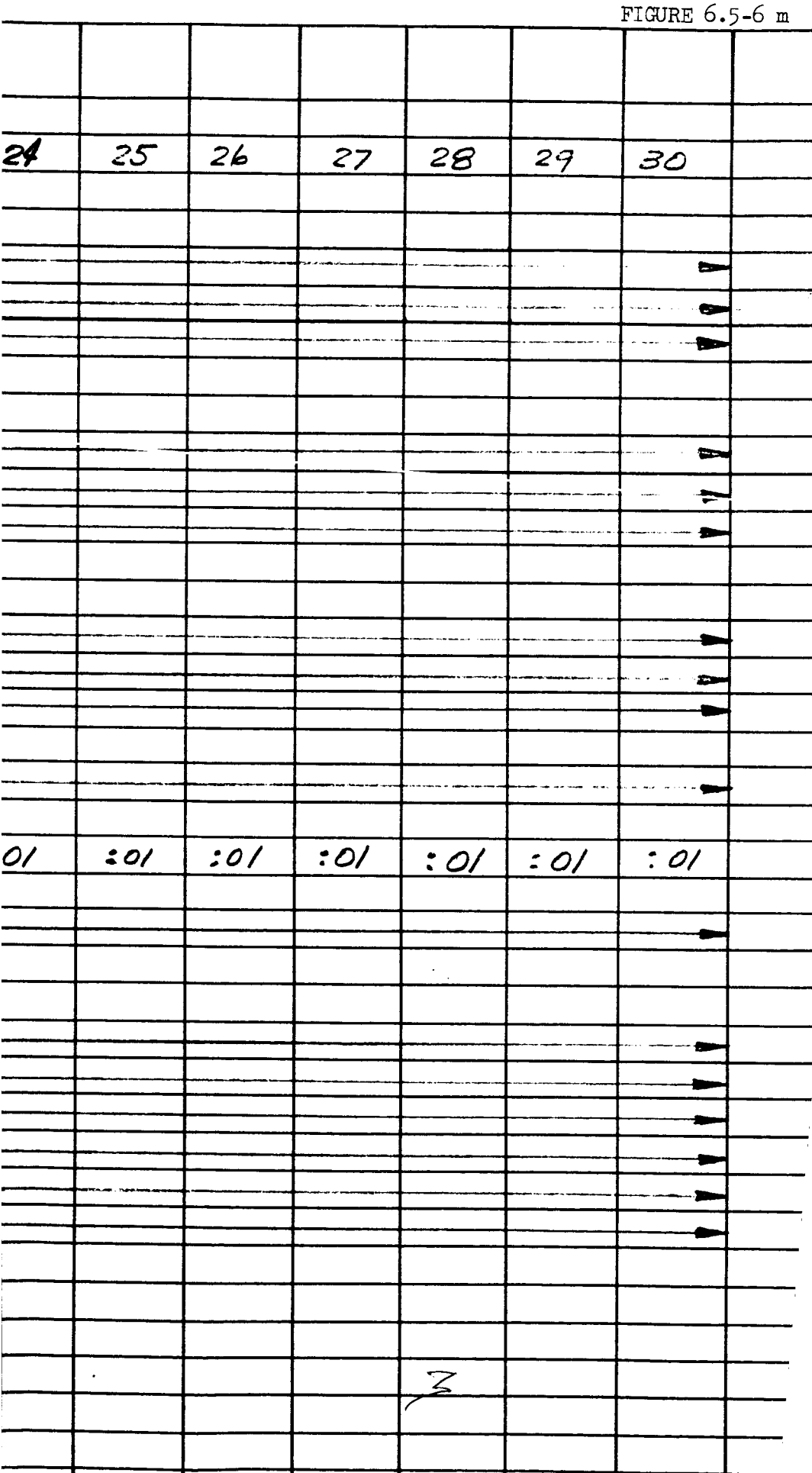

PESCO PRODUCTS DIVISION
BORG-WARNER CORPORATION

PHASE B LIQUID HYDROGEN			
DATA TIME - HR:MIN	CYCLE 31	32	33
VOLTAGE - L-N			
PHASE A	122		
PHASE B	120		
PHASE C	122		
CURRENT - AMPS			
PHASE A	1.09		
PHASE B	1.07		
PHASE C	1.00		
WATTAGE - WATTS			
PHASE A	7.5		
PHASE B	27.5		
PHASE C	13.0		
SPEED - RPM	11880		
SPIN DOWN TIME - MIN	:01	:01	:01
FREQUENCY - CPS			
TEMPERATURE - °F			
FRONT BEARING	-425		
REAR BEARING	-425		
FRONT WNDG TURNS	-425		
REAR WNDG TURNS	-425		
STATOR CORE	-425		
AIR GAP	-425		

34	35	36	37	38	39	40	41
:01	:01	:01	:01	:01	:01	:01	:01

400 ± 1 cps

FIGURE 6.5-6 n

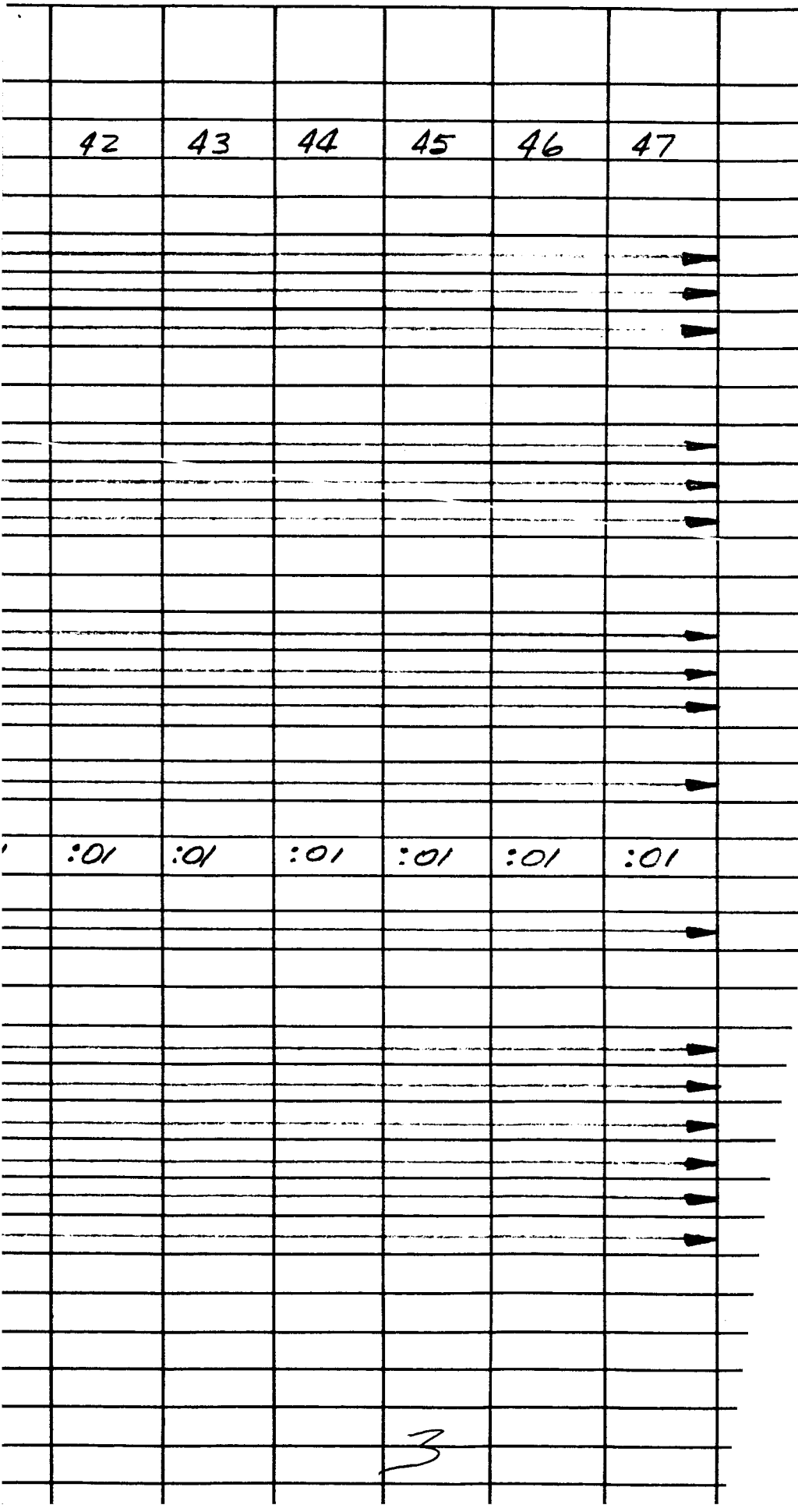

PESCO PRODUCTS DIVISION
BORG-WARNER CORPORATION

PHASE B LIQUID HYDROGEN				
DATA TIME - HR:MIN	CYCLE 48	49	50	8
VOLTAGE - L-N				
PHASE A	122			1
PHASE B	120			1
PHASE C	122			1
CURRENT - AMPS				
PHASE A	1.09			1
PHASE B	1.07			1
PHASE C	1.00			1
WATTAGE - WATTS				
PHASE A	7.5			
PHASE B	27.5			2
PHASE C	13.0			1
SPEED - RPM	11880			11
SPIN DOWN TIME - MIN	:01	:01	:01	
FREQUENCY - CPS		400 ± 1 CPS		
TEMPERATURE - °F				
FRONT BEARING	-425			-
REAR BEARING	-425			-
FRONT WNDG TURNS	-425			-
REAR WNDG TURNS	-425			-
STATOR CORE	-425			-
AIR GAP	-425			-

			STOP	B5-2-42			END
:30	8:45	9:00	9:15	9:30	9:45	10:00	
22						→	
20						→	
22						→	
.09						→	
07						→	
00						→	
7.5						→	
7.5						→	
8.0						→	
880						→	
		— 400 ± 1 cfs —				→	
425						→	
425						→	
425						→	
425						→	
425						→	
425						→	

FIGURE 6.5-6 o

PHASE B

ELECTRICAL LAB CHECK - AIR AT STP

120
120
120

.84
.87
.85

13.5
15
13.5

11880

:04

100

70
70
70
70
70
70

6.5.3.1.2 Phase B (LH_2)

Phase voltages (L-N) were constant and balanced at 120 volts and phase currents were in the range of 0.99 to 1.09 amperes. Phase wattages were again unbalanced, but constant during this phase of the test. The speed remained constant at 11880 rpm as in Phase A. All motor and bearing temperatures were constant at the liquid hydrogen temperature (-425°F), as was to be expected since only a locked rotor condition caused by bearing seizure could bring about a temperature increase large enough to be sensed by the thermocouples. Reference to Figures 6.5-6 b and 6.5-6 j through o give a detailed analysis of the reduced data for this phase.

6.5.3.1.3 Bearing Analysis

Upon completion of test phases A and B, the unit was disassembled and the bearings removed for analysis. In this section and subsequent sections, reference to front and rear bearings will be as follows:

1.) The front bearing is located on the preload spring end of the shaft, and 2.) The rear bearing is located near the magnetic speed pickup. (See Figure 6.5-2). Barden SR4ABSS bearings are the angular contact type and operate without conventional lubrication (maximum rated temperature +575°F). Close examination of both front and rear bearings revealed the following: 1) No indication of interference between the bearing and motor housing, 2) A slight even wear pattern could be seen in the raceway of the outer and inner races located on the thrust side just off the centerline of the raceways. This was due to the no load condition and the preload spring, 3) These wear patterns could be seen only under magnification, 4) The wear patterns were parallel to the raceways indicating the bearings were mounted squarely on the shaft, 5) The balls from both bearings showed a slight running pattern, but no galling or other signs of stress were visible, 6) Neither separator showed wear or failure of material. Figures 6.5-7 and 6.5-8 illustrate the disassembled front and rear bearings respectively.

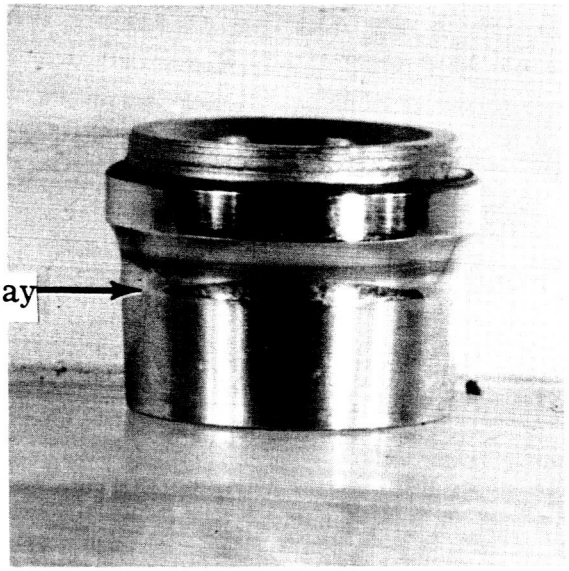

Inner Race

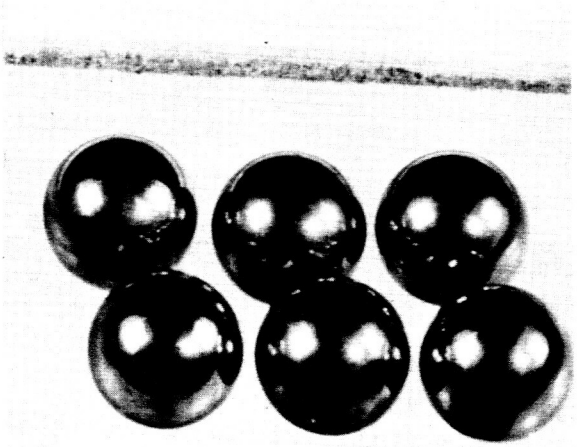

Bearing Balls

Test Bearing
(Front)
Figure 6.5-7

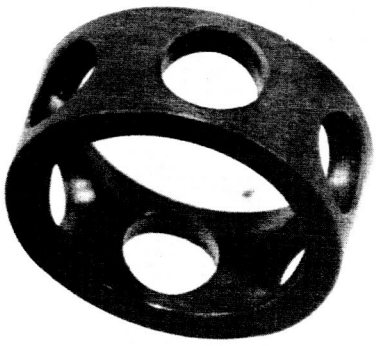

Separator

Outer Race

Inner Race

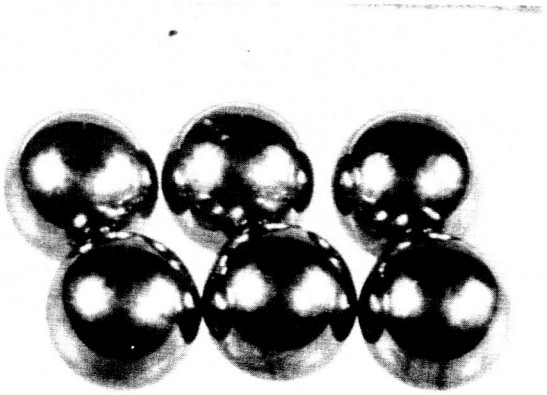

Bearing Balls

Test Bearing
(Rear)
Figure 6.5-8

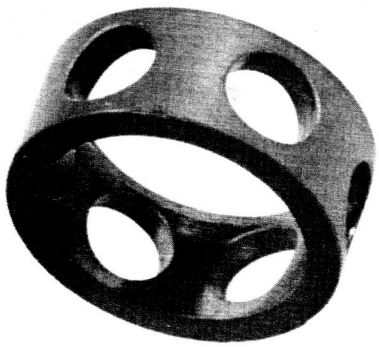

Separator

Outer Race

USAF ZERO DEFECTS

aerospace equipment BORG WARNER

6.5.3.2 Second Test Unit

6.5.3.2.1 Phase B (LH_2)

The results of this phase were identifical to those obtained for the first test unit, (see Section 6.5.3.1.2), therefore no further discussion is given.

6.5.3.2.2 Phase A (Gaseous Helium)

A slight modification of this test was introduced to try to increase the bearing and motor temperatures. The voltage was raised to 135 volts (L-N), but this brought about no appreciable increase in temperature. The purpose of this modification was to help substantiate the motor design and bearing performance at increased temperatures. The increase in voltage caused the phase currents and phase wattages to increase to 0.90 and 18-22 watts respectively.

6.5.4 Discussion

Although the test program was of limited duration, it is deemed sufficient to establish the feasibility of the bearing and housing design. It is evident by the appearance of the test parts and the stability of speed and temperatures during testing that no unusual or severe stresses radial or axial were imposed on the bearing. Visual running patterns as noted on the examination are expected as the solid lubricant is wiped from the cage by the balls and deposited on raceways. The testing accomplished does not assure long life but does encourage life verification testing on the described or similar design.

APPENDIX I

SAMPLE CALCULATIONS

1. Circumferential Stresses Due to Differential Contractions

The cylindrical surfaces involved are the core, the bearing outer races, the sleeves and the housing. Excepting the core, the others can be treated as thin cylinders. To simplify calculations, each one of these was treated as thin cylinders for all the designs studied, only the final design was checked with the necessary cylinders treated as thick cylinders. Both the thin and thick cylinder theories are briefly reviewed below.

Thin Cylinder Theory

(Timoshenko - Strength of Materials pt. I)

Subscript 1 refers to the outer cylinder
Subscript 2 refers to the inner cylinder

No pressure exists between the cylinders at the high temperature t. The stresses at another temperature t_o are given by -

$$\sigma_1 = \frac{pd}{2\delta_1} \quad \& \quad \sigma_2 = \frac{pd}{2\delta_2}$$

where δ_1 and δ_2 are the thicknesses, d is the common diameter and p is the pressure between the two cylinders, at any temperature circumferential contraction for both the cylinders is the same, then

$$\alpha_1 (t - t_o) - \frac{pd}{2E_1\delta_1} = \alpha_2 (t - t_o) + \frac{pd}{2E_2\delta_2}$$

USAF ZERO DEFECTS

aerospace equipment BORG WARNER®

where α's are the coefficients of thermal expansion and E's are the moduli of elasticity.

Solving this equation for pd and substituting, we get,

$$\sigma_1 = \frac{(\alpha_1 - \alpha_2)(t - t_o) E_1}{1 + \frac{\delta_1}{\delta_2} \frac{E_1}{E_2}}$$

and

$$\sigma_2 = \frac{(\alpha_1 - \alpha_2)(t - t_o) E_2}{1 + \frac{\delta_2}{\delta_i} \frac{E_2}{E_i}}$$

Thick Cylinder Theory

(Timoshenko - Strength of Materials pt. II)

Subscript a refers to the inner cylinder
Subscript b refers to the outer cylinder

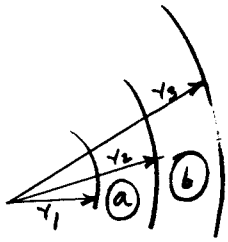

r_1 the inner radius of a

r_2 the inner radius of b and the outer radius of a

r_3 the outer radius of b

The external radius of the inner cylinder in an unstressed condition is larger than the internal radius of the outer cylinder by δ.

Then $$\frac{r_2 p}{E_b}\left(\frac{r_2^2 + r_3^2}{r_3^2 - r_2^2} + \mu_b\right) + \frac{r_2 p}{E_a}\left(\frac{r_1^2 + r_2^2}{r_2^2 - r_1^2} - \mu_a\right) = \delta$$

where p is the pressure between the two cylinders

and

$$\delta_{r_1} = -\frac{2 r_1 r_2^2 p}{E_a (r_2^2 - r_1^2)}$$

$$\sigma_{a\ max.} = -\frac{2 p r_2^2}{r_2^2 - r_1^2}$$

$$\sigma_{b\ max.} = \frac{p (r_1^2 + r_2^2)}{r_2^2 - r_1^2}$$

Illustrative Example

Consider the design represented by Figure 6 . All the cylindrical sections will be treated as thin cylinders.

Section A

Core is made of 1020 steel with 2.31 O.D. and 2.06 I.D., aluminum housing is made of 7075 bar with .125" wall thickness.

Assume that I.D. of Al Housing and O.D. of core are in-line at 350°F, then the stresses at -450°F are given by -

$$\sigma_1 = \frac{(370 + 430 - 190 - 200) \times 10^{-5} \times 12 \times 10^6}{1 + \frac{12 \times 10^6}{31.5 \times 10^6} \times \frac{.125}{.125}} = 35,600 \text{ psi}$$

and $$\sigma_2 = \frac{410 \times 10^{-5} \times 31.5 \times 10^6}{1 + \frac{31.5 \times 10^6}{12 \times 10^6} \times \frac{.125}{.125}} = 35,600 \text{ psi}$$

Strain in the core $\varepsilon_2 = \frac{35,600}{31.5 \times 10^6} = 1.13 \times 10^{-3}$ ins/in change of internal radius (originally 1.31/2) of the core due to strain

$$\Delta r_{2i} = \frac{1.312}{2} \times 1.13 \times 10^{-3} = .0007 \text{ inches}$$

If we had assumed a radial clearance between the housing and the core at .001" at 350°F, from 68°F to 350°F

$$\Delta\alpha = \frac{(370 - 190) \times 10^{-5}}{282} = .638 \times 10^{-5} \text{ in/in/°F}$$

and to contract Al housing .002" on 2.31 inches, required

$$\Delta t = \frac{.002}{2.31 \times .638 \times 10^{-5}} = \frac{200}{2.31 \times .638} = 135°F$$

$$\therefore \Delta\alpha \Delta t \approx \left(1 - \frac{135}{800}\right) \times 445 = (1 - .169) \times 445 = 370$$

and $\sigma_1 = \frac{370}{445} \times 35,600 = 29,600$ psi at -450°F so the stress is reduced from 35,600 psi to 29,600 psi.

Section B

Bearing outer race is made of 440 C and has .75 O.D. and .04" wall. Al housing is of 7075 with .125" wall.

Assume in-line at 350°F

Then the stress in Al housing at the section B and at -450°F is

$$\sigma_1 = \frac{445 \times 10^{-5} \times 12 \times 10^6}{\frac{12 \times 10^6}{33 \times 10^6} \times \frac{.125}{.04}} = \frac{53,400}{1 + 1.172} = 24,600 \text{ psi}$$

APPENDIX II

BIBLIOGRAPHY

I. Sources

A. Technical Abstracts

1. Engineering Indix 1956 - 1965
2. Applied Science and Technology Index 1958 - 1964
3. British Technology Index
4. U. S. Armed Services Technical Information Agency Technical Abstract Bulletin 1957 - 1963
5. U. S. Government Research Reports 1956 - 1965
6. U. S. NASA Technical Publications Announcements 1958 - 1962
   U. S. NASA Scientific and Technical Aerospace Reports 1963 - 1965.

B. Cryogenic Conferences' Reports and Technical Journals

1. Advances in Cryogenic Engineering 1954 - 1964
2. Cryogenics 1960 - 1962
3. Low Temperature Physics and Chemistry

C. Pesco's In-house Reports and Data

D. U. S. Government Agencies

The following seven (7) were very cooperative and supplied us with considerable amount of information. We gratefully acknowledge their efforts.

1. Cryogenic Properties of Solids, Cryogenic Division, Cryogenic Engineering Laboratory, National Bureau of Standards, Boulder, Colorado.

2. Research Institute, University of Dayton,
300 College Park, Dayton, Ohio 45409
(Serving, Air Force Materials Laboratory, Research and
Technical Division, AFSC, Wright Patterson
A. F. Base, Dayton, Ohio 45433)

3. Analysis and Research Unit, Technical Service Branch,
Scientific and Technical Information Division, National
Aeronautics and Space Administration, ATSS,
Washington, D.C. 20546

4. Defense Documentation Center's Computer Type Bibliography
Service, DDC/OSB, Camerson Station, Alexander, Virginia
22314
(Serving, Defense Supply Agency, Dayton Field Service,
Defense Documentation Center for Scientific
and Technical Information, Building 47, Area B,
Wright-Patterson AFB, Ohio 45433)

5. Mechanical Properties Data Center,
Air Force Materials Information Center,
Sutton Bay, Michigan 49682

6. Thermophysical Properties Research Center,
Purdue University Research Park,
2595 Yeager Road, Lafayette, Indiana

7. National Bureau of Mines
Helium Research Center
Amerillo, Texas, 79105

II. References

A. Structural Materials

1. A Compendium of the Properties of Materials at Low Temperature (Phase I)
Victor J. Johnson, General Editor
WADD Technical Report 60-56 (Prepared by NBS Eng. Lab.)
Part I (July, 1960), Part II (Oct., 1960), Part III (Oct., 1960)
Published by U.S.A.F.

2. A Compendium of the Properties of Materials at Low Temperature (Phase II)
Richard B. Stewart and Victor J. Johnson, General Editors
WADD Technical Report 60-56 (Prepared by NBS Eng. Lab.)
Part IV (December, 1961) Published by U.S.A.F.

3. Aluminum Alloys for Cryogenic Service
J. E. Campbell
Matls. Research & Standards, v4 n10 Oct., 1964 p540-8.

4. Cryogenic Materials Data Handbook
13th Progress Report, Air Force Matls. Lab., Res. & Tech. Div., AFSC, Wright-Patterson A.F. Base.

5. Cryogenics (Structural Materials for Electric & Electronic Devices)
Electro-Technology, v68 n3 September 5, 1961 p 121-33
also November p 76-84.

6. Cryogenic Testing of Structural Solids
R. M. McClintock
Am. Soc. Metals, Metals Eng. Quart. 2, No. 1, Feb., 1962
p 28-35.

7. Enthalpy - Entropy Chart for Helium
(3 to 25°K, 1 to 100 atm)
NBS - CEL, 1964.

8. Low Temperature Metals
A. Hurlich
Chem. Eng. v70 n24 November 25, 1963 p 104-12.

9. Low Temperature Thermal Conductivity of Some Commercial Coppers
R. L. Powell, H. M. Roder and W. M. Rogers
J. Appl. Phys. 28, 1282-1288, November, 1957.

10. Low-Temperature Tensile Properties of Copper and Four Bronzes
R. M. McClintock, D. A. VanGundy and R. H. Kropschot
ASTM Bull. No. 240, September, 1959, p 47-50.

11. Low-Temperature Transport Properties of Commercial Metals and Alloys, II, Aluminum.
R. L. Powell, W. J. Hall and H. M. Roder
J. Appl. Phys. 31, 496-503, March, 1960.

12. Low-Temperature Transport Properties of Commercial Metals and Alloys, III Gold-Cobalt
R. L. Powell, M. D. Bunch and E. F. Gibson
J. Appl. Phys. 31, 504-505, March, 1960.

13. Mechanical Properties of Structural Materials at Low Temperatures; A Compilation from the Literature
R. M. McClintock and H. P. Gibbons
Natl. Bur. Stds. (U.S.) Monograph No. 13, June 1, 1960)

14. Properties of Materials at Low Temperatures
R. J. Corruccini
Chem. Engr. Progr. 53, Part 1, 262-267, Part 2, 342-346, Part 3, 397-402, June, July, August, 1957.

15. Some Low Temperature Properties of Materials
R. H. Kropschot
Proceedings Mountain States Navy Res. & Dev. Clinic
September, 1961.

16. Specific Heats and Enthalpies of Technical Solids at Low Temperatures; A Compilation from the Literature)
R. J. Corruccini and J. J. Gniewek
U. S. Bur. Stds. Monograph n21 October, 1960 20 p.

17. A Survey of the Literature on Heat Transfer from Solid Surfaces to Cryogenic Fluids
R. J. Richards, W. G. Steward, and R. B. Jacobs
Natl. Bur. Stds, (U.S.) Tech. Note No. 122 (PB161623)
October, 1961.

18. Temperature - Entropy Diagram for Helium
(3 to 25°K; 0.5 to 100 atm)
NBS - CEL, 1964.

19. Temperature - Entropy Diagram for Helium
(0 to 50°K, 0.5 to 200 atm)
Zelmanov's and Keesom's data, 1957.

20. Temperature - Entropy Diagram for Helium
(15 to 300°K; 0.1 to 100 atm)
NBS - CEL, 1964.

21. Thermal Conductivities of Common Commercial Aluminum Alloys
W. J. Hall, R. L. Powell and H. M. Roder
Paper G-6, Proceedings 1957 Cryo. Eng. Conf. p 408-415.

22. Thermal Conductivities of Copper and Copper Alloys
R. L. Powell, W. M. Rogers and H. M. Roder
Paper E-3, Proceedings 1956 Cryo. Eng. Conf. p 166-171.

23. Thermal Conductivity of Metals and Alloys at Low Temperatures
R. L. Powell and W. A. Blanpied
Natl. Bur. Stds. (U.S.) Circ. No. 556, September 1, 1954.

24. Thermal Conductivity of Solids at Low Temperatures
R. L. Powell and D. O. Coffin
Paper G-5, Proceedings 1954 Cryo. Eng. Conf. p 262-266.

25. The Thermodynamic Properties of Helium from 6 to 540°R between 10 and 1500 psia
Douglas B. Mann
Natl. Bur. Stds. (U.S.) Tech. Note 154, January, 1962

26. The Thermodynamic Properties of Helium from 3 to 300°K between 0.5 to 100 Atmospheres
Douglas B. Mann
Natl. Bur. Stds. (U.S.) Tech. Note 154, January, 1962.

27. Thermal and Electrical Conductivity of Aluminum and Aluminum Alloys
W. J. Hall, H. M. Roder and R. L. Powell
Low Temperature Physics and Chemistry 1958 (5th Int. Natl. Conf.) p 389-391.

28. Thermal Expansion of Technical Solids at Low Temperatures; A Compilation from the Literature
R. J. Corruccini and J. J. Gniewek
Natl. Bur. Stds. (U.S.) Monograph No. 29, May 19, 1961.

29. Thermal Expansion of Some Engineering Materials from 20 to 293°K
V. Arp, J. H. Wilson, L. Winrich and P. Sikora
Cryogenics 2, June, 1962 p 230-236.

30. The Tensile Property Evaluation of One 5000-Series Aluminum Alloy at the Temperature of Liquid Helium
L. P. Rice, J. E. Campbell and W. F. Simmons
Advances in Cryo. Eng. v8 1962 p 671-677.

31. Which Metals for Cryogenic Applications
H. Hamilton and M. Katcher
Matls. in Design Eng. v59 n5 May, 1964 p 83-6.

B. Magnetic Materials

32. Magnetic Losses at Low Temperatures
E. H. Borwn and J. R. Brennand, Jr.
Proceedings 1958 Cryo. Eng. Conf. p 65-70.

33. Properties of Electronic and Magnetic Materials at Cryogenic Temperatures
J. G. Daunt
DDC AD-608 041 September, 1964 12 p

34. Temperature Dependence of Magnetic Losses
J. J. Gniewek and R. L. Powell
Advances in Cryo. Eng. v7 1961 p 303-310.

C. Conductor Materials

35. Cryogenic Characteristics of Alloy Wires
A. B. Kaufman
Instruments and Control Systems p 119-121, March, 1964.

36. Dielectric Strength of Some Common Electrical Insulators in Liquid Helium and Nitrogen
F. T. Stone and R. McFee
The Review of Scientific Instruments v32, No. 12, December 1961.

37. Electrical Contact Resistance of Copper-Copper Junctions at Low Temperatures
R. L. Powell and A. A. Aboud
Rev. Sci. Instr. 29, March, 1958, p 248-249.

38. Low Temperature Electrical Resistance of Fifteen Commercial Conductors
O. E. Park, M. M. Fulk and M. M. Reynolds
Paper D-3, Proceedings 1954 Cryo. Eng. Conf. p 156-157.

39. Low Temperature Mechanical Properties of Copper and Four Copper Alloys
R. H. McClintock, D.A. VanGundy, and R. H. Kropschot
NBS Report 5505, August 1957.

40. Properties of Copper Alloys at Cryogenic Temperatures
C. L. Bulow
Engineering Design News, June 1964.

41. Properties of Dielectrics at Cryogenic Temperatures
K. N. Mathes
Westinghouse Elect. & Mfg. Co. - Dielectrics in Space Symposium, Collected Papers 10 1963 14 p.

42. Electrical and Thermal Resistivity of Transition Elements at Low Temperatures
G. K. White and S. B. Woods
Roy. Soc. Lond. Philosophical Trans. Series A
v251 n995 March 12, 1959 p 273-302.

D. Insulation Material

43. Electrical Insulation Applications
J. A. Milek
Polyimide Plastics: A State-of-the-Art Report,
Report No. S-8, Chapter IV, September 1965.

44. Electrical Insulation at Cryogenic Temperatures
K. N. Mathes
Electro-Technology v72 n3 September, 1963 p72-7.

45. Electrical Insulation for Application at Cryogenic Temperatures
K. N. Mathes and E. C. McKannon
Nat. Research Council - Publ. 1080, 1963, p 29-31.

46. Evaporation of Helium I Due To Current-Carrying Leads
H. Sobol and J. J. McNichol
Rev. Sci. Instr. v33 n4 April, 1962 p 473-7.

47. Thermal Contact with Electrical Insulation for Cryogenic Applications
R. L. Chaplin and P. E. Shearin
Rev. Sci. Inst. v33 n12 December, 1962 p 1466-7

E. Bearing Materials

48. The Application of Gas-Lubricated Bearings to a Miniature Helium Expansion Turbine
B. W. Birmingham, H. Sixsmith and W. A. Wilson
Advances in Cryo. Eng. v7 1961 p 30-32.

49. Cryogenic Bearings
H. Hanan
Machine Design v36 n13 June 4, 1964 p 122-8.

50. Dry Gas Operation of Ball Bearings at Cryogenic Temperatures
L. E. Scott, D. B. Cheiton, and J. A. Brennan
Advances in Cryo. Eng. v7 1961 p 273-276.

51. Elastomeric Seals and Materials at Cryogenic Temperatures
D. H. Weitzel, P. R. Ludtke, Y. Ohori, R. F. Robbins, and F. B. Peterson
NBS Report 7603, Quarterly Report for June, 1962 to August, 1962.

52. Electrical and Mechanical Behaviors of Polymers at Cryogenic Temperatures
K. N. Mathes
SPE Technical Papers, 20th Annual Tech. Conf. v10 (1964)

53. Electromagnetic Bearing
H. Sixsmith
Rev. Sci. Instr. 32, November, 1961, p 1196 - 1197.

54. Evaluation of Ball Bearing Separator Materials Operating Submerged in Liquid Nitrogen
W. A. Wilson, K. B. Martin, J. A. Brennan and B. W. Birmingham
ASLE Trans. 4, 1961 p 50-58.

55. Load Carrying Capacity of Gas-Lubricated Bearings with Inherent Orifice Compensation Using Nitrogen and Helium Gas
H. Sixsmith, W. A. Wilson and B. W. Birmingham
Natl. Bur. Stds. (U.S.) Tech. Note No. 115 (PB161616) August, 1961.

56. Operation of Bearings and Pumps at Low Temperatures
K. B. Martin, R. B. Jacobs and R. J. Hardy
Proceedings 1957 Cryo. Eng. Conf. p 209-216.

57. Self-Lubricating Materials Developed by Westinghouse
Sci. Lubrication v15 n8 August, 1963 p22-4.

58. Some Mechanical Properties of Mylar and Dacron Polyester Strands at Low Temperatures
R. P. Reed and R. P. Mikesell
Rev. Sci. Instr. 29, 734-736, August, 1958.

59. A Survey Materials Report on Tetrafluoroethylene (TFE) Plastics
J. T. Milek
Electronic Properties Information Center, September, 1964.

60. Testing of Ball Bearings with Five Different Separator Materials at 9200 RPM in Liquid Nitrogen
J. A. Brennan, W. A. Wilson, R. Radebaugh and B. W. Birmingham
Paper G-2 in Advances in Cryo. Eng. Vol. 7, 1961 Conf. p 262-272.

61. The Theory of Stable High-Speed Externally Pressurized Gas-Lubricated Bearing
H. Sixsmith and W. A. Wilson
J. Res. 68C (Eng. and Instr.) No. 2, 101-14, April-June, 1964.

62. Testing and Operation of Ball Bearings Submerged in Liquefied Gases
K. B. Martin and R. B. Jacobs
Proceedings 1958 Cryo. Eng. Conf. p 476-486.

F. Miscellaneous

63. Cryogenics
A. E. Javitz
Electro-Technology p 121-133 September, 1961.

64. The Cryogenic Challenge
J. H. Lieb and R. E. Mowers
The Insulation Challenge, February, 1962.

65. Epoxy Resins as Cryogenic Structural Adhesives
R. M. McClintock and M. J. Hiza
Paper F-3, Proceedings 1957 Cryo. Eng. Conf. p 305-315
also in Modern Plastics 35, 172-174, 176, 237, June, 1958.

66. Low-Temperature Strength of Epoxy-Resin Adhesives
Natl. Bur. Stds. (U.S.) Tech. News Bull. 42
May, 1958, p 84-85.

67. An Operational Information Retrieval System in the Field of Cryogenics
N. A. Obien
Automation and Sci. Communication pt. 2 26th Annual Meeting 1963 p 157-158.

68. Program of Testing Non-metallic Materials at Cryogenic Temperatures, Final Report R-3498
Rocket Propulsion Laboratories
Edwards, California
December 1962.

69. Properties of Lead Thermal Switches at Low Temperatures
W. Reese and W. A. Steyert, Jr.
Rev. Sci. Instr. v33 n1 January, 1962 p 43-7.

70. The Role of Materials in Cryogenics
D. Perkner and M. W. Riley
Materials in Design Engineering, Special Report No. 185, July, 1961.

ADDENDUM I

MOTOR SELECTION GUIDE

The purpose of this addendum is to provide a Motor Selection Guide for motors operating in helium at temperatures from -453°F to +70°F and pressures from 10 psia to 3000 psia. An additional purpose is to provide a comparison to a motor designed to operate solely in helium at -453°F.

The first purpose is accomplished in Figures 1 and 2. Figure 1 is a chart of envelope dimensions, volume, and weight of 17 motors ranging in horsepower from .012 to 6.9 and operating speeds from 5,000 to 20,000 rpm. Figure 2 is data presented in curve form such that a designer knowing the required horsepower and speed for a given application may determine the envelope dimensions and volume of the motor.

The ambient is defined above, however, this alone is not sufficient to complete the design definition. The motors described in Figures 1 and 2 are designed to the following requirements:

1) Ambient: Helium at -453°F to +70°F, 10 psia to 3000 psia.

2) Type of Load: Centrifugal Device or equivalent type load.

3) Power Input: 3-phase, 400 cps, 115/200 volts (Figures will apply also to other design voltages within range of 50 to 400).

The mechanical construction of these units is essentially the same throughout the range described. One peculiarity, however, is that all the 2-pole (20,000 rpm) motors and the two smallest 4-pole (10,000 rpm) motors have the bearings and pre-load springs beyond the stator end turn extension.

The larger 4-pole motors and all the 8-pole motors have a sufficiently large end turn I. D. that most of the bearing assembly can fit inside the end turns. The result is obvious on the drive end bearing extension as shown on Figures 1 and 2 as dimensions Le and De. This same length increase, of course, occurs at the other end resulting in a discontinuity in the L/D ratio, but is not apparent from the envelope drawing. The lengths shown also include the internal motor cooling fan.

To determine the motor dimensions for a required continuous horsepower output and speed using Figure 2 simply requires entering the upper curve at the appropriate horsepower and determining the basic volume at the required speed. At this same volume, the L/D ratio can be determined for the required speed. The output and L/D ratio are ordinates plotted against the common abscissa of basic volume for ease of reading. The envelope volume, the motor case diameter, and the motor length can then be computed from the equations in Figure 2, and by reference to Figure 1 for the drive end bearing extension dimensions.

The additional purpose of indicating the size advantage to be gained from cryogenic operation is accomplished by reference to the tabulation below. The computor print-out for this design is shown in Figure 3 with the maximum torque (T_m) marked and the rated torque (T_r) point also marked. The rated torque is determined as 1/1.7 of the maximum torque and the actual value falls between two of the computed points. The performance at T_r is simply a matter of extrapolation and the small differences between computed points allows for accuracy with the ease of linear extrapolation. The cryogenic and room ambient helium motors are compared for approximately the same volume and also for approximately the same output in the table below.

Ambient	Envelope Vol. In^3	RTD RPM	RTD HP	HP/ In^3	WGT. Lbs.	HP/ Lb.
He, -453°F	26.7	11,420	6.0	.225	3.8	1.58
He, -453°F to +70°F	158	10,000	5.5	.0348	20.1	.274
He, -453°F to +70°F	28.5	10,000	.38	.0133	3.4	.112

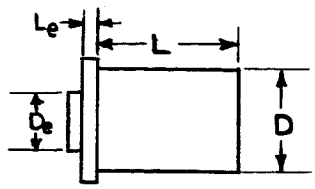

Rated RPM	Rated HP	D In	De In	L In	Le In.	Envelope Vol.[7] In^3	Wgt. Lbs.	Basic Vol.[8] In^3	Brg. Ext. Vol. In^3
20,000[6]	.012	1.62	.81	3.62	1.0	7.98	.9	7.47	.51
20,000[6]	.066	1.92	.81	3.97	1.0	12.0	1.4	11.5	.51
20,000[6]	.18	2.34	1.06	4.44	1.0	20.0	2.2	19.1	.88
20,000[6]	.70	2.87	1.06	4.85	1.0	32.3	3.7	31.4	.88
20,000[4,6]	1.8	3.51	1.37	5.62	1.12	56.0	6.6	54.3	1.65
20,000[4,6]	3.7	4.37	1.60	6.38	1.12	97.8	11.7	95.6	2.25
20,000[4,6]	6.9	5.34	1.70	7.40	1.25	168.5	20.5	165.7	2.83
10,000[6]	.023	2.01	.81	3.60	1.0	11.9	1.3	11.4	.51
10,000[6]	.10	2.39	1.06	4.07	1.0	19.1	2.1	18.25	.88
10,000	.38	2.96	1.06	4.10	.25	28.5	3.4	28.3	.22
10,000	1.0	3.64	1.37	4.73	.3	49.6	6.1	49.2	.44
10,000	2.5	4.56	1.60	5.51	.35	90.7	11.3	90.0	.70
10,000	5.5	5.61	1.70	6.36	.4	158.4	20.1	157.5	.91
5,000	.092	3.09	1.06	3.90	.25	29.4	3.5	29.2	.22
5,000	.34	3.79	1.37	4.48	.3	52.0	6.3	51.6	.44
5,000	1.0	4.75	1.60	5.01	.35	89.5	11.2	88.8	.70
5,000	3.0	5.91	1.70	5.73	.4	157.7	20.2	156.8	.91

NOTE:

(1) Ambient: Helium at -453°F to +70°F, 10 to 3000 psia.

(2) Type of Load: Centrifugal Device

(3) Power Input: 3-Phase, 400 cps, 115/200 Volts (Table will apply also to other design voltages within range of 50 to 400)

(4) The bearing Dn values for these units are beyond presently published experience, therefore caution must be exercised.

(5) Table contains ratings for 2, 4, and 8 pole speeds, 6 pole also available (6600 rpm.)

(6) Bearings extend beyond stator end turn extension, do not fit inside end turn extension.

(7) Envelope Volume includes drive end bearing extension.

(8) Basic Volume is volume defined by D and L and is basic motor volume excluding drive end bearing extension, but including fan.

CONTINUOUS OUTPUT AVAILABLE FROM VARIOUS VOLUMES & WEIGHTS

FIGURE 1

USAF ZERO DEFECTS

aerospace equipment BORG WARNER®

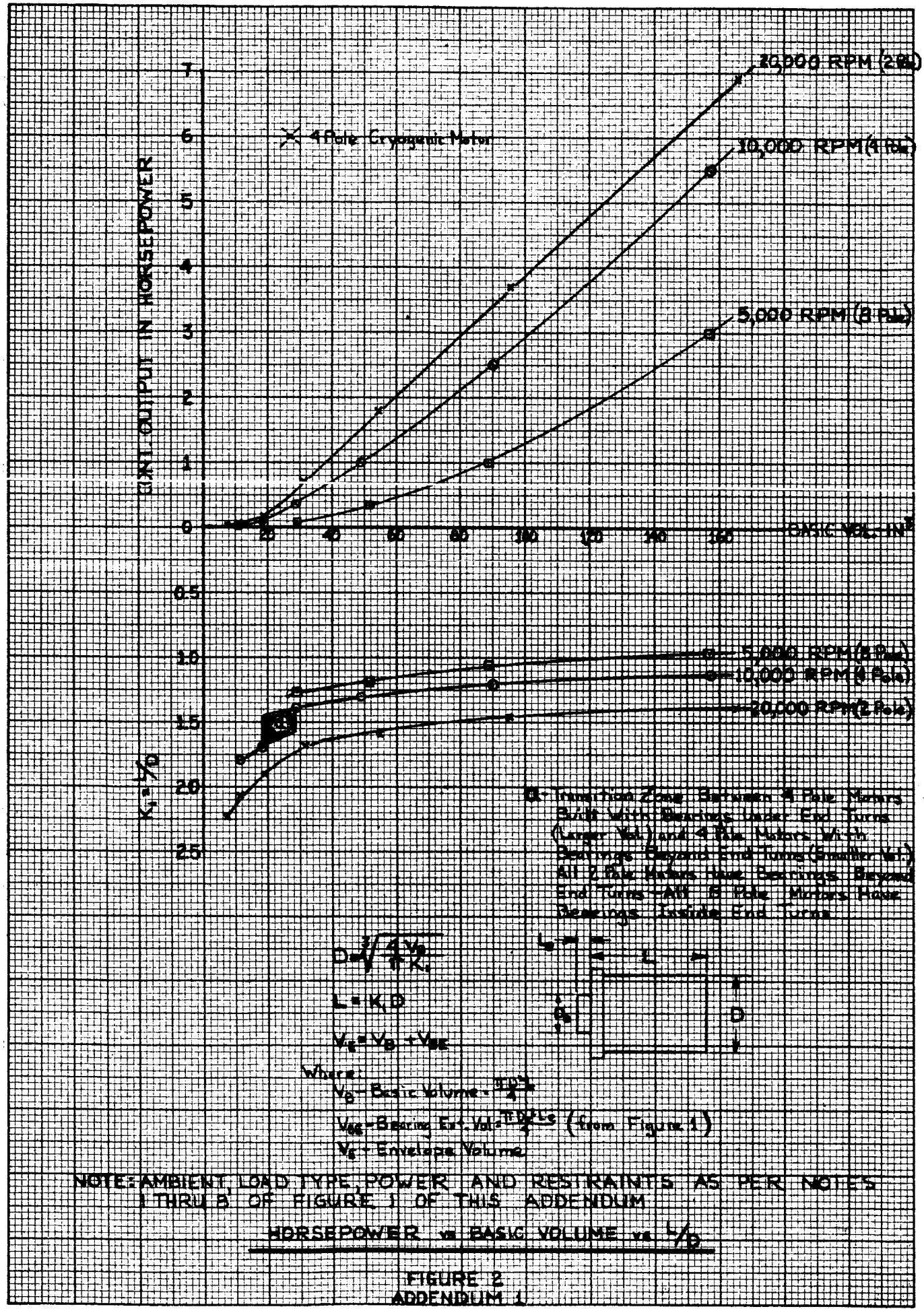

NOTE: AMBIENT, LOAD TYPE, POWER AND RESTRAINTS AS PER NOTES 1 THRU 8 OF FIGURE 1 OF THIS ADDENDUM

HORSEPOWER vs BASIC VOLUME vs L/D

FIGURE 2
ADDENDUM 1

K&E 10 X 10 TO 1/4 INCH 7 X 10 INCHES KEUFFEL & ESSER CO. MADE IN U.S.A. 46 1322

PESCO AC MOTOR COMPUTER CALCULATIONS

	SLIP	TORQUE IN.LB	RPM	HP	I AMPS	EFF	PF	WATTS	VA	PRI LOSS	SEC LOSS	IRON LOSS	F W LOSS
	0.30	2.06	11964.	0.391	6.678	61.48	20.58	474.	2304.	1.9	1.0	140.0	39.8
	0.60	4.39	11928.	0.831	7.004	76.97	33.34	806.	2417.	2.1	4.0	140.0	39.5
	1.00	7.48	11880.	1.411	7.660	84.52	47.11	1245.	2643.	2.5	11.0	140.0	39.2
	1.30	9.78	11844.	1.837	8.282	87.24	54.99	1571.	2857.	2.9	18.6	140.0	39.0
	1.60	12.05	11808.	2.257	8.987	88.90	61.08	1894.	3100.	3.5	28.0	140.0	38.7
	2.00	15.02	11760.	2.803	10.021	90.24	67.02	2317.	3457.	4.3	43.5	140.0	38.4
	2.30	17.21	11724.	3.201	10.846	90.86	70.25	2629.	3742.	5.0	57.1	140.0	38.2
	2.60	19.36	11688.	3.589	11.700	91.26	72.69	2934.	4036.	5.9	72.5	140.0	37.9
	3.00	22.15	11640.	4.089	12.867	91.59	75.04	3331.	4439.	7.1	95.5	140.0	37.6
	3.30	24.18	11604.	4.451	13.755	91.71	76.29	3620.	4745.	8.1	114.6	140.0	37.4
	3.60	26.15	11568.	4.799	14.647	91.76	77.21	3902.	5053.	9.2	135.1	140.0	37.2
	4.00	28.69	11520.	5.244	15.837	91.74	78.04	4264.	5464.	10.8	164.5	140.0	36.9
	4.30	30.53	11484.	5.561	16.725	91.68	78.43	4525.	5770.	12.0	188.1	140.0	36.6
T_R= 33.2	4.60	32.30	11448.	5.865	17.607	91.58	78.66	4778.	6074.	13.3	212.7	140.0	36.4
	5.00	34.55	11400.	6.249	18.768	91.40	78.76	5100.	6475.	15.1	247.2	140.0	36.1
	5.30	36.16	11364.	6.520	19.627	91.25	78.72	5330.	6771.	16.5	274.2	140.0	35.9
	5.60	37.71	11328.	6.776	20.473	91.07	78.59	5551.	7063.	18.0	302.0	140.0	35.6
	6.00	39.66	11280.	7.097	21.579	90.81	78.30	5830.	7445.	20.0	340.2	140.0	35.3
	6.30	41.04	11244.	7.320	22.392	90.61	78.02	6027.	7725.	21.5	369.5	140.0	35.1
	6.60	42.35	11208.	7.530	23.189	90.39	77.68	6215.	8000.	23.1	399.4	140.0	34.9
	7.00	43.99	11160.	7.788	24.227	90.08	77.17	6450.	8358.	25.2	439.9	140.0	34.6
	7.30	45.14	11124.	7.966	24.987	89.84	76.74	6615.	8620.	26.8	470.7	140.0	34.4
	7.60	46.23	11088.	8.131	25.729	89.60	76.27	6770.	8876.	28.4	501.7	140.0	34.2
	8.00	47.57	11040.	8.331	26.692	89.26	75.61	6963.	9209.	30.6	543.4	140.0	33.9
	8.30	48.50	11004.	8.467	27.393	89.00	75.09	7097.	9451.	32.2	574.7	140.0	33.6
	8.60	49.37	10968.	8.590	28.078	88.74	74.55	7222.	9687.	33.8	606.1	140.0	33.4
	9.00	50.44	10920.	8.737	28.964	88.38	73.80	7375.	9992.	36.0	647.9	140.0	33.1
	9.30	51.17	10884.	8.834	29.608	88.11	73.23	7480.	10215.	37.6	679.1	140.0	32.9
	9.60	51.84	10848.	8.921	30.235	87.83	72.64	7577.	10431.	39.2	710.2	140.0	32.7
	10.00	52.65	10800.	9.020	31.045	87.46	71.84	7694.	10710.	41.3	751.3	140.0	32.4
	10.30	53.20	10764.	9.084	31.633	87.18	71.23	7774.	10913.	42.9	781.8	140.0	32.2

	SLIP	TORQUE IN.LB	RPM	HP	I AMPS	EFF	PF	WATTS	VA	PRI LOSS	SEC LOSS	IRON LOSS	F W LOSS
	10.60	53.70	10728.	9.138	32.204	86.89	70.62	7846.	11110.	44.5	812.1	140.0	32.0
	11.00	54.29	10680.	9.197	32.941	86.51	69.79	7931.	11365.	46.6	851.9	140.0	31.7
	11.30	54.67	10644.	9.232	33.476	86.22	69.17	7988.	11549.	48.1	881.4	140.0	31.5
	11.60	55.02	10608.	9.259	33.994	85.93	68.54	8038.	11728.	49.6	910.5	140.0	31.3
	12.00	55.42	10560.	9.283	34.663	85.54	67.70	8097.	11959.	51.5	948.6	140.0	31.0
	12.30	55.67	10524.	9.294	35.147	85.24	67.08	8134.	12126.	53.0	976.7	140.0	30.8
	12.60	55.88	10488.	9.298	35.618	84.94	66.45	8166.	12288.	54.4	1004.4	140.0	30.6
	13.00	56.12	10440.	9.294	36.223	84.55	65.62	8200.	12497.	56.3	1040.5	140.0	30.3
	13.30	56.25	10404.	9.284	36.661	84.25	65.00	8221.	12648.	57.7	1067.1	140.0	30.1
	13.60	56.36	10368.	9.270	37.086	83.95	64.38	8237.	12795.	59.0	1093.2	140.0	29.9
	14.00	56.46	10320.	9.243	37.633	83.55	63.56	8253.	12983.	60.8	1127.2	140.0	29.6
	14.30	56.50	10284.	9.217	38.029	83.25	62.95	8259.	13120.	62.0	1152.2	140.0	29.4
T_M	14.60	56.51	10248.	9.187	38.413	82.95	62.35	8263.	13253.	63.3	1176.7	140.0	29.2
	15.00	56.49	10200.	9.141	38.907	82.54	61.55	8262.	13423.	64.9	1208.5	140.0	28.9
	20.00	53.87	9600.	8.204	43.661	77.43	52.48	7904.	15063.	81.8	1536.5	140.0	25.6
	30.00	44.57	8400.	5.939	48.451	67.15	39.47	6598.	16716.	100.7	1907.2	140.0	19.6
	40.00	36.52	7200.	4.171	50.561	56.99	31.30	5459.	17444.	109.7	2083.9	140.0	14.4
	50.00	30.53	6000.	2.906	51.640	47.02	25.87	4610.	17816.	114.4	2177.7	140.0	10.0
	60.00	26.09	4800.	1.986	52.256	37.25	22.06	3978.	18028.	117.1	2232.4	140.0	6.4
	70.00	22.72	3600.	1.298	52.639	27.68	19.26	3497.	18160.	118.9	2267.0	140.0	3.6
	80.00	20.10	2400.	0.765	52.892	18.28	17.11	3123.	18248.	120.0	2290.0	140.0	1.6
	90.00	18.02	1200.	0.343	53.067	9.06	15.42	2823.	18308.	120.8	2306.2	140.0	0.4
	95.00	17.13	600.	0.163	53.135	4.51	14.70	2695.	18332.	121.1	2312.5	140.0	0.1
	98.00	16.63	240.	0.063	53.171	1.80	14.31	2624.	18344.	121.3	2315.8	140.0	0.0
	99.00	16.48	120.	0.031	53.183	0.90	14.18	2602.	18348.	121.3	2316.9	140.0	0.0

MODEL NO.116115A
CALC.NO. 1001
MARCH 3,1966

E	115.000	PHI	3.000	RPM-SYNC	12000.000
R1-HOT	0.014	R2-HOT	0.313	X	2.140
XO	17.600	KP	0.937	FE LOSS	140.000
F AND W-SYNC	40.0				

Typical Cryogenic Motor Performance

Figure 3

Addendum 1

aerospace equipment BORG WARNER